

**THE ROLE OF BEDROCK GROUNDWATER IN HEADWATER CATCHMENTS:
PROCESSES, PATTERNS, STORAGE AND TRANSIT TIME**

A Thesis Submitted to the College of
Graduate and Postdoctoral Studies
In Partial Fulfillment of the Requirements
For the Degree of Doctor of Philosophy
In the School of Environment and Sustainability
University of Saskatchewan
Saskatoon

By

CHRISTOPHER P. GABRIELLI

© Copyright Christopher Gabrielli, November, 2017.

All rights reserved.

PERMISSION TO USE

In presenting this thesis/dissertation in partial fulfillment of the requirements for a Postgraduate degree from the University of Saskatchewan, I agree that the Libraries of this University may make it freely available for inspection. I further agree that permission for copying of this thesis/dissertation in any manner, in whole or in part, for scholarly purposes may be granted by the professor or professors who supervised my thesis/dissertation work or, in their absence, by the Head of the Department or the Dean of the College in which my thesis work was done. It is understood that any copying or publication or use of this thesis/dissertation or parts thereof for financial gain shall not be allowed without my written permission. It is also understood that due recognition shall be given to me and to the University of Saskatchewan in any scholarly use which may be made of any material in my thesis/dissertation.

DISCLAIMER

Reference in this thesis/dissertation to any specific commercial products, process, or service by trade name, trademark, manufacturer, or otherwise, does not constitute or imply its endorsement, recommendation, or favoring by the University of Saskatchewan. The views and opinions of the author expressed herein do not state or reflect those of the University of Saskatchewan, and shall not be used for advertising or product endorsement purposes.

Requests for permission to copy or to make other uses of materials in this thesis/dissertation in whole or part should be addressed to:

Executive Director
School of Environment and Sustainability
University of Saskatchewan
Room 323, Kirk Hall
117 Science Place
Saskatoon, Saskatchewan S7N 5C8 Canada

OR

Dean
College of Graduate and Postdoctoral Studies
University of Saskatchewan
105 Administration Place
Saskatoon, Saskatchewan S7N 5A2 Canada

ABSTRACT

Understanding the role of groundwater contributions to headwater rainfall-runoff processes, storages and transit times remains a major challenge in hydrology. Bedrock groundwater contributions to the stream channel can significantly augment streamflow, mediate water quality and control the age of water discharging from catchments. Yet, the hydroclimatic and bedrock characteristics that control these dynamics are not fully understood. Direct observation of bedrock groundwater dynamics, storages and surface water connections remain limited, challenging our ability to fully constrain new catchment scale models that are needed to aid future resource management decisions. I undertook a large field campaign at a well-studied research site in New Zealand. Bedrock groundwater dynamics were monitored for one year and combined with bedrock characterization, tritium-based age dating and hydrochemical analysis to constrain a new conceptual model of the headwater aquifer. Findings were used to develop a new index to identify the controls of bedrock permeability and landscape structure on the time scales of catchment storage-release processes. The three major findings of this research were firstly, that unfractured low-permeability bedrock underlying the research catchment limited to deep flowpaths. Minimal bedrock groundwater flux combined with large bedrock storage resulted in significantly older bedrock groundwater that contributed minimally to catchment discharge. Second, unfractured low-permeability bedrock was a primary control on bedrock groundwater recharge seasonality. Groundwater movement occurred as matrix flow, requiring long durations of high catchment-wetness for considerable recharge to occur, a condition that was only attained during cold-season months when evapotranspiration rates were low and catchment wetness was high. Third, permeability contrasts at the soil-bedrock interface and landscape structure were highly correlated with mean transit time for eight catchments in geologically diverse regions, suggesting that subsurface anisotropy is a major control on setting streamwater age. Overall, through the coupled analysis of the processes, patterns, storages and transit times, this research has advanced our understanding of the role of bedrock groundwater in headwaters. The findings presented here offer new insights into the function of deeper hydrologic layers and have implications for future models of headwater catchment function – models that need to better incorporate the influence of deep flowpaths and storages in groundwater-surface water and rainfall-runoff predictions.

ACKNOWLEDGEMENTS

No single person has shaped my academic career more than my supervisor, Jeffrey J. McDonnell. His passion for the subject, generosity of time, ability to impart wisdom and his patience to let me find my way has had a profound and lasting effect on me. Thank you Jeff, it has truly been a pleasure. I wish to also thank my committee members – Lee Barbour, Chris Spence, Andrew Ireson and Grant Ferguson – for their advice and continued support, and for helping me think beyond the confines of my discipline. Thank you to Anna Coles, Willemijn Appels, Julian Klaus, Cody Hale, Uwe Morgenstern, Mike Stewart, Nik Aksamit, and Nico Leroux for conversation, math and modeling lessons, and for being part of this entire process; and to others in the McDonnell Watershed Hydrology lab over the years – Kim and Daryl Janzen, Cody Miller, Luke Pangle, Winnie Seifert, Jaivime Evaristo, Jay Frentress, Dyan Pratt, Natalie Orlowski, Ali Ameli, Veva McDonnell, and many other visitors – for helpful discussions, pints and laughs. I owe a huge debt of gratitude to Christie Thomson, Matt Taylor and Laurent Gourdol for suffering through the steep slopes, bush lawyer, torrential rain and long days that defined our 8 months living on site at the Maimai. A special thanks to John Payne for keeping Maimai alive long enough to let me have my go at it. Your legacy at Maimai will be long and enduring, and from all of us who have stepped foot within its boundaries, thank you John. To my Kiwi community, specifically Shaun and Jacqui McCrackenberry, and Emma and Bob Noonan, thank you from the bottom of my heart. Your help, generosity and endless support were critical to the success of this project. I am lucky to have been part of this incredible and supportive community and feel grateful for our time together.

DEDICATION

For my parents, for always letting me find my own path, no matter how circuitous

TABLE OF CONTENTS

PERMISSION TO USE.....	i
DISCLAIMER	i
ABSTRACT.....	ii
ACKNOWLEDGEMENTS.....	ii
DEDICATION.....	iv
TABLE OF CONTENTS.....	v
LIST OF TABLES.....	x
LIST OF FIGURES	xi
LIST OF ABBREVIATIONS.....	xii
CHAPTER 1: INTRODUCTION.....	1
1.1 Introduction.....	1
1.2 Research goals and thesis outline	3
1.3 References.....	10
CHAPTER 2: BEDROCK GROUNDWATER AGE, WATER TABLE DYNAMICS AND TIME-VARYING TRANSIT TIME AT THE MAIMAI WATERSHED.....	17
2.1 Abstract.....	17
2.2 Introduction.....	18
2.3 Study Site	20
2.4 Dataset and methods	23
2.4.1 Bedrock characterization and well installation.....	23
2.4.2 Hydrometric data and bedrock groundwater dynamics and flux	24

2.4.3 Transit time analysis	25
2.4.4 Silica analysis and catchment MTT	27
2.5 Results.....	28
2.5.1 Bedrock characterization.....	28
2.5.2 Bedrock groundwater position.....	28
2.5.3 Bedrock groundwater dynamics	33
2.5.4 Bedrock groundwater gradients	34
2.5.5 Tritium measurements and MTT	37
2.5.6 Silica analysis and time-varying streamwater MTT	40
2.6 Discussion.....	42
2.6.1 Bedrock groundwater location and dynamics.....	42
2.6.1.1 Water table position	42
2.6.1.2 Water table dynamics.....	44
2.6.2 The bedrock groundwater domain: gradients, age and streamflow contributions	45
2.6.2.1 Vertical bedrock groundwater gradients.....	45
2.6.2.2 Bedrock groundwater MTT	46
2.6.3 Time-varying streamwater transit time.....	48
2.6.4 An evolving perceptual model of Maimai hydrology.....	50
2.7 Conclusion	53
2.8 Transition statement.....	54
2.9 Acknowledgments.....	54
2.10 Author contributions	55
2.11 References.....	56

Chapter 3: GEOLOGIC CONTROL ON THE SEASONALITY OF RECHARGE IN THE CRITICAL ZONE	67
3.1 Abstract.....	66
3.2 Introduction.....	68
3.3 Study site.....	71
3.4 Data and methods.....	74
3.4.1 Bedrock characteristics and recharge mechanisms.....	74
3.4.1.1 Hydraulic conductivity.....	74
3.4.1.2 Sprinkler Experiment: Bedrock infiltration rate and mechanisms of recharge.	74
3.4.2 Recharge seasonality.....	76
3.4.2.1 Noble gas measurements.....	76
3.4.2.1 Stable isotope measurements	77
3.4.3 Climatic and hydrologic seasonality.....	77
3.4.4 Bedrock groundwater recharge model	78
3.4.4.1 The model	78
3.4.4.2 Parameter identification and model input filtering	80
3.4.4.3 Soil water comparison.....	81
3.5 Results.....	11
3.5.1 Mode of recharge: Bedrock sprinkler experiment and bedrock characterization	82
3.5.1.1 Bedrock Characterization.....	81
3.5.1.2 Sprinkler Experiment	82
3.5.2 Bedrock groundwater recharge seasonality	85
3.5.3 Bedrock groundwater recharge model	86
3.5.3.1 DS(t) filter and Parameter Identification	86

3.5.3.2 Intra-annual and inter-annual recharge patterns	90
3.5.3.3 Soil water comparison.....	93
3.6 Discussion.....	96
3.6.1 Geologic control on groundwater recharge.....	96
3.6.2 Summer runoff but no summer recharge: Seasonality is crucial	97
3.6.3 Review of the groundwater recharge model	101
3.6.4 What is the role of soil for groundwater recharge at Maimai?	102
3.7 Conclusion	103
3.8 Transition statement.....	104
3.9 Acknowledgements.....	105
3.10 Author contributions	106
3.11 References.....	105

CHAPTER 4: A LANDSCAPE ANISOTROPY INDEX TO QUANTIFY THE
RELATIONSHIP BETWEEN GEOLOGY, LANDSCAPE STRUCTURE AND WATER

TRANSIT TIME THROUGH CATCHMENTS	118
4.1 Abstract.....	118
4.2 Introduction.....	119
4.3 Theory.....	122
4.4 Methods.....	124
4.5 Results.....	127
4.6 Discussion.....	131
4.6.1 On the value of the new index	131
4.6.2 On the meaning of the anisotropy index.....	131
4.6.3 Beyond the initial Pacific Rim testing	133

4.7 Summary	135
4.8 Transition statement.....	135
4.9 Acknowledgments.....	135
4.10 Author contributions	136
4.11 References.....	137
Chapter 5: CONCLUSIONS AND FUTURE WORK	147
5.1 Conclusions.....	147
5.2 References.....	152

LIST OF TABLES

Table 2.1a Bedrock well characteristics 2.1a.....	29
Table 2.1b Bedrock well characteristics 2.1b	30
Table 2.2 Tritium units and corresponding MTT for sampled waters	38
Table 3.1 Landscape position and Ksat bedrock wells	82
Table 3.2 Hydroclimatic variables and modeled bedrock groundwater recharge.....	91
Table 4.1 Summary of catchment characteristics.....	124
Table 4.2 Summary of catchment MTT characteristics	126
Table 4.3 Catchment variables used to calculate the Anisotropy Index.	127
Table 4.4 Flowpath length, downslope travel distance, AI, and percent $AI_{>1}$	128

LIST OF FIGURES

Figure 2.1 Map of the Maimai Experimental Watershed.....	21
Figure 2.2 Depth to water table for the underlying headwater aquifer	32
Figure 2.3 Water table elevation time series.....	33
Figure 2.4 Vertical groundwater gradients between	36
Figure 2.5 Bedrock groundwater, soil water and streamwater MTT.....	39
Figure 2.6 Relationship between M8 discharge and silica concentration.....	41
Figure 2.7 Time series of streamwater silica concentration and streamwater MTT.....	42
Figure 2.8 Conceptual model of the bedrock groundwater flow domain	52
Figure 3.1 Maimai Experimental Watershed.	72
Figure 3.2 Stage height time series of sprinkler stilling basin.....	83
Figure 3.3 Bedrock sprinkler experiment photos.....	84
Figure 3.4 NGT and dual isotope plots.....	86
Figure 3.5 Annual recharge temperature magnitude.....	87
Figure 3.6 Modeled bedrock groundwater recharge and dynamic storage	89
Figure 3.7 Mean monthly bedrock groundwater recharge.....	90
Figure 3.8 Mean monthly recharge versus P, Q_{tot} , Q_{dir} , Q_{base} , PET.	92
Figure 3.9 Yearly recharge versus P, Q_{tot} , Q_{dir} , Q_{base} , PET.....	93
Figure 3.10 Soil water and modeled recharge for 2015.....	95
Figure 3.11 Conceptual model of seasonal catchment water balance fluxes.....	100
Figure 4.1 Anisotropy Index theory.....	123
Figure 4.2 The sequence of analysis to calculate the Anisotropy Index.....	129
Figure 4.3 Relationship between the AI and catchment MTT.....	130
Figure 4.4 Regression fit between catchment mean AI and MTT.	130

LIST OF ABBREVIATIONS

AI	Anisotropy index
$AI_{>1}$	Binary Anisotropy index
API	Antecedent precipitation index
Ar	Argon
C_n	Saturated bedrock thickness
DEM	Digital elevation model
DS(t)	Dynamic storage
GRACE	Gravity recovery and climate experiment
ha	hectare
I	Bedrock groundwater recharge/infiltration
Ksat	Saturated hydraulic conductivity
L_d	Downslope travel distance
L_f	Flowpath length
LMWL	Local meteoric water line
MAAT	Mean annual air temperature
MTT	Mean transit time
N_2	Nitrogen
N	Saturated soil thickness
NGT	Noble gas recharge temperature
P	Precipitation
PET	Potential evapotranspiration
PVC	Polyvinyl chloride
Q_{base}	Baseflow discharge
Q_{dir}	Direct flow discharge
Q_{tot}	Total discharge
SBI	Soil bedrock interface
TT	Turnover time
T_R	Bedrock groundwater recharge temperature
TU	Tritium units
TWI	Topographic wetness index
WT	Water Table

CHAPTER 1

INTRODUCTION

1.1 Introduction

Headwater, or first order catchments are the building blocks of the hydrological landscape. They are the main sources of water, nutrients and sediment that sustain the health of ecosystems and humans downstream. They contribute up to half of the mean water volume and nitrogen fluxes for fourth and higher-order rivers in the USA (*Alexander et al.*, 2007) and have recently been associated with greater contributions to groundwater recharge than lower lying downstream regions (*Jasechko et al.*, 2016). The total storage volume of a headwater catchment, in part, controls the length and time scales over which water is captured, stored and released from the landscape. These scales, in turn, are critical in setting the timing, quantity and quality of water that is discharged into stream channels.

Most headwater hydrology research to date that has examined storage and release processes has focused on the thin veneer of soil that mantles the watershed. Early work showed that this soil depth was a first order control on the factors that affect runoff in headwaters (*Hewlett and Hibbert*, 1967). Since then, countless studies have shown how the high permeability and porosity of soil acts as a primary medium of storage and flow for incoming precipitation (e.g. *Pearce et al.* (1986), *Jones and Grant* (1996), *Kirchner* (2003)). Compared to deeper layers, the soil mantle is relatively easy to access and study. And in most headwater modeling exercises, the underlying bedrock has been assumed impermeable – further emphasizing the upper soil horizons as the zone of hydrologic interest.

But what of the deeper layers? The C horizon, saprolite, weathered bedrock and fresh bedrock that all underlie soil do not exist in isolation from the hydrologic, geochemical and biologic processes that occur above. These horizons, and the critical zone in general, are now perhaps the biggest

focus of National Science Foundation sponsored research in the hydrological sciences (*Brantley et al.*, 2007).

So while catchment storage is a known primary control of both discharge dynamics and subsurface mixing processes (*Kirchner*, 2009; *Salve et al.*, 2012; *Creutzfeldt et al.*, 2014), the changes in headwater storage below the soil mantle remain poorly characterized (*McNamara et al.*, 2011). In particular, the contribution of bedrock groundwater to the storage-discharge relationship is difficult to understand and assess, and, as a result, total catchment storage is still largely unknown in most research sites (*Sayama et al.*, 2011). We are simply unable to predict, a priori, how much water a headwater catchment can store and then release, and we still lack clear understanding of the location of a headwater catchments lower boundary. While much new process discovery has focused on extraction of stored water by plants (*Brooks et al.*, 2010; *Overeem et al.*, 2013), process studies of deep catchment storage dynamics have received less attention and relied heavily on empirical approaches. Baseflow recession analysis (*Wittenberg*, 2003) and GRACE-based (*Doell et al.*, 2014; *Sproles et al.*, 2015) methods have provided insights into catchment scale storage-discharge relationships. However, these black-box approaches fail to resolve internal processes, structures and patterns - information necessary to drive the next generation of catchment scale models (*Rinaldo et al.*, 2015).

Recent work by *Birkel et al.* (2011) has highlighted the complexities of catchment storages, identifying both active and passive components that influence differentially, discharge volumes, transit times and solute fluxes. Seasonal changes in catchment storage, both active and passive, are a direct result of storage changes in the entire catchment subsurface volume, not solely in the soil, indicating that the often ignored bedrock volume is contributing considerably to quantity, quality and timing observations made in surface water runoff measurements. Indeed, *Katsuyama et al.* (2010) recently identified connections between stream water mean transit times and bedrock groundwater recharge/discharge dynamics, and *Brantley et al.* (2016) connected critical zone weathering rates and landscape formation with bedrock characteristics and bedrock groundwater dynamics. The influence of bedrock as an additional storage volume, with its associated flowpaths, mixing processes and solute loads (beyond the soil mantle) remains a great source of uncertainty.

A more complete description of the catchment control volume, and thus a more complete description of total headwater hydrologic functioning remains a key research challenge.

Bedrock poses two major challenges to headwater process investigations: (1) the logistical challenges associated with gaining access into bedrock in steep, remote and often roadless terrain and (2), the often complex fracture-dominated flowpaths that can govern bedrock systems. Both of these have historically thwarted attempts to directly study flowpath dynamics, often leaving studies focused on bedrock spring discharge as a proxy for deeper processes (e.g. *Asano et al. (2009)*, *Millares et al. (2009)*, *Katsuyama et al. (2010)*, *Uchida and Asano (2010)*, *Asano and Uchida (2012)*). Additionally, where direct measurement of bedrock groundwater dynamics have been made, they have often been limited to the plot or hillslope scale (*Anderson et al., 1997*; *Montgomery et al., 1997*). Geophysical techniques offer a promising way forward (*Binley, 2010*), however, interpretation of results are often ambiguous without significant ground truthing. Recent advancements in mobile drilling technology, however, have made the direct observation of bedrock groundwater dynamics in difficult to access headwater catchments more readily available (*Gabrielli and McDonnell, 2012*).

1.2 Research goals and thesis outline

This thesis focuses on the Maimai watershed in New Zealand, building on the scores of hydrological process studies conducted at this site (for review see *McGlynn et al. (2002)*). The 280 ha Maimai experimental watershed lies 15 km inland on the northwest coast of New Zealand's South Island near the township of Reefton. Maimai initially came into existence in the mid-1970's as a research catchment to study the hydrologic impact of different logging and harvesting techniques in New Zealand's burgeoning plantation forest industry. Over the 40 years since Maimai's inception it has grown to be one of the most-studied headwater catchments in hillslope hydrology literature. It has been described by Beven (2006, pp. 336) as the 'quintessential wet, steep, forested catchment'.

Previous work at Maimai by *Graham et al.* (2010) and *Gabrielli et al.* (2012) suggested that bedrock groundwater dynamics and storage may play a larger role in streamflow generation than previously thought. The bedrock underlying Maimai was initially considered essentially impermeable (*Pearce et al.*, 1986), leading most additional studies to focus solely on soil-based runoff generation processes. However, work by *Woods and Rowe* (1996) revealed that the rainfall-runoff ratio of hillslope runoff from an instrumented hillslope was significantly less than that of the entire catchment (~15% versus 60%, respectively). This indicated (although not discussed by *Woods and Rowe*) that precipitation might be infiltrating into the hillslope bedrock, traversing bedrock flowpaths and re-emerging into the stream channel to augment catchment discharge. Further, more recent analysis identified moderately permeable bedrock just 1 order of magnitude lower than the lower permeability limit of the mineral soil (*Graham et al.*, 2010), as well as large bedrock water table dynamics occurring on storm-event time scales (*Gabrielli et al.*, 2012). Both observations directly supported a possible new conceptual model of considerable contributions of bedrock groundwater to Maimai's rainfall-runoff processes. Yet, streamwater mean transit time (MTT) was determined to be on the order of 4 months - among the youngest recorded streamwater transit times (*Pearce et al.*, 1986; *Stewart and McDonnell*, 1991). These observations appeared contradictory because the large storage volume associated with the recently observed hydrologically active bedrock formation should lead to long, not short, streamwater transit times. Pilot work examining tritium-based bedrock groundwater age (*Mike Stewart*, personal communication, Feb 13, 2014) further exacerbated these inconsistencies, revealing much older, decadal-age bedrock groundwater and suggesting deeper and more complex catchment scale storage patterns.

This unresolved question of how Maimai could seemingly contain both hydrologically active bedrock *and* short streamwater MTT highlighted a lack of understanding of how bedrock characteristics influence headwater function – even in this, one of the worlds most studied headwater catchments. This question ultimately shaped the overarching objectives of my PhD research, which aimed to mechanistically assess bedrock characteristics at the Maimai to understand how they influenced the timing and magnitude of bedrock groundwater recharge,

controlled bedrock groundwater discharge, and influenced the nature of the streamwater transit time.

I organized my research into three sections – consistent with the 3 research chapters presented in this dissertation – each of which directly sought to answer specific questions regarding bedrock form, function and influence in headwater processes. Specifically:

1. What are the bedrock groundwater dynamics, age and contributions to runoff at the Maimai Experimental Watershed, and how do these factors impact the time varying nature of streamwater transit time? [Chapter 2]
2. How do geologic properties control the seasonality of bedrock groundwater recharge in headwaters? [Chapter 3]
3. Does a simple relation exist between geologic characteristics, landscape topographic form and catchment mean transit time that can explain observed differences in mean transit time across different geologies? [Chapter 4]

This thesis is presented in a ‘dissertation by manuscript’ style as outlined in School of Environment and Sustainability Graduate Student Handbook. Following this introductory chapter, Chapters 2, 3, and 4 are structured as standalone manuscripts intended for direct submission to peer-reviewed journals. Chapter 5 presents the conclusions of my research, discusses linkages between the three manuscript chapters, and suggests avenues for future research.

My main objective in Chapter 2 was to understand how bedrock properties controlled the storage, flux and age of groundwater within the bedrock, and how the spatial distributions of these characteristics influenced streamwater transit times under varying catchment wetness conditions. Although the influence of bedrock properties and the contributions of bedrock groundwater to

headwater processes has received continued interest over the last two decades (*Wilson and Dietrich, 1987; Welch and Allen, 2014; Pfister et al., 2017*), there exists a critical absence of direct whole-catchment observation. As noted above, most studies have been limited to either indirect bedrock spring discharge observations (*Uchida and Asano, 2010; Asano and Uchida, 2012; Oda et al., 2013*) or to direct observation limited to the plot (*Masaoka et al., 2016*) or hillslope scale (*Katsura et al., 2014*). Bedrock properties, however, can vary considerably throughout a single catchment. Therefore, to understand how these spatially diverse characteristics drive the integrated catchment-scale storage-release relationship that influences the time varying nature of streamwater transit time, we need to directly characterize how the spatial distribution of bedrock properties and its control on groundwater age and dynamics varies across different landscape structures catchment-wide.

To achieve the objectives established for Chapter 2, I completed a large scale field campaign that installed 65 wells – 40 into bedrock and 25 into the soil mantle – across the 3 main landscape units (i.e. hillslopes, hollows and riparian zone) that make up the 4.5 ha Maimai M8 research catchment (the site of many previous investigations by *Mosley (1979), Pearce et al. (1986), McDonnell (1990)*, and many others in recent years). Bedrock properties were characterized through downhole testing, and soil and bedrock water tables dynamics were monitored along with other hydrometric data for a full year. Tritium-based water age dating was conducted on 28 bedrock groundwater, soil water and streamwater samples. I developed a silica-based regression model to identify the relation between streamwater age and silica concentration to extend the time series analysis of streamwater age throughout a 1-year monitoring period. This work leveraged the rich history of research previously conducted at Maimai and provided significant new insights into the factors controlling catchment storage, streamwater age and the role of bedrock properties. I also contextualize the findings at Maimai to research conducted at other internationally recognized research catchments.

This study was submitted in August 2017 for potential publication in *Water Resources Research*, and is currently in review: Gabrielli, C.P., McDonnell, J.J., Morgenstern, U., Stewart, M., 2017.

Bedrock groundwater age, water table dynamics and time varying transit time at the Maimai watershed. *Water Resources Research*. In review.

The goal of Chapter 3 was to identify how bedrock properties, in concert with hydroclimatic forcing, controlled the seasonality of groundwater recharge in the bedrock aquifer. Groundwater is a critical resource to humanity, supplying nearly 70% of all water used for agriculture (*Margat and Van der Gun, 2013*) and making up nearly half of the global drinking water budget (*Smith et al., 2016*). Recent work has shown the critical importance of steep headwaters to global groundwater recharge and streamwater mean transit times (*Jasechko et al., 2016*). However, bedrock groundwater recharge in steep mountainous terrain has often been studied in the context of mountain block recharge (*Wilson and Guan, 2004*). This regional scale perspective does not always provide the spatial and temporal process-based understanding needed to identify how specific catchment properties interact to control recharge at the individual headwater scale. We also currently lack complete understanding of the interactions and feedbacks between the geologic characteristics of catchments and the timing and spatial scales of bedrock recharge and subsurface stormflow (*Winter, 2007; Gleeson et al., 2010*), a critical piece of knowledge needed to inform future models to protect and manage our groundwater resources.

In Chapter 3, I used isotopic and noble gas data extracted from bedrock groundwater samples to identify a distinct summer-winter seasonal cycle of groundwater recharge at Maimai. I leveraged a long-term rainfall-runoff and air-temperature data set to compare seasonal patterns in hydroclimatic forcing with the observed seasonality of recharge to identify possible controls. A simple energy balance based empirical recharge model was constructed and an inverse modeling approach was taken to match observed annual recharge depth and temperature with model output. This knowledge was synthesized along with previous understanding of rainfall-runoff processes and subsurface storm flow mechanisms at Maimai to show how specific bedrock properties, as characterized in Chapter 2, control the basic subsurface flow regime that drives the observed seasonal patterns of bedrock groundwater recharge.

This study was submitted in Sept 2017 for potential publication in *Water Resources Research*, and is currently in review: Gabrielli, C.P., McDonnell, J.J., 2017. Geologic and hydroclimatic controls on the seasonality of recharge in a steep, wet headwater catchment. *Water Resources Research*. In review.

Finally, in Chapter 4, I aimed to synthesize my understanding of the control of bedrock properties on the storage-release characteristics of the Maimai and of headwater catchments in general. Many studies have attempted to identify simple terrain-based metrics that capture relationships between headwater characteristics and the MTT of the water they discharge (*McGlynn et al.*, 2003; *McGuire et al.*, 2005; *McNamara et al.*, 2011; *Heidbüchel et al.*, 2013). But while these efforts have been fruitful in some locations, there lacks consistency in relationships from one research location to another and no single metric has been developed that is capable of capturing the variability of streamwater MTT observed between multiple catchments in different geologic settings. Identifying such an index, although simple compared to current complex particle tracking models (*Davies et al.*, 2013) and storage-selection functions (*Rinaldo et al.*, 2015), would present a simple means to identify how the underlying bedrock structure and landscape form controls the mechanisms and time scales over which the landscape redistributes water in the subsurface.

In this final chapter, I explored how catchment topographic characteristics and soil and bedrock permeability contrasts reveal landscape-scale patterns of subsurface water redistribution and how this influences the time scales over which catchments store and release water. I expanded on a previously established metric known as the downslope travel distance (*Jackson et al.*, 2014) to develop a new index that describes the tendency for landscapes to shed water laterally downslope towards the stream channel or to infiltrate water vertically to depth. I conducted a small meta-data analysis and applied the new index to 8 headwater catchments in 4 geologically distinct regions within the Pacific Rim. I tested the hypothesis that landscapes with a greater tendency to shed water laterally would have younger streamwater MTT. The new index was compared to previously established streamwater MTTs for each of the 8 catchments and showed a strong inverse correlation, explaining 77% of the observed variability in MTT across the 8 catchments. This work revealed that a simple index derived from readily available data can capture the complex

interconnected relationship between landscape form, geologic properties and headwater storage-release processes.

This study will be submitted in late 2017 for potential publication in *Water Resources Research* as: Gabrielli, C.P. and McDonnell 2017. A landscape anisotropy index to quantify the relationship between geology, landscape structure and water transit time through catchments. *Water Resources Research*. In prep.

1.3 References

Alexander, R.B., E.W. Boyer, R.A. Smith, G.E. Schwarz and R.B. Moore (2007), The role of headwater streams in downstream water quality, *JAWRA Journal of the American Water Resources Association*, 43(1), 41-59.

Anderson, S.P., W.E. Dietrich, D.R. Montgomery, R. Torres, M.E. Conrad and K. Loague (1997), Subsurface flow paths in a steep, unchanneled catchment., *Water Resour. Res.*, 33(12), 2637-2653. 10.1029/97WR02595.

Asano, Y., T. Uchida, Y. Mimasu and N. Ohte (2009), Spatial patterns of stream solute concentrations in a steep mountainous catchment with a homogeneous landscape, *Water Resour. Res.*, 45(10).

Asano, Y. and T. Uchida (2012), Flow path depth is the main controller of mean base flow transit times in a mountainous catchment, *Water Resour. Res.*, 48(3), W03512. 10.1029/2011WR010906.

Beven, K.J. (2006), *Streamflow generation processes*, IAHS Press.

Binley, A.E.A. (2010), *Hydrogeophysics: Opportunities and challenges*.

Birkel, C., C. Soulsby and D. Tetzlaff (2011), Modelling catchment-scale water storage dynamics: Reconciling dynamic storage with tracer-inferred passive storage, *Hydrol. Processes*, 25(25), 3924-3936. 10.1002/hyp.8201.

Brantley, S.L., M.B. Goldhaber and K.V. Ragnarsdottir (2007), Crossing disciplines and scales to understand the critical zone, *Elements*, 3(5), 307-314.

Brantley, S.L., M.I. Lebedeva, V.N. Balashov, K. Singha, P.L. Sullivan and G. Stinchcomb (2016), Toward a conceptual model relating chemical reaction fronts to water flow paths in hills, *Geomorphology*.

Brooks, J.R., H.R. Barnard, R. Coulombe and J.J. McDonnell (2010), Ecohydrologic separation of water between trees and streams in a mediterranean climate, *Nature Geoscience*, 3(2), 100-104.

Creutzfeldt, B., P.A. Troch, A. Güntner, T.P.A. Ferré, T. Graeff and B. Merz (2014), Storage-discharge relationships at different catchment scales based on local high-precision gravimetry, *Hydrol. Processes*, 28(3), 1465-1475. 10.1002/hyp.9689.

Davies, J., K. Beven, A. Rodhe, L. Nyberg and K. Bishop (2013), Integrated modeling of flow and residence times at the catchment scale with multiple interacting pathways, *Water Resour. Res.*, 49(8), 4738-4750. 10.1002/wrcr.20377.

Doell, P., H. Mueller Schmied, C. Schuh, F.T. Portmann and A. Eicker (2014), Global-scale assessment of groundwater depletion and related groundwater abstractions: Combining hydrological modeling with information from well observations and grace satellites, *Water Resour. Res.*, 50(7), 5698-5720.

Gabrielli, C.P. and J.J. McDonnell (2012), An inexpensive and portable drill rig for bedrock groundwater studies in headwater catchments, *Hydrol. Processes*, 26(4), 622-632. 10.1002/hyp.8212.

Gabrielli, C.P., J.J. McDonnell and W.T. Jarvis (2012), The role of bedrock groundwater in rainfall-runoff response at hillslope and catchment scales, *J. Hydrol.*, 450, 117-133. 10.1016/j.jhydrol.2012.05.023.

Gleeson, T., J. Vandersteen, M.A. Sophocleous, M. Taniguchi, W.M. Alley, D.M. Allen and Y. Zhou (2010), Groundwater sustainability strategies, *Nature Geoscience*, 3(6), 378.

Graham, C.B., R.A. Woods and J.J. McDonnell (2010), Hillslope threshold response to rainfall: (1) a field based forensic approach, *J. Hydrol.*, 393(1-2), 65-76. 10.1016/j.jhydrol.2009.12.015.

Heidbüchel, I., P.A. Troch and S.W. Lyon (2013), Separating physical and meteorological controls of variable transit times in zero-order catchments, *Water Resour. Res.*, 49(11), 7644-7657. 10.1002/2012WR013149.

Hewlett, J.D. and A.R. Hibbert (1967), Forest hydrology. Sopper, W.E. and Lull, H.W. (eds), pp. 275-291, Pergamon Press, New York.

Jackson, C.R., M. Bitew and E. Du (2014), When interflow also percolates: Downslope travel distances and hillslope process zones, *Hydrol. Processes*, 28(7), 3195-3200. 10.1002/hyp.10158.

Jasechko, S., J.W. Kirchner, J.M. Welker and J.J. McDonnell (2016), Substantial proportion of global streamflow less than three months old, *Nature Geosci*, 9(2), 126-129. 10.1038/ngeo2636.

Jones, J.A. and G.E. Grant (1996), Peak flow responses to clear-cutting and roads in small and large basins, western cascades, oregon, *Water Resour. Res.*, 32(4), 959-974.

Katsura, S.Y., K.I. Kosugi, Y. Yamakawa and T. Mizuyama (2014), Field evidence of groundwater ridging in a slope of a granite watershed without the capillary fringe effect, *J. Hydrol.*, 511. 10.1016/j.jhydrol.2014.02.021.

Katsuyama, M., M. Tani and S. Nishimoto (2010), Connection between streamwater mean residence time and bedrock groundwater recharge/discharge dynamics in weathered granite catchments, *Hydrol. Processes*, 24(16), 2287-2299. 10.1002/hyp.7741.

Kirchner, J.W. (2003), A double paradox in catchment hydrology and geochemistry, *Hydrol. Processes*, 17(4), 871-874.

Kirchner, J.W. (2009), Catchments as simple dynamical systems: Catchment characterization, rainfall-runoff modeling, and doing hydrology backward, *Water Resour. Res.*, 45(2), W02429. 10.1029/2008WR006912.

Margat, J. and J. Van Der Gun (2013), *Groundwater around the world: A geographic synopsis*, CRC Press.

Masaoka, N., K.I. Kosugi, Y. Yamakawa and D. Tsutsumi (2016), Processes of bedrock groundwater seepage and their effects on soil water fluxes in a foot slope area, *J. Hydrol.*, 535, 160-172. 10.1016/j.jhydrol.2016.01.081.

Mcdonnell, J.J. (1990), A rationale for old water discharge through macropores in a steep, humid catchment, *Water Resour. Res.*, 26(11), 2821-2832. 0.1029/WR026i011p02821.

Mcglynn, B., J. Mcdonnell, M. Stewart and J. Seibert (2003), On the relationships between catchment scale and streamwater mean residence time, *Hydrol. Processes*, 17(1), 175-181. 10.1002/hyp.5085.

Mcglynn, B.L., J.J. Mcdonnell and D.D. Brammer (2002), A review of the evolving perceptual model of hillslope flowpaths at the maimai catchments, new zealand, *J. Hydrol.*, 257, 1-26. 10.1016/S0022-1694(01)00559-5.

Mcguire, K.J., J.J. Mcdonnell, M. Weiler, C. Kendall, B.L. McGlynn, J.M. Welker and J. Seibert (2005), The role of topography on catchment-scale water residence time, *Water Resour. Res.*, 41(5). 10.1029/2004WR003657.

Mcnamara, J.P., D. Tetzlaff, K. Bishop, C. Soulsby, M. Seyfried, N.E. Peters, B.T. Aulenbach and R. Hooper (2011), Storage as a metric of catchment comparison, *Hydrol. Processes*, 25(21), 3364-3371. 10.1002/hyp.8113.

Millares, A., M.J. Polo and M.A. Losada (2009), The hydrological response of baseflow in fractured mountain areas, *Hydrol. Earth Syst. Sci.*, 13(7), 1261-1271. 10.5194/hess-13-1261-2009.

Montgomery, D.R., W.E. Dietrich, R. Torres, S.P. Anderson, J.T. Heffner and K. Loague (1997), Hydrologic response of a steep, unchanneled valley to natural and applied rainfall, *Water Resour. Res.*, 33(1), 91-109. 10.1029/96WR02985.

Mosley, M.P. (1979), Streamflow generation in a forested watershed, *Water Resour. Res.*, 15, 795-806. 10.1029/WR015i004p00795.

Oda, T., M. Suzuki, T. Egusa and Y. Uchiyama (2013), Effect of bedrock flow on catchment rainfall-runoff characteristics and the water balance in forested catchments in tanzawa mountains, japan, *Hydrol. Processes*, 27(26), 3864-3872. 10.1002/hyp.9497.

Overeem, A., H. Leijnse and R. Uijlenhoet (2013), Country-wide rainfall maps from cellular communication networks, *Proceedings of the National Academy of Sciences*, 110(8), 2741-2745.

Pearce, A.J., M.K. Stewart and M.G. Sklash (1986), Storm runoff generation in humid headwater catchments: 1. Where does the water come from?, *Water Resour. Res.*, 22, 1263-1272. 10.1029/WR022i008p01263.

Pfister, L., N. Martínez-Carreras, C. Hissler, J. Klaus, G.E. Carrer, M.K. Stewart and J.J. McDonnell (2017), Bedrock geology controls on catchment storage, mixing and release: A comparative analysis of 16 nested catchments, *Hydrol. Processes*, 31(10), 1828-1845. 10.1002/hyp.11134.

Rinaldo, A., P. Benettin, C.J. Harman, M. Hrachowitz, K.J. McGuire, Y. Van Der Velde, E. Bertuzzo and G. Botter (2015), Storage selection functions: A coherent framework for quantifying how catchments store and release water and solutes, *Water Resour. Res.*, 51(6), 4840-4847. 10.1002/2015WR017273.

Salve, R., D.M. Rempe and W.E. Dietrich (2012), Rain, rock moisture dynamics, and the rapid response of perched groundwater in weathered, fractured argillite underlying a steep hillslope, *Water Resour. Res.*, 48(11). 10.1029/2012WR012583.

Sayama, T., J.J. McDonnell, A. Dhakal and K. Sullivan (2011), How much water can a watershed store?, *Hydrol. Processes*, 25, 3899-3908. 10.1002/hyp.8288.

Smith, M., K. Cross, M. Paden and P. Laban (2016), Spring – managing groundwater sustainably, *IUCN, Gland, Switzerland*.

Sproles, E., S. Leibowitz, J. Reager, P. Wigington Jr, J. Famiglietti and S. Patil (2015), Grace storage-runoff hystereses reveal the dynamics of regional watersheds, *Hydrol. Earth Syst. Sci.*, 19(7), 3253-3272.

Stewart, M.K. and J.J. McDonnell (1991), Modeling base flow soil water residence times from deuterium concentrations, *Water Resour. Res.*, 27(10), 2681-2693. 10.1029/91WR01569.

Uchida, T. and Y. Asano (2010), Spatial variability in the flowpath of hillslope runoff and streamflow in a meso-scale catchment, *Hydrol. Processes*, 24(16), 2277-2286. 10.1002/hyp.7767.

Welch, L. and D. Allen (2014), Hydraulic conductivity characteristics in mountains and implications for conceptualizing bedrock groundwater flow, *Hydrogeol. J.*, 22(5), 1003-1026.

Wilson, C. and W.E. Dietrich (eds) (1987) The contribution of bedrock groundwater flow to storm runoff and high pore pressure development in hollows, Association of Hydrological Sciences, Wallingford, U.K.

Wilson, J.L. and H. Guan (2004), Mountain-block hydrology and mountain-front recharge, *Water Science and Application*, 9, 113-137. 10.1029/009WSA08.

Winter, T.C. (2007), The role of ground water in generating streamflow in headwater areas and in maintaining base flow, *JAWRA Journal of the American Water Resources Association*, 43(1), 15-25.

Wittenberg, H. (2003), Effects of season and man-made changes on baseflow and flow recession: Case studies, *Hydrol. Processes*, 17(11), 2113-2123.

Woods, R. and L. Rowe (1996), The changing spatial variability of subsurface flow across a hillside, *Journal of Hydrology New Zealand*, 35(1), 51-86.

CHAPTER 2

BEDROCK GROUNDWATER AGE, WATER TABLE DYNAMICS AND TIME-VARYING TRANSIT TIME AT THE MAIMAI WATERSHED

Status: Submitted September 2017

Citation: Gabrielli, C.P., J.J. McDonnell, U. Morgenstern and M. Stewart (2017), Bedrock groundwater age, water table dynamics and time varying transit time at the Maimai watershed

Water Resources Research, In Review.

2.1 Abstract

The influence of bedrock groundwater aquifers on runoff generation processes and their control of time-variant streamwater mean transit time (MTT) in headwater catchments is still not well understood. Here we present new tritium age dating and hydrogeological characterization data from 40 bedrock wells at the intensively-studied Maimai Experimental Watershed in New Zealand. We investigate the extent, dynamics and age of a 4.5 ha headwater aquifer over a 400 day period capturing 70 storm events to identify bedrock controls on aquifer dynamics, the aquifer flow domain and its influence on time varying streamwater MTT. We show that the unfractured low permeability hillslope bedrock hinders deep recharge, thereby regulating groundwater age, streamwater MTT and surface water-groundwater interaction. This establishes a compartmentalized bedrock groundwater storage unit with long turnover times due to minimal groundwater flux; groundwater ages averaged 5.7 years and varied from 0.1 to 23.5 years. Catchment storage is formed by two sharply contrasting and distinct hydrogeological units: shallow young soil storage, and deep much older bedrock groundwater. This storage pairing produces a bimodal seasonal streamwater MTT response where during the 8 month wet season, streamwater MTT was young (mean: 0.44 y) and stable (standard deviation: 0.14 y) due to high antecedent wetness conditions and minimal available soil storage. While during the slightly drier

summer season, streamwater MTT ranged between 0.37 and 2.5 y and was highly dynamic, fluctuating between young event-driven discharge and older baseflow conditions.

2.2 Introduction

Recent increases in computational power have led to stunning new simulations of groundwater contributions to streamflow (*Ebel and Loague, 2006; Maxwell and Condon, 2016*). While these and other simulations are inspiring, much basic process work still needs to be done to age date and understand bedrock groundwater flow processes in the headwaters and to quantify its link to streamflow. Without hard-fought field measurements, we lack the means to ground and support model assumptions and approaches. Basic field-based process work examining groundwater-streamflow interactions in headwater catchments have previously been conducted in the USA (*Frisbee et al., 2011; Salve et al., 2012; Ward et al., 2013*), Europe (*Haria and Shand, 2004; Soulsby et al., 2015*) and Japan (*Kosugi et al., 2011; Iwasaki et al., 2014*). One iconic field site where little direct surface water-groundwater interaction exploration has occurred is the Maimai watershed in New Zealand. This is ironic, as Maimai is often viewed as an exemplar for how steep, wet catchments generate runoff (*Mosley, 1979; Pearce et al., 1986*). The Maimai catchment is known for its flashy and responsive hydrograph, extremely high runoff ratios and young streamwater discharge. For nearly 40 years it has existed as a testing ground for hypothesis testing in hillslope hydrology, revealing insights on the mechanisms and timing of subsurface stormflow (*Mosley, 1979; Pearce et al., 1986; Sklash et al., 1986*), on mixing and effusion of old and new water (*McDonnell, 1990*) and on the spatial and time source components of runoff generation and its control on streamwater chemistry (*McGlynn and McDonnell, 2003; McGlynn et al., 2004*).

The implied simplicity of the hydrologic system combined with the wealth of available long term data has also made the Maimai an effective testbed for model structure development (*Seibert et al., 2003*). This has led to the development of soft data concepts (*Seibert and McDonnell, 2003*), virtual experiments (*Weiler and McDonnell, 2004*), the incorporation of lateral preferential flow networks into hillslope runoff models (*Weiler and McDonnell, 2007*) and the use of streamwater age and tracers in rejectionist catchment modeling (*Vaché and McDonnell, 2006; Sayama and McDonnell, 2009*).

But missing in the lexicon of Maimai hydrology has been an examination of the role of deep bedrock groundwater and its impact on flow and mean transit time of streamwater. Initial water balance studies concluded that the bedrock underlying Maimai was “essentially impermeable” (Pearce *et al.*, 1977), a notion adopted by subsequent studies (O’Loughlin *et al.*, 1978; McDonnell, 1990; McGlynn *et al.*, 2002) and cemented into the evolving perceptual rainfall-runoff model for nearly 40 years (despite no actual testing of the bedrock itself). The Pearce *et al.* (1977) water balance suggested that water loss to the deeper groundwater system was 100 mm/y. Indeed, an extremely young streamflow age (0.4 y (Pearce *et al.*, 1986)), combined with a flashy hydrograph (Mosley, 1979) and high runoff ratios supported a shallow subsurface flow conceptual model. However, possible inconsistencies were reported in the Maimai literature suggesting a more complex subsurface system below the soil mantle. Measured hillslope runoff ratios of only ~13% (Woods and Rowe, 1996) contrasted with a catchment scale runoff ratio of nearly 60% (Pearce *et al.*, 1977) hinting at some loss of subsurface stormflow to the bedrock and potential riparian zone subsidies of water from these deeper hillslope segments.

More recently, bedrock testing at Maimai has revealed bedrock saturated hydraulic conductivities that question initial claims of ‘impermeability’ (Graham *et al.*, 2010), with bedrock groundwater dynamics observed on storm-event time scales (Gabrielli *et al.*, 2012). This has suggested a deeper hydrologically active zone than previously thought. If bedrock groundwater were active and contributing to runoff processes this would imply considerable stores of subsurface water and extended flowpath lengths and transit times, due to the extreme steepness of the topography and the large prism of bedrock storage. Yet Maimai stream water is some of the youngest documented in the isotope hydrology literature with MTT estimates on the order of only 4 months (Pearce *et al.*, 1986). And to date, no direct observation of bedrock groundwater connectivity to the stream has been made. It is clear that despite decades of research, the mechanisms contributing to and controlling the rainfall-runoff response at the Maimai watershed, still remain incomplete.

Here we present new results from an intensive field campaign that combines hydrometric, geochemical and tritium based analyses with groundwater monitoring to characterize the underlying headwater bedrock aquifer and its connection and contribution to streamflow and

streamwater age. We installed 40 wells down to ~9 m with a backpackable drill rig (modified from *Gabrielli and McDonnell (2012)*) and sampled for groundwater tritium concentration. We monitored water table dynamics for 400 days. Except for *Kosugi et al. (2011)*, we believe that this is the highest density of bedrock wells ever drilled in a small headwater research catchment. We use the approach of *Morgenstern et al. (2010)* to translate tritium values into robust water ages and then relate this to the bedrock aquifer flow structure, groundwater dynamics and streamwater silica concentration to determine the controls and connections to the time-varying streamwater transit time. Specifically, we address the following research questions:

- i. What are the permeability characteristics of the underlying bedrock formation?
- ii. What are the spatial and temporal dynamics of bedrock groundwater recharge, discharge and water table position within the catchment?
- iii. How old is bedrock groundwater and how does it vary spatially?
- iv. To what extent is bedrock groundwater connected to the stream and how does this influence time-varying streamwater transit time?

2.3 Study Site

The 280 ha Maimai Experimental Watershed is located on the northwest coast of the South Island, New Zealand in the Tawhai State Forest (Figure 2.1; 42°05'S 171°47'E). This work focused specifically on the 4.5 ha sub-watershed known as M8 (the original site of work by *Mosley (1979)* and *McDonnell (1990)* and subsequent papers). Elevation within M8 ranges from 251 to 348 m.a.s.l. The landscape is highly dissected and dominated by 3 main geomorphic landscape units: highly convergent and divergent hillslopes, steep ephemeral hollows and a gently sloping riparian zone (*Weiler et al., 2003*). Hillslopes are short (< 100 m) and steep (range: 15° to 65°, average: 34°).

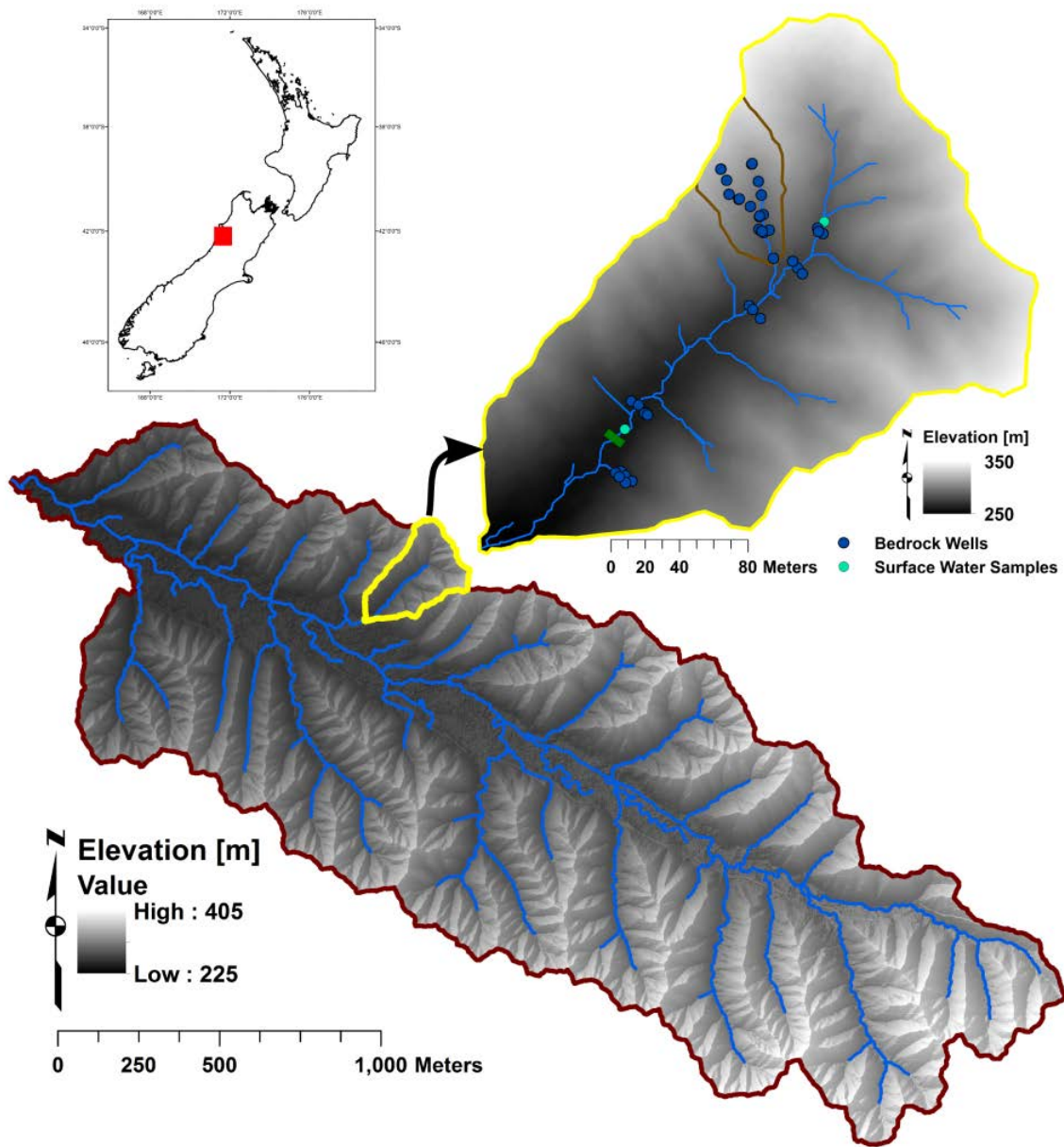


Figure 2.1 Map of the Maimai Experimental Watershed and sub-catchment M8 with vicinity map inlay showing Maimai’s general location within the country of New Zealand. The M8 sub-catchment also shows the location of bedrock wells and the two surface water sampling locations. The green bar shows the location of the M8 weir and is the reference point for watershed area (4.5 ha).

Soils are thin, averaging 0.6 m deep with a range of 0.1 to 1.8 m, and highly transmissive. Infiltration capacity in the top 170 mm humic horizon is as high as 6100 mm/h and average hydraulic conductivity of the upper mineral soil is on the order of 250 mm/h (McDonnell, 1990).

Hillslope soils are characterized as podsolized to mottled yellow-brown earths, while wetter convergent hollows and riparian zones are heavily gleyed (*McKie, 1978*). The bedrock underlying the catchment is a conglomerate known as Old Man Gravel (OMG) belonging to a larger unit known as the Old Man Group (*Bowen, 1967*). The gravel (now a weakly lithified conglomerate) was laid down in the early Pleistocene as a thick (> 400 m) layer of glacial outwash during an erosional sequence in the formation of the Southern Alps (*Mortimer et al., 2001*). The conglomerate is composed primarily of well-rounded sandstone clasts (greywacke) with small additions of schist and granite in a compact sandy-clay matrix. The rounded clasts range in size from 10 to 400 mm in diameter, but are primarily less than 150 mm (*Mortimer et al., 2001*). Over the scale of a few meters the bedrock displays heterogeneity in clast size, however, over 10s to 100s of meters the bedrock is remarkably homogeneous (*Nathan et al., 1986*).

The entire M8 catchment, with the exception of the riparian zone (~ 5% of total area), was cleared of its native southern beech (*Fuscospora spp.*) and podocarp (*Podocarpaceae spp.*) forest in the 1970's and replanted with radiata pine (*pinus radiata*). The replanted forest was unmanaged and has proven susceptible to local fungal attacks and windfall, leading to low stand densities and a thick undergrowth of invasive and native woody and herbaceous species. Rainfall interception losses for the original native vegetation, which is likely similar to the current vegetation cover, were measured by *Pearce and Rowe (1979)* and equal to ~ 670 mm/y or ~ 26% of the 2600 mm gross annual rainfall. Rainfall is spread over ~ 150 rain-days per year with a slight seasonality where drier conditions prevail through mid-summer months (Jan-Mar). Storms are generally characterized by their low-intensity and long duration. Mean rainfall intensity is 1.2 mm/h (*Rowe and Pearce, 1994*), although intensities >30 mm/h have been observed. Single event rainfall totals commonly exceed 100 mm. The catchment's low elevation and proximity to the Tasman Sea result in mild winters. Temperatures remain mostly above freezing, limiting snowfall occurrences to 1 to 2 days per year with melt occurring rapidly within hours to days.

The thin soils, high frequency of storm events and considerable precipitation maintain high soil water content throughout much of the year resulting in a highly responsive rainfall-runoff regime (*Mosley, 1979*). The Maimai has been described as the 'quintessential steep humid catchment'

(*McGlynn et al.*, 2002). Runoff ratios are among the highest of any research catchment in recorded literature. Mean annual runoff is 1550 mm, equal to nearly 60% of annual rainfall, and quickflow, as defined by *Hewlett and Hibbert* (1967), makes up >65% of annual runoff.

2.4 Dataset and methods

2.4.1 Bedrock characterization and well installation

Forty bedrock wells were drilled and completed within the M8 catchment for water table observation and groundwater extraction. Wells were strategically located in key landscape positions to capture the three main hydrologic response units (i.e. hillslopes, hollows and riparian zones) that have been previously identified to control runoff generation at the Maimai (*McGlynn and McDonnell*, 2003b; *Weiler et al.*, 2003). Fifteen wells were installed in hillslope positions, 14 in riparian and toe-slope positions, and 11 within the gut of a previously studied ephemeral hollow (*McDonnell*, 1990; *Mosley*, 1979) (Figure 2.1).

Bedrock wells were installed using a modified version of the portable bedrock drilling system described by *Gabrielli and McDonnell* (2012). Bores were drilled to a diameter of 63 mm and to varying depths depending on water table location (see Tables 2.1a and 2.1b for details). PVC casing (25.4 mm inner diameter) was installed down the length of each bore and screened across the lower interval. Screened length was between 0.3 and 1.0 m, dependent on the completed depth into bedrock. We backfilled the well annulus with clean sand to a position 0.15 m above the top of the screened section and a bentonite slurry filled the remainder of the bore length to the soil surface. In locations where soil depth was greater than 0.15 m, a soil well was co-located with each bedrock well. Soil wells were completed to the depth of the soil bedrock interface, screened across the lower 0.15 – 0.3 m dependent on soil depth, and backfilled in a manner similar to the bedrock bores.

Bedrock saturated hydraulic conductivity (Ksat) was determined in the field through falling head slug tests in each of the 40 bedrock bores. Slug tests were conducted by introducing a small volume of water instantaneously into the bore and monitoring the return of the water table to its

initial depth. Slug test data was analyzed by implementing the Hvorslev method (*Hvorslev*, 1951) within the Aqtesolv software package. Tests were performed 1-3 times and in locations where more than one slug test was conducted the average value was calculated. Individual well values are reported, as well as geometric mean of wells in similar landscape units.

Bedrock porosity was measured from bedrock samples ($\sim 0.04 \text{ m}^3$) cut from the surface of the intact bedrock formation using a concrete cutting chainsaw (Stihl GS 461). Samples were transported to the University of Saskatchewan where porosity was determined using a water-displacement method. A sample was slowly saturated from the bottom up to reduce pore-space air entrapment and left submerged for 20 days. Saturated mass was measured and the sample was oven dried at 60° C until recursive weight measurements showed no additional mass loss, establishing the oven dry mass. Mass difference between saturated and oven-dry states was converted to water volume, which is presumed equal to bedrock pore space, and this value was divided by total sample volume to calculate porosity.

2.4.2 Hydrometric data and bedrock groundwater dynamics and flux

Hydrometric data was collected for streamflow, precipitation, and soil and bedrock water table position from Dec 11, 2014 to Jan 31, 2016, representing 416 days of monitoring. Streamflow was measured at the M8 catchment outlet at 10 minute intervals using a 90° V-notch. Stage height was converted into specific discharge using a standard rating curve for 90° sharp crested v-notch weirs (*Rantz*, 1982). Rainfall was recorded using a 0.2 mm tipping bucket rain gauge located within the M8 catchment 20 m downstream of the main weir in a small forest clearing (Figure 2.1).

Soil and bedrock wells were instrumented with absolute pressure transducers (OnSet Loggers© or Heron Instrument©) or capacitance rods (Tru-Track© or Odyssey Instruments©) to record water table location and dynamics in each well at 10 minute intervals. Two dedicated pressure transducers were located within a research hut 100 m from the M8 outlet to record barometric pressure in order to correct absolute pressure readings from the deployed pressure transducers. Tru-Track© and Odyssey© capacitance rods had a blanking distance of 75 mm and 35 mm,

respectively, which prevented the observation of saturated conditions below these lower ranges for soil and bedrock wells instrumented with this equipment.

We used basic metrics to quantify the spatial and temporal patterns of event-based and seasonal water table fluctuations for each bedrock well, and identified average values for wells clustered within similar landscape units. We calculated storm response, defined as millimeters of water table displacement per millimeter of rainfall for each storm event. We also calculated a storm transmissivity change metric, equal to the change in water table depth multiplied by local bedrock hydraulic conductivity, where the change in depth was defined as the difference in water table elevation between pre-storm and storm-peak levels. This value allows for a more consistent comparison of water table dynamics between wells in different landscape units by accounting for the effect of spatially varying hydraulic conductivity. Higher values of transmissivity change are associated with greater groundwater flux. Additionally, Spearman Rank Correlation Coefficient (Rho), a nonparametric measure of statistical dependence between two variables, was used to test the relationship between water table fluctuations and catchment discharge.

Potentiometric surface was used to calculate vertical head gradients between each co-located soil and bedrock well, establishing general spatial and temporal trends of vertical bedrock groundwater movement across the catchment. Analyses were conducted using a conditional interpretation where gradients were categorized as vertically upward or vertically downward. Due to data uncertainty in some well location surveys and water table records, we additionally identified gradients as hydrostatic if differences in potentiometric surfaces were ± 20 mm.

2.4.3 Transit time analysis

Tritium (^3H) based MTT estimates were conducted on water samples collected during a synoptic sampling campaign during a low-flow period on Feb 24, 2015. Two surface water, 3 soil water and 23 bedrock groundwater samples were taken from locations within M8. MTT estimates were determined by employing a lumped parameter convolution approach as outlined in *Morgenstern and Taylor (2009)*:

$$C_{out}(t) = \int_0^{\infty} g(\tau)C_{in}(t - \tau)e^{-\lambda\tau} d\tau$$

where $C_{out}(t)$ is the ^3H concentration of individual samples at time t , $g(\tau)$ is the transit time distribution, C_{in} is the ^3H concentration of precipitation into the system, and $e^{-\lambda\tau}$ is the radioactive decay term to account for the natural decay of the tritium isotope, where the decay constant $\lambda = \ln(2/T_{1/2})$ and $T_{1/2} = 12.32$ years for ^3H . C_{in} was determined from long-term monthly tritium measurements made at the Kaitoke reference station near Wellington, New Zealand, approximately 150 km north of Maimai. We scaled rainfall input at Maimai by a factor of 1.15 based on a standard latitude adjustment and verified this scaling factor with tritium measurements taken from 2 aggregated rainfall samples collected over a 10-month period at the outlet and upper elevations of the larger Maimai watershed that M8 is located within.

Tritium concentrations, used to define C_{out} , were analyzed by the GNS Science Water Dating Laboratory (Lower Hutt, New Zealand) using electrolytic enrichment and liquid scintillation counting (*Morgenstern and Taylor, 2009*). Recent advancements in this method have led to further tritium enrichment that is now >90-fold, leading to a lower detection limit of 0.02 Tritium Units (TU). Calibration of the tritium enrichment for each individual sample via deuterium enrichment allows for a reproducibility of the tritium enrichment of better than 1%. The decay of tritium that remains in the New Zealand hydrologic system to levels below pre 1950 atomic bomb testing levels results in MTT estimates that are relatively insensitive to the model choice (i.e. $g(\tau)$) when estimating the transit time distribution of the studied flow system – meaning model choice is no longer critical for accurate and unambiguous MTT estimates (*Morgenstern et al., 2010*). We used a uniform exponential piston flow model with 70% exponential flow within the total flow volume – found to be a reasonable ratio by *Morgenstern et al. (2010)* – to estimate $g(t)$ as follows (*Maloszewski and Zuber, 1982*):

$$g(\tau) = 0 \quad \text{for } \tau < \tau_m(1 - f) \quad (\text{Eq. 2.2})$$

$$g(\tau) = (f\tau_m)^{-1} \exp\left[-\left(\frac{\tau}{f\tau_m}\right) + \left(\frac{1}{f}\right) - 1\right] \quad \text{for } \tau \geq \tau_m(1 - f) \quad (\text{Eq. 2.3})$$

Where f represents the ratio of the exponential flow volume to total flow volume, and τ_m is the MTT in years. We recognize that by convention, the age value of groundwater sampled from wells is referred to as “groundwater age” or “mean residence time” and reflects the mean elapsed time from when the water molecules entered the groundwater body to when they discharged from the system, in our case, when sampled from the wells (Kazemi *et al.*, 2006).

2.4.4 Silica analysis and catchment MTT

To estimate time-varying streamwater transit time of catchment M8 discharge we followed an approach similar to Peters *et al.* (2014) where an empirically derived relationship between groundwater silica concentration, tritium-based MTT and streamwater silica concentrations is used to estimate streamwater MTT. Dissolution from water-rock interactions tends to increase groundwater silica concentrations with increased subsurface contact time (Edmunds and Smedley, 2000; Burns *et al.*, 2003; Katz *et al.*, 2004; Stewart *et al.*, 2007), allowing silica to be used as a proxy for MTT. We established two regression relationships; one between catchment discharge volume and catchment discharge silica concentration, and a second between silica concentration in soil and bedrock water samples and tritium-based MTT measured in those sampling locations. The discharge-silica relationship was developed from grab samples collected during a moderate sized storm event from the M8 catchment outlet at intervals which captured pre-event, event and recession conditions. Water samples were collected in 250 mL HDPE bottles, filtered using 0.45 μm cellulose acetate syringe filters and refrigerated within 24 hours of sampling. Analysis was conducted at the Oregon State University Collaboratory using an ion chromatograph (Dionex ICS-1500). We applied the discharge-silica regression model to a time series of catchment runoff to produce an estimated streamwater silica concentration at 10 minute intervals for 1 year (Dec 25, 2015 to Dec 24, 2016). We then applied the silica-MTT regression model to the silica time series to estimate streamwater MTT over the same period. This produced a 1-year time series of streamwater MTT covering more than 60 storm events through seasonal shifts in catchment wetness conditions and water balance.

We estimated silica concentrations using a discharge value equal to the flow condition under which tritium samples were collected. The resulting silica concentration was applied to the silica-MTT

regression model and an estimated MTT was calculated. Both estimated silica and MTT values were compared to measured silica and tritium based streamwater MTT values in our grab samples as a means to test the validity of the two regression models.

2.5 Results

2.5.1 Bedrock characterization

Laboratory based porosity measurements of bedrock samples taken from the upper 1 m of bedrock had an average value of 0.21 (n = 3, standard deviation = 0.03), and fall within the range of established porosities for sandstone (*Freeze and Cherry, 1979*).

Variability in Ksat for all bedrock wells spanned 5 orders of magnitude from 5.42E-9 m/s to 6.99E-5 m/s (Table 2.1a and 2.1b). Slug tests revealed spatial patterns broadly following geomorphic landscape units. The geometric mean hydraulic conductivity increased from hillslopes to hollows to the riparian zone with mean values each of 1.7E-08 m/s, 1.2E-07 m/s and 4.9E-06 m/s, respectively. The increase in conductivity with increasing upslope accumulated area may indicate that wetter zones with greater upslope area undergo greater mineral weathering resulting in more permeable bedrock.

2.5.2 Bedrock groundwater position

Tables 2.1a and 2.1b show the average depth to water table for bedrock wells within the M8 catchment. Bedrock groundwater was present in the majority of wells over the entire study period; however, during an unusually dry period between Dec 2014 and February 2015, water tables dropped below well screens in some riparian and ephemeral hollow locations. We note that January, 2015 was the single driest month in 55 years of record at the Reefton meteorological station 5 km southeast of Maimai.

Table 2.1a Bedrock well characteristics: position within the landscape, physical characteristics, associated bedrock characteristics and water table dynamics.

Bedrock Well	Landscape Unit ^a	Total Depth, m	Depth into bedrock, m	Screen length, m	Distance to Stream, m	TWI	Mean Ksat ± 1 SD, m/s	Mean landscape Mean depth to Water table			Transmissivity, m ² /s	
								unit Ksat, m/s (±SD)	Water Table, m	fluctuation range, m		sensitivity, mm/mm
1	Hillslope	7.00	7.00	-	15.2	6.1	1.31E-08	6.89 ± 0.23	0.85	1.3 ± 2.3	0.65	1.8E-01
2	Hillslope	3.95	3.95	-	9.0	2.9	1.31E-08	3.54 ± 0.11	0.52	1.4 ± 1.2	0.60	5.0E-04
3	Hillslope	7.14	7.14	-	12.3	3	6.9E-09	-	-	-	-	-
4	Hillslope	1.51	1.51	0.5	5.8	2.2	2.48E-07 ± 2.25E-07	0.75 ± 0.16	0.81	4.7 ± 5.0	0.66	2.6E-02
5	Hillslope	4.46	4.46	1.0	5.6	2.2	1.60E-08 ± 7.62E-09	3.89 ± 0.16	0.85	3.9 ± 1.9	0.60	6.0E-04
6	Hillslope	3.86	3.16	0.5	14.5	3.6	7.18E-09 ± 3.52E-09	1.7E-8	-	-	-	-
7	Hillslope	6.33	5.67	1.0	14.4	3.6	2.77E-08 ± 1.65E-08	-	-	-	-	-
8	Hillslope	6.49	5.69	1.0	26.8	5	1.50E-08 ± 4.56E-09	4.12 ± 0.11	0.45	1.6 ± 0.9	0.57	6.0E-04
9	Hillslope	5.57	4.15	1.0	35.3	4.6	2.97E-08 ± 1.43E-08	4.22 ± 0.14	0.71	2.0 ± 1.4	0.41	1.4E-03
10	Hillslope	8.80	7.49	1.0	35.1	4.6	6.26E-09 ± 3.22E-09	7.65 ± 0.09	0.36	1.0 ± 0.7	-0.30	2.0E-04
11	Hillslope	8.03	7.55	1.0	40.8	1.4	1.18E-08 ± 1.48E-09	6.19 ± 0.08	0.4	1.7 ± 1.3	0.20	4.0E-04
12	Hillslope	7.54	7.04	1.0	49.9	2.6	2.72E-07 ± 1.92E-07	6.84 ± 0.03	0.14	1.1 ± 0.8	0.71	5.1E-03
13	Hollow	1.49	0.94	0.3	0.8	9.1	4.00E-06 ± 1.97E-06	0.3 ± 0.18	0.91	6.0 ± 7.1	0.81	5.0E-01
14	Hollow	3.94	3.94	1.0	8.2	2.8	5.42E-09 ± 3.43E-09	3.55 ± 0.03	1.12	4.5 ± 7.3	0.56	2.0E-04
15	Hollow	1.50	0.93	0.5	0.4	8.3	9.04E-08 ± 4.84E-08	0.52 ± 0.12	0.71	4.31 ± 5.1	0.76	9.7E-03
16	Hollow	1.42	0.82	0.5	1.4	5.5	1.38E-06 ± 6.91E-07	0.88 ± 0.08	0.42	3.6 ± 3.3	0.56	7.4E-02
17	Hollow	2.73	2.28	0.5	1.7	5.5	6.75E-07 ± 4.64E-07	1.67 ± 0.06	0.38	2.8 ± 2.5	0.71	3.5E-02
18	Hollow	2.81	2.15	0.5	4.2	3.4	4.42E-08 ± 1.77E-08	1.86 ± 0.14	0.78	2.6 ± 1.6	0.54	3.1E-03
19	Hollow	1.49	0.99	0.5	0.6	6.9	1.68E-08 ± 9.48E-10	1.15 ± 0.09	0.5	2.9 ± 5.3	0.25	1.1E-03
20	Hollow	1.80	1.68	0.5	1.4	7.9	5.81E-09 ± 6.41E-10	0.9 ± 0.09	0.52	1.4 ± 0.9	0.18	2.0E-04
21	Hollow	1.22	1.07	0.5	0.1	7.3	3.13E-08	0.47 ± 0.06	0.36	1.3 ± 1.2	0.85	1.3E-03
22	Hollow	2.25	1.36	0.5	14.3	3.7	7.65E-07	-	-	-	-	-
23	Hollow	6.02	5.11	1.0	14.3	3.7	4.84E-07 ± 3.14E-07	4.55 ± 0.05	0.38	2.9 ± 1.9	0.86	2.9E-02

^aLandscape positions classified as Riparian/Hill indicate wells located on hillslopes but drilled to a depth such that the screened interval is equal to or deeper than the ground surface of the local riparian zone.

Table 2.1b Bedrock well characteristics: position within the landscape, physical characteristics, associated bedrock characteristics and water table dynamics.

Bedrock Well	Landscape Unit ^a	Total Depth, m	Depth into bedrock, m	Screen length, m	Distance to Stream, m	TWI	Mean Ksat \pm 1 SD, m/s	Landscape unit geometric mean Ksat	Mean depth to Water table Water Table, fluctuation range, m	Water table sensitivity, mm/mm	Spearman Rank (Rho)	Transmissivity, m ² /s
24	Riparian	4.01	2.27	1.0	9.8	4.3	3.50E-05		1.57 \pm 0.05	3.6 \pm 2.5	0.69	2.9E+00
25	Riparian	2.79	0.81	0.3	8.7	5.1	1.09E-05 \pm 5.22E-06		1.33 \pm 0.1	3.3 \pm 2.0	0.95	1.1E+00
26	Riparian	1.90	0.95	0.3	0.6	13.2	2.59E-05 \pm 2.27E-05		0.41 \pm 0.13	6.3 \pm 4.9	0.43	4.1E+00
27	Riparian	0.75	0.54	0.3	0.2	11.1	1.87E-05 \pm 1.14E-05		0.26 \pm 0.06	2.6 \pm 2.7	0.87	1.3E+00
28	Riparian	2.05	1.63	0.5	3.3	3.7	6.98E-06 \pm 2.29E-06		1.27 \pm 0.09	4.2 \pm 2.6	0.93	5.9E-01
29	Riparian	1.87	0.93	0.5	1.8	8.6	5.66E-06 \pm 6.03E-07		0.55 \pm 0.12	5.1 \pm 5.5	0.46	8.1E-01
30	Riparian	4.00	3.62	1.0	4.6	5.6	1.93E-06 \pm 2.08E-07		2.38 \pm 0.15	6.2 \pm 3.7	0.78	1.8E-01
31	Riparian	1.33	1.25	0.5	6.0	3.9	1.02E-06 \pm 5.15E-07	4.9E-6	0.98 \pm 0.09	2.3 \pm 1.4	0.92	6.3E-02
32	Riparian	1.69	1.35	0.5	1.2	7.4	7.01E-07 \pm 1.46E-07		0.47 \pm 0.05	3.1 \pm 1.8	0.83	5.2E-02
33	Riparian	2.06	0.97	0.5	3.7	5.6	1.40E-06 \pm 9.88E-07		1.06 \pm 0.07	3.6 \pm 2.6	0.65	6.1E-02
34	Riparian/Hill	5.60	5.60	-	6.5	7.1	6.99E-05		3.3 \pm 0.06	1.5 \pm 0.6	0.82	3.5E+00
35	Riparian/Hill	5.87	5.87	-	8.9	7.1	6.22E-06		5.68 \pm 0.08	1.7 \pm 1.3	0.74	1.5E+00
36	Riparian/Hill	3.34	3.34	-	5.0	5.4	2.38E-05		1.42 \pm 0.04	1.6 \pm 0.8	0.50	2.0E-04
37	Riparian/Hill	3.01	1.64	0.5	10.3	5.8	3.31E-06 \pm 2.29E-06		2.05 \pm 0.04	0.9 \pm 0.6	0.61	8.8E-02
38	Riparian/Hill	3.36	1.44	0.5	7.5	5.2	2.48E-07 \pm 2.75E-08		2.56 \pm 0.22	6.0 \pm 6.2	0.54	5.0E-02
39	Riparian/Hill	4.19	4.07	1.0	10.1	0.9	9.02E-06 \pm 3.56E-06		3.34 \pm 0.14	2.8 \pm 2.6	0.63	4.2E-01
40	Riparian/Hill	5.08	3.85	1.0	7.1	3.2	4.98E-07 \pm 1.18E-07		3.5 \pm 0.23	4.0 \pm 2.2	0.79	3.2E-02

^aLandscape positions classified as Riparian/Hill indicate wells located on hillslopes but drilled to a depth such that the screened interval is equal to or deeper than the ground surface of the local riparian zone.

Water table depths ranged from 0.26 to 7.65 m below the ground surface. Generally, the water table was shallower in the riparian zone and at the center of the hillslope hollows and deeper in toe-slope and upper hillslope positions. We fit a relation between depth to water table and distance to stream channel with a power-law regression ($R^2 = 0.72$) and applied this to a 1 m grid DEM of M8 to produce a catchment scale water table map (Figure 2.2). Figure 2.2 shows the shallow water table in topographically convergent areas and a rapid deepening of the water table with distance from the stream channel. Estimated depth to water table ranged from 0.98 m in the near-stream riparian corridor to approximately 10.5 m at ridgeline. Mean, median and standard deviation of depth to water table over the entire catchment domain was 5.25 m, 5.43 m and 2.03 m, respectively.

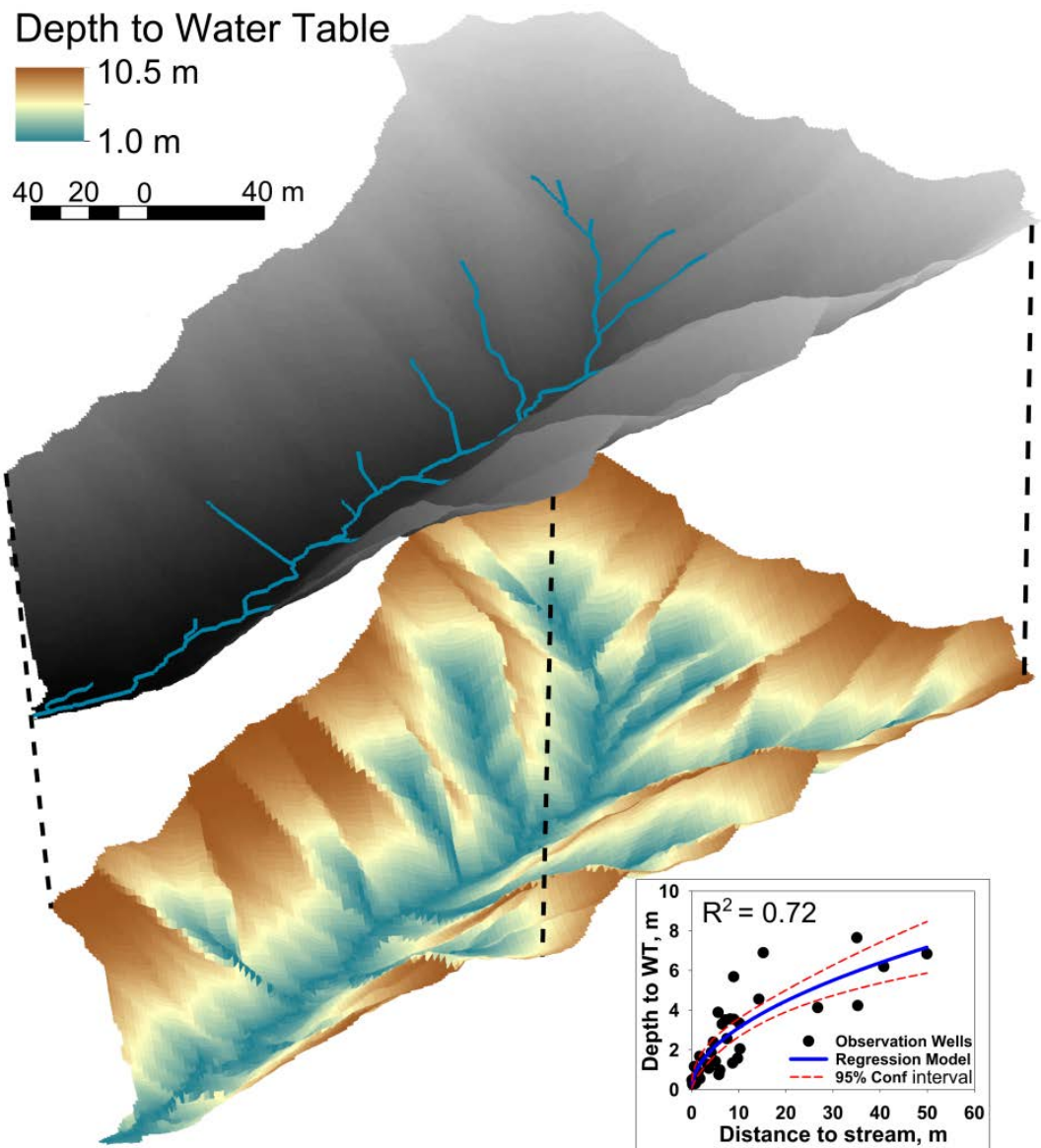


Figure 2.2 Depth to water table for the underlying headwater bedrock aquifer based on average water table depths over 400 days from 36 monitored bedrock wells. Depth to water table is overlaid on the 3-dimensional representation of the bedrock aquifer free-water surface. The M8 3-dimensional DEM is included above the water table layer for visual comparison. The inset scatter plot shows the relationship between distance to stream and depth to water table ($R^2 = 0.72$).

2.5.3 Bedrock groundwater dynamics

A representative example of water table dynamics for each of the three main landscape positions is shown in Figure 2.3. Although there was variability within each landscape position, event based water table fluctuations, seasonal fluctuations, storm response and transmissivity change metrics all captured consistent trends delineating the three landscape units. Generally, lower-lying areas had greater range and variability, while dynamics became more attenuated with distance from the stream channel.

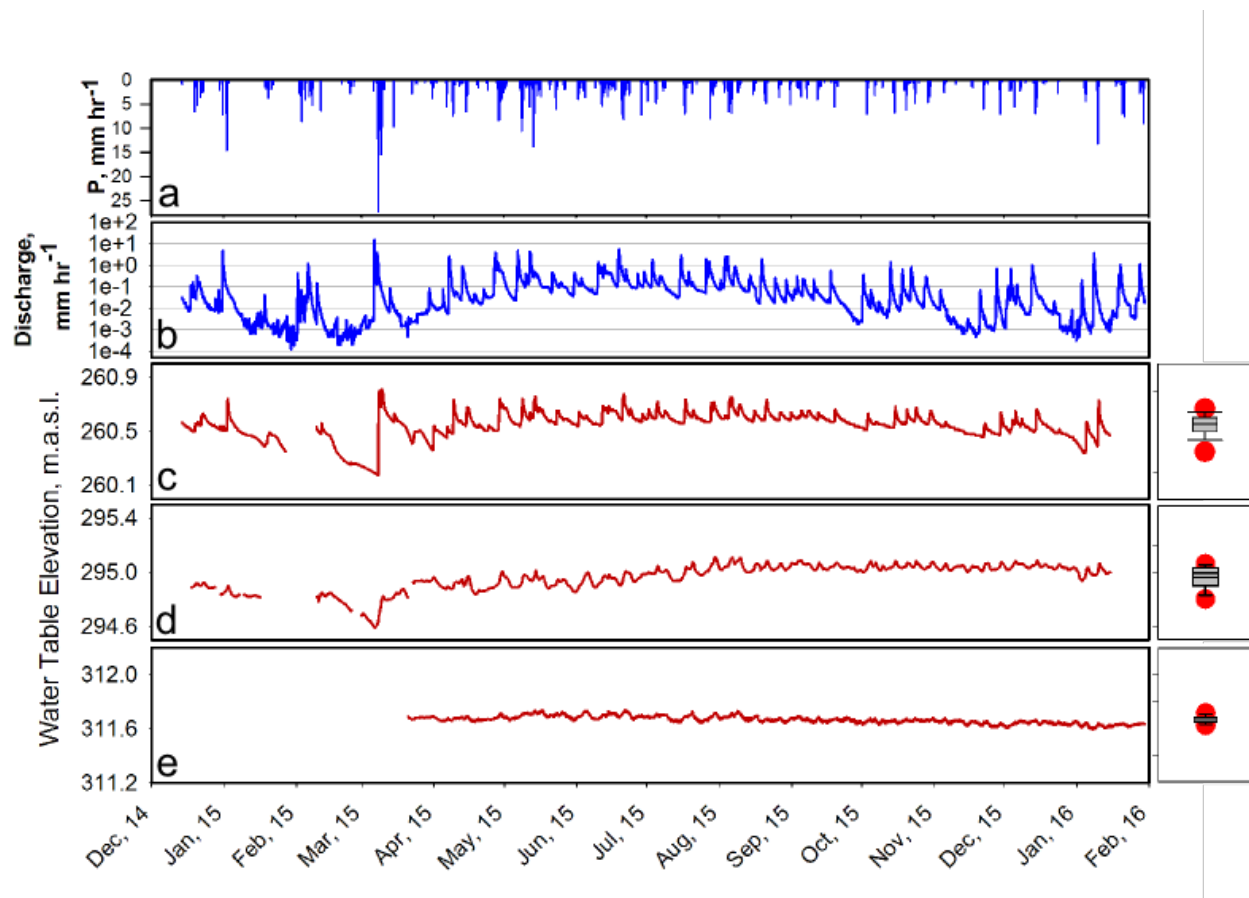


Figure 2.3 Water table elevation data from a representative riparian (c), hollow (d), and hillslope (e) well, with corresponding rainfall (a) and runoff (b) time series. Box and whisker plots show median, and 1st and 3rd quartiles of the water table dynamics for each of the 3 landscape positions.

Seasonally, maximum water table fluctuation for all wells over the monitoring period ranged from 0.14 to 1.36 m. The greatest range in seasonal water table fluctuations was found in the shallower riparian and toe-slope zones. Seasonal fluctuations decreased in wells located in the center of hollows and decreased further in the upper hillslope positions (i.e. wells 8, 9, 11, 12). Upper hillslope wells displayed almost no seasonal fluctuations, with the most near-ridge well (well 12) fluctuating only 0.14 m cm during the study period, which included one of the driest periods on record.

Average event-based water table response (measured as mm change in water table per mm of rainfall) for each well over the 70 monitored storm events is presented in Table 2.1a and 2.1b. Spatially averaged response was 3.9 mm/mm, 3.23 mm/mm and 1.96 mm/mm for riparian, hollow and hillslope locations, respectively. Water table response and transmissivity change captured similar spatial trends to those observed for average event-based and seasonal water table fluctuations, generally indicating greater damping with distance from the stream channel (Tables 2.1a & 2.1b). Mean bedrock transmissivities increased progressively from hillslope to hollow to riparian zone by an order of magnitude for each landscape unit (3.76×10^{-8} , 4.79×10^{-7} , $5.35 \times 10^{-6} \text{ m}^2\text{s}^{-1}$, respectively).

Spearman rank correlation coefficients for each well are shown in Tables 2.1a and 2.1b. Values decreased from the riparian zone to hollow to hillslope. Riparian zone wells were extremely responsive to precipitation inputs with rapid water table rises and recessions in phase with the storm hydrograph ($\text{Rho} = 0.71$). Ephemeral hollow wells responded to individual storm events but were slightly more delayed and attenuated than the riparian zone ($\text{Rho} = 0.61$), while hillslope wells showed an even more attenuated storm response. Water table rise and fall was not always attributable to specific storm events ($\text{Rho} = 0.52$) (Figure 2.3).

2.5.4 Bedrock groundwater gradients

Vertical hydraulic head gradients were measured at 19 soil and bedrock well pairs and between 3 pairs of vertically nested bedrock wells. Figure 2.4 shows a subset of the 416 day time series (data

logger failure prevents full display—however, trends in the overall data do not deviate significantly from the subset).

Groundwater gradients across the catchment were predominantly downward in all landscape positions indicating that the catchment is continuously recharging surface and soil water into the bedrock groundwater aquifer. Hillslope gradient calculations were sporadic based on the transient nature of saturated hillslope soils which occurred only during high antecedent conditions or during larger storm events. Within the ephemeral hollow, soil-bedrock well pairs showed consistent downward gradients across all wetness conditions and storm intensities, with the exception of the most downslope well pair (well 13 and associated soil well). Transient flow reversals occurred during storm event peaks under high antecedent conditions, resulting in hydrostatic conditions or upward groundwater gradients at the base of the hollow.

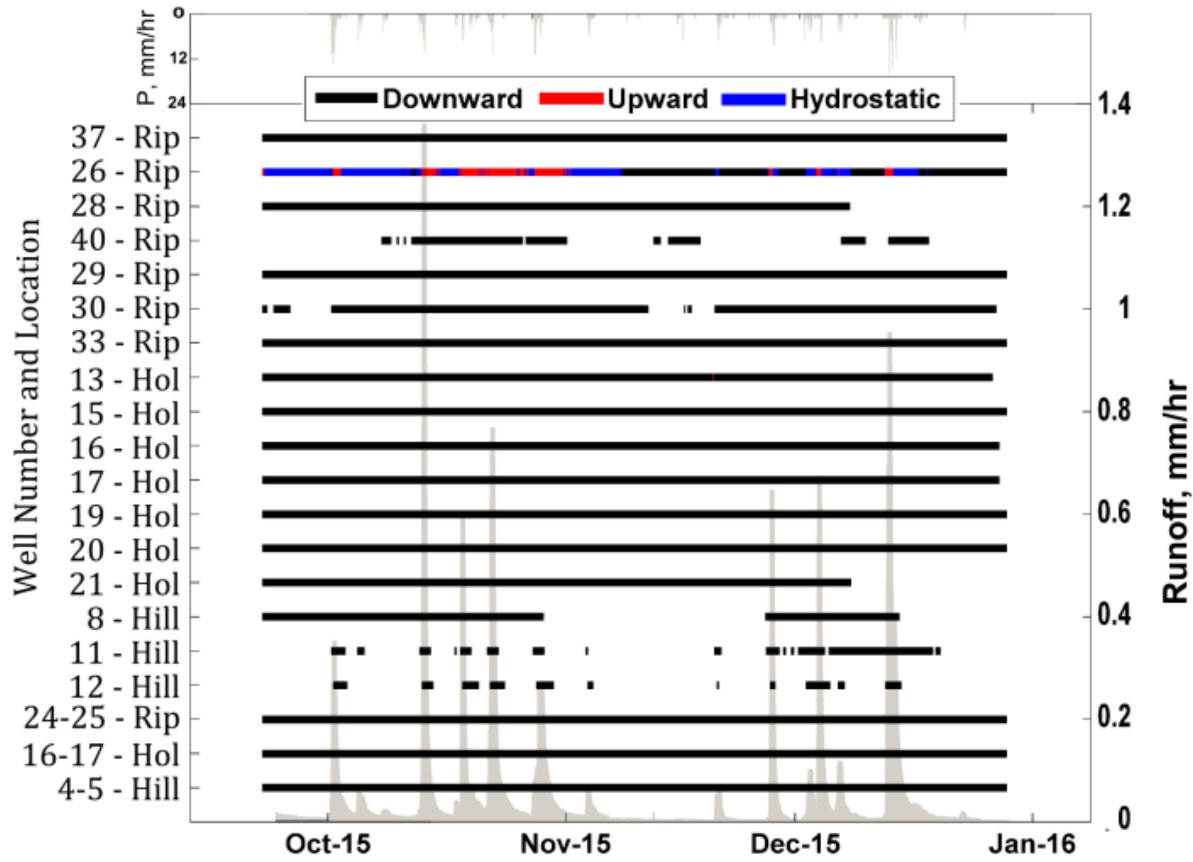


Figure 2.4 Vertical groundwater gradients between nested soil-bedrock wells (shown by a single well number on the y-axis) and nested bedrock-bedrock wells (shown as two well numbers on the y-axis). Colored horizontal bars represent gradient direction. The white space within horizontal bars is indicative of dry periods when no soil-water was present in the wells, thus no gradient was calculated. The exception to this is the late periods wells 28 and 21 which were missing data due to instrument failure. Additionally, rainfall and runoff data are displayed for the corresponding time period.

Riparian corridor groundwater flux was also consistently downward through the duration of the observation period for all well pairs under both low and high antecedent conditions and during inter and intra storm periods. The exception to this trend was the most downstream well pair (well 26 and associated soil well) located 15 m upstream from the M8 weir. Under high antecedent conditions the hydraulic gradient remained hydrostatic between storm events and briefly switched upwards during rainfall periods. Under lower antecedent conditions gradients also switched to upward (or hydrostatic) during rainfall events, but remained downward between events. Under extremely dry conditions (not shown in Figure 2.4) upward gradients prevailed, indicating bedrock

groundwater subsidies to baseflow (as discussed below). For this well pair (well 26), gradients were upward, hydrostatic and downward for 27%, 26% and 47% of the monitoring period.

2.5.5 Tritium measurements and MTT

A synoptic sampling of 30 locations on Feb 24, 2015 within the M8 catchment produced tritium-based age estimates for 2 surface water samples, 3 soil water samples and 23 bedrock groundwater samples. The catchment was under extremely low baseflow conditions with a 30 day antecedent precipitation index (API) value of 25.2 mm, and a catchment discharge of 0.00075 mm/h corresponding to a flow exceedance probability of 99%. Table 2.2 presents tritium concentrations and estimated MTT for each sampling location. MTT from all bedrock wells averaged 5.3 ± 7.5 years and ranged from less than 0.1 to 23 years (>2.50 to 0.97 TU, respectively). The three soil water samples taken from hillslope, toe-slope and riparian positions had MTT values less than 0.5 years. Soil water sample 43, collected from a perennial soil seep within the instrumented hollow, was the youngest of all waters tested with a value of >2.50 TU. This was similar in concentration to recent precipitation, indicating extremely short travel times. Sample 42 from the most upstream portion of the riparian zone had a value of 2.15 TU, corresponding to an MTT of 0.3 years, and identical to the MTT for surface water collected in the same location (sample 44). Soil water sample 41, collected from a perennially saturated soil well at the base of a short planer hillslope near the catchment outlet, had a tritium concentration of 2.05 TU, corresponding to an MTT of 0.5 years.

Table 2.2 Tritium units and corresponding MTT for sampled bedrock, soil and streamwater samples within the M8 catchment. Samples 41, 42 and 43 are soil wells, sample 44 is a stream sample from the same catchment location as soil well 42, and sample 45 is from the main M8 weir.

Well/sample name	Landscape position	Tritium Units, TU	± 1 SD, TU	MTT, y
8	Hillslope	1.38	0.03	10.5
12	Hillslope	1.65	0.04	6.5
13	Hollow	2.11	0.04	0.3
16	Hollow	2.14	0.04	0.3
17	Hollow	2.01	0.04	0.3
21	Hollow	1.87	0.04	1.3
23	Hollow	1.73	0.03	5.3
24	Riparian	1.24	0.03	13.5
25	Riparian	1.85	0.03	2.5
26	Riparian	1.98	0.03	0.7
27	Riparian	2.10	0.04	0.3
28	Riparian	2.17	0.04	0.3
29	Riparian	2.05	0.04	0.3
30	Riparian	2.06	0.03	0.3
32	Riparian	2.13	0.04	0.3
33	Riparian	2.18	0.05	0.3
34	Riparian/Hill	0.97	0.02	23
35	Riparian/Hill	1.01	0.03	22
36	Riparian/Hill	1.02	0.02	22
37	Riparian/Hill	1.72	0.03	5.5
38	Riparian/Hill	2.16	0.04	0.3
39	Riparian/Hill	1.72	0.03	5.3
40	Riparian/Hill	2.17	0.04	0.3
41	Riparian/Hill - Soil	2.05	0.04	0.5
42	Riparian - Soil	2.15	0.04	0.3
43	Hollow - Soil	2.50	0.05	0.1
44	Stream – Upper Riparian	1.85	0.03	0.3
45	Stream - Weir	2.11	0.04	2.5

Bedrock groundwater within M8 ranged in tritium concentration from 2.18 to 0.97 TU (MTT 0.3 to 23 y, respectively) indicating that the water in the underlying aquifer includes a wide range of ages representing heterogeneous flowpaths (Figure 2.5). The bedrock groundwater MTT varied both spatially and with depth, revealing complex spatial patterns associated with the groundwater flow structure. MTT showed a weak linear relationship ($R^2 = 0.32$) with well depth. All

groundwater samples older than 2.5 years were found at depths greater than 2.8 m, while the youngest waters were found predominantly in shallower wells. No significant correlation was found between groundwater MTT and depth to water table, upslope accumulated area or the topographic wetness index (*Beven and Kirkby, 1979*).

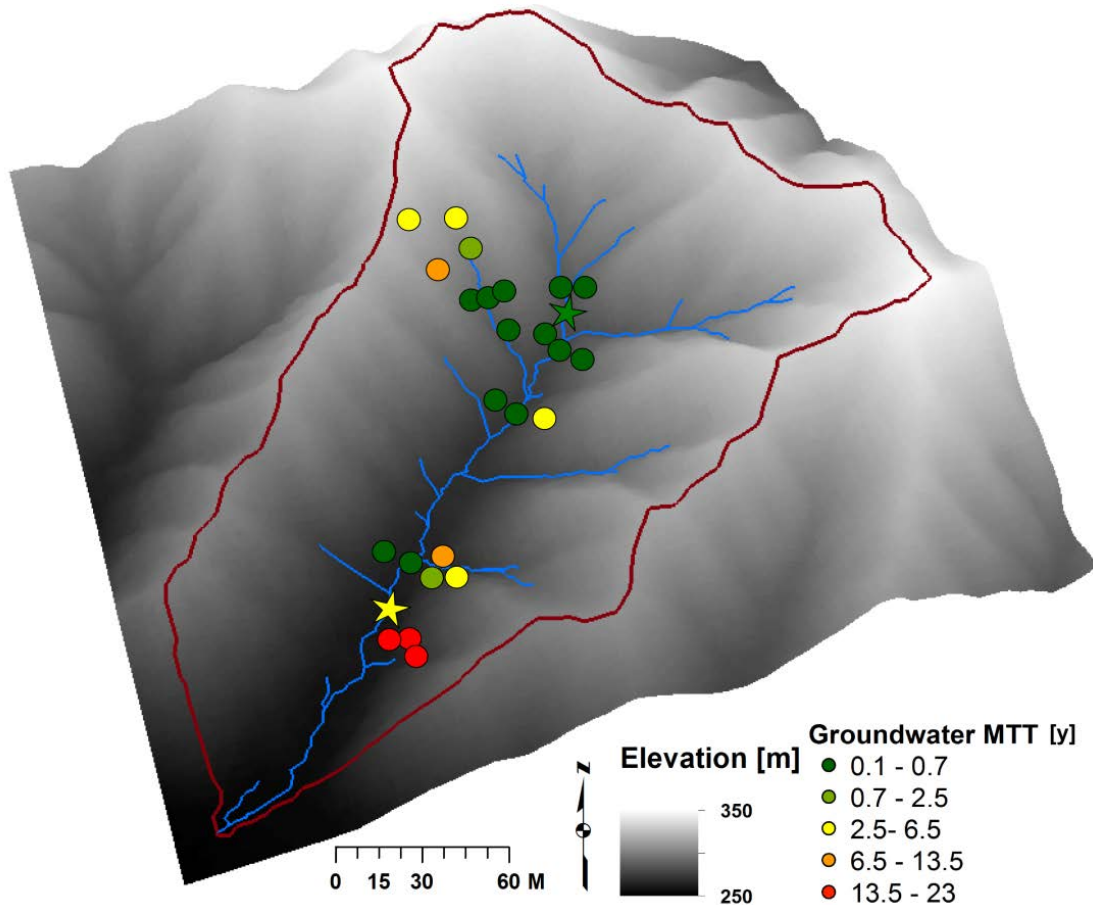


Figure 2.5 Spatial distribution of bedrock groundwater, soil water and streamwater MTT across the M8 catchment. Bedrock and soil samples are indicated by colored circles and surface samples by stars.

Generally, upper hillslope and deep riparian and toe-slope positions contained the oldest water, while younger water was found primarily in shallow bedrock wells within hollow and riparian positions. Bedrock wells along the entire length of the ephemeral hollow generally had younger water. All MTT estimates for wells within the hollow were less than 1.3 y old (> 1.87 TU), with the exception of the most upslope well, well 23, which had an MTT of 5.3 y (1.73 TU). The

location, depth to water table and water table dynamics of well 23 were more characteristic of other hillslope wells, as opposed to hollow wells, and as such, the older groundwater at this location was expected. The two upper hillslope samples (wells 8 and 12), collected at depths greater than 7 m, had MTTs of 6.5 and 10.5 y, respectively (1.65 and 1.38 TU, respectively)

Riparian zone and toe-slope wells had the greatest water age range from 0.1 to 23 y (2.5 and 0.97 TU). All toe-slope and riparian wells in the upper portion of the catchment, regardless of exact landscape position, contained young waters less than 0.3 y (TU > 2.01). Further downstream in the riparian zone, shallow wells remained young while deeper wells contained older water (> 5 y, TU < 1.72). The oldest waters were found in toe-slope positions on the east side of the catchment within 20 m upstream and downstream of the gauged weir. These wells (24, 34, 36, 37 and 39), all with sampling depths greater than 3.0 m, had MTT age estimates of 23, 22, 5.5, 13.5 and 5.3 y, respectively.

2.5.6 Silica analysis and time-varying streamwater MTT

Catchment discharge versus silica concentration data and the regression model fit to this relationship is shown in Figure 2.6a. The regression model captured a strong linear relation between the log transformed values of discharge and silica ($R^2 = 0.98$). Silica concentration showed a strong dilution gradient with increasing discharge. We applied this relationship to 1 year of catchment runoff. The estimated catchment discharge silica concentration is shown in Figure 2.7b. Silica concentration dropped to a low of 3.14 mg/l during peak storm events and rose to a high of 19.4 mg/l during an extended dry period in early 2015.

Using the relation between silica concentration and MTT (Figure 2.6b, $R^2 = 0.92$) we estimated stream water MTT from the 1 year time series of silica concentration (Figure 2.7c). MTT ranged from 0.37 to 2.5 years. Time-weighted mean MTT was 0.62 years and volume-weighted mean was 0.41 years. The MTT time series showed a distinct bi-modal age distribution that followed seasonal catchment wetness conditions and discharge volume. During the drier months of December through February, the catchment was in a state of older low-flow discharge punctuated by occasional precipitation inputs that transiently flushed young water to the stream channel.

Baseflow conditions quickly reestablished post storm-hydrograph peaks and MTT increased. Beginning in March, precipitation became more persistent, the growing season slowed and temperatures declined, reducing the evapotranspiration budget. Baseflow discharge increased between events as the catchment wetted up, available storage declined and the streamflow became younger. Catchment wet-up continued through April until soil water storage filled and antecedent wetness remained high between events, indicated by sustained levels of high runoff. This tipped the catchment into a state of young water discharge and streamwater MTT remained young and relatively stable through the remainder of the wet season. Beginning in October/November the catchment began to dry up as the next growing season initiated. As a result, streamwater MTT became much more dynamic and again fluctuated between older low-flow and young event-driven periods.

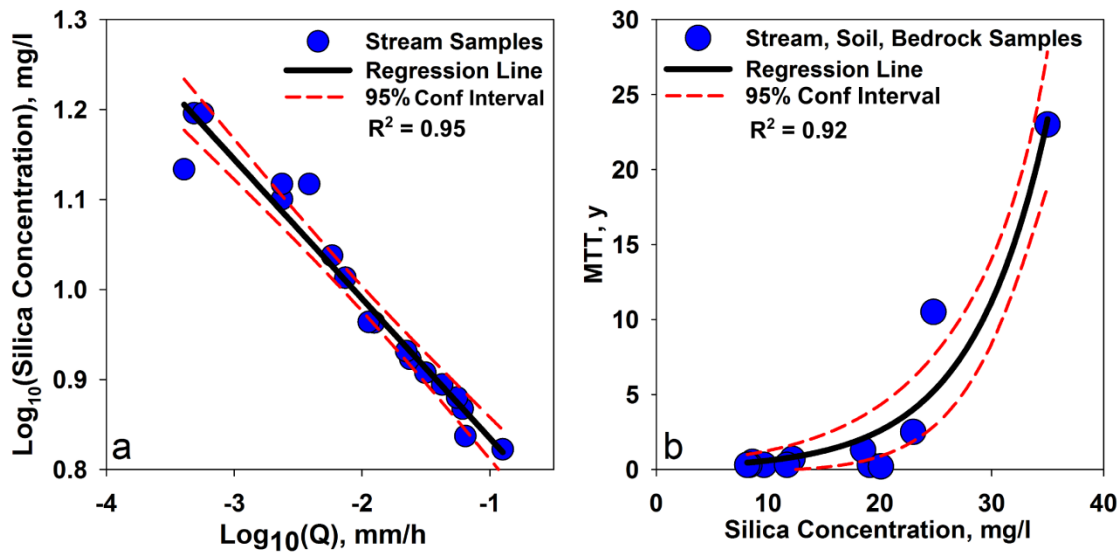


Figure 2.6 The linear relationship between the log-transformed M8 stream specific discharge and log-transformed streamwater silica concentration (a), and the non-linear relationship between silica concentration in bedrock groundwater, soil water and streamwater samples and measured MTT values (b). Both plots show values for individual grab samples, the fitted regression model and 95% confidence interval.

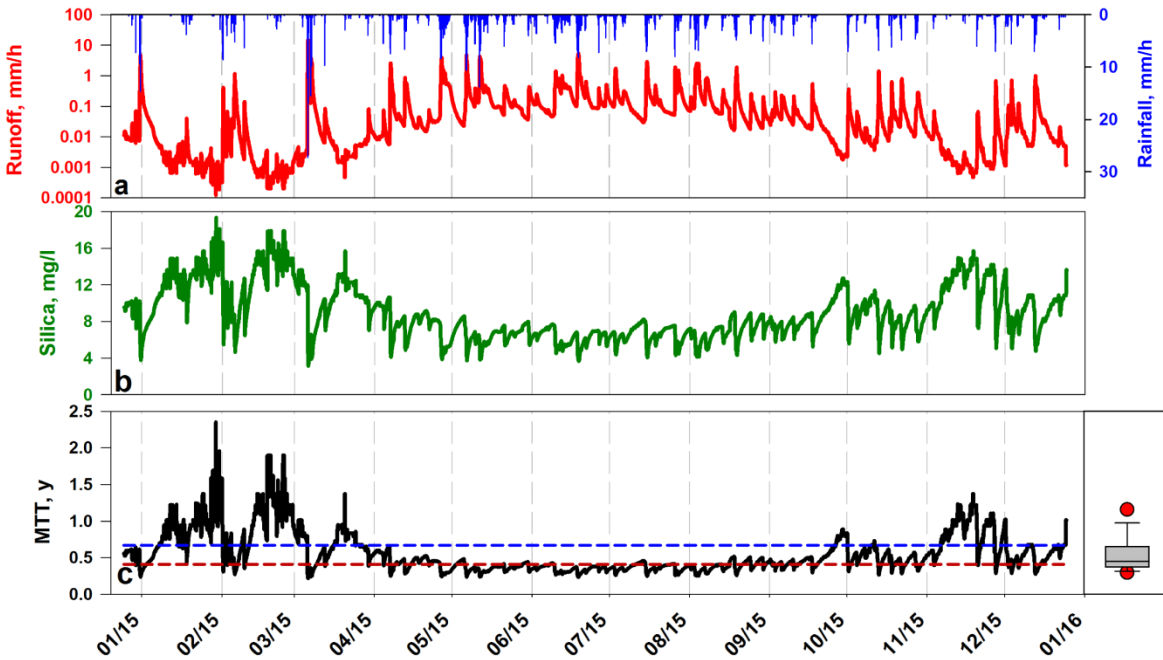


Figure 2.7 Time series of precipitation and runoff (a), estimated streamwater silica concentration (b) and estimated streamwater MTT (c). The blue hashed line represents the time-weighted streamwater MTT (0.62 y) and the red hashed line represents the volume weighted streamwater MTT (0.41 y). The box plot shows median, 1st and 3rd quartiles. Whiskers are equal to the 10th and 90th percentiles and red dots are outliers at the 5th and 95th percentiles.

2.6 Discussion

Our intensive hydrometric, hydrochemical and isotopic field campaign focused directly on characterizing the location, dynamics and age of the underlying bedrock aquifer and its contributions to streamflow. In so doing, our study advances the evolving perceptual model of hydrologic processes governing the Maimai watershed and offers insights on the control of deeper subsurface architecture on catchment processes for watershed conceptualizations elsewhere.

2.6.1 Bedrock groundwater location and dynamics

2.6.1.1 Water table position

We found that the shape of the underlying bedrock aquifer reflected a subdued replica of the land surface. This was consistent with other field and modeling studies in humid regions and suggests a topographically controlled water table (Sanford, 2002; Winter *et al.*, 2003; Haitjema and

Mitchell-Bruker, 2005). While the topographic control on water table position is not surprising given early descriptions of this (*Todd*, 1956), what was surprising was the particularly shallow ridgeline water table positions in the M8 catchment. This is in stark contrast to catchments in other geologic settings with similar climatic regimes (*Haria and Shand*, 2004; *Katsura et al.*, 2008; *Hale et al.*, 2016) and especially other watersheds where we have worked – e.g. WS 10 at the HJ Andrews Watershed, where ridgeline water tables were very deep and fluctuated greatly from dry to wet season (*Harr*, 1977). The depth to ridgeline water table exemplifies the complex interrelationship between climate, topography and geology, representing the balance point between recharge inputs from above and the ability of the bedrock formation to transmit water down-gradient (*Jamieson and Freeze*, 1982). In a simple sense, the Maimai’s shallow ridgeline water tables represent reduced groundwater flux compared to other sites with deeper water tables under similar recharge and geologic conditions (*Fetter*, 2000). Our site’s lower hydraulic conductivity limits flux rates, forcing the water table to rise, increasing the hydraulic gradient until recharge is balanced with discharge. As a metric, ridgeline water table depth, when considered along with the local precipitation regime, can provide insight on the landscape scale hydrologic activity of bedrock in terms of the extent of water movement. This also provides some understanding into the relative amounts of active storage and total catchment storage and their links to flow and transport. For example, a high water table in a hydrologically responsive catchment would imply a reduced vertical groundwater flux and greater horizontal partitioning of precipitation inputs to shallower flowpaths, thus greater volumes of younger water contributing to runoff. Conversely, a high ridgeline water table in a catchment with a dampened stream response would indicate greater vertical recharge to depth, larger active groundwater storage and greater volumes of older water contributing to runoff (*Tague and Grant*, 2004).

Gleeson and Manning (2008) used 3-D numerical simulations to explore the control of recharge rates and hydraulic conductivity on water table location. They found that increasing the ratio of recharge (R) to hydraulic conductivity (K) resulted in higher water table elevations. Indeed, the R/K ratio at Maimai is 0.64 (recharge 200 mm/y and bedrock hydraulic conductivity of 1.0×10^{-8} m/s), equal to the highest R/K value explored by *Gleeson and Manning* (2008). The high R/K ratio that we observed at M8 is consistent with the *Gleeson and Manning* (2008) prediction of the shallow ridgeline water table at our site.

2.6.1.2 Water table dynamics

Groundwater dynamics at M8 were spatially and temporally variable with some distinctions between the three major landscape units. The spatially variable water table dynamics revealed locally complex interactions between topography, aquifer characteristics, recharge source and timing, as well as pressure propagation through the vadose zone.

Seasonally, water table dynamics were most variable in the riparian zone and hollow positions and least variable in near-ridge wells. This trend was opposite to what we expected. During drier summer months as the landscape drained, we expected that hillslope water table positions would drop significantly and the riparian water table position to remain relatively constant, as has been reported in hillslope studies in other humid catchments (*Katsuyama et al.*, 2005; *Kosugi et al.*, 2006; *Iwagami et al.*, 2010; *Kosugi et al.*, 2011; *Hale et al.*, 2016). The absence of this trend at Maimai, where the near-ridge water table levels showed little seasonality, is likely due to the geologic properties of the OMG formation, with its low hydraulic conductivity – a first order control on storage and groundwater movement. The scarcity of bedrock fracturing at M8 forces recharge to occur through the bedrock's primary porosity, instead of through preferential fracture-based recharge, a flow process that has been previously attributed to large and rapid water table fluctuations (*Montgomery et al.*, 1997; *Gleeson et al.*, 2009; *Praamsma et al.*, 2009; *Gabrielli et al.*, 2012). Additionally, unsaturated bedrock storage increased with distance to the ridge as the vadose zone overlying the aquifer thickened. This unsaturated low permeability wedge likely acts to smooth and buffer seasonal variations of bedrock infiltration (percolation), while also delivering a relatively constant rate of recharge to the free-water surface. These factors combined maintained the observed near-stationary hillslope water table position near the ridgeline.

In lower lying wetter zones where bedrock water tables were shallow, more pronounced dynamics were observed in response to both storm and seasonal fluctuations. The thin or nonexistent unsaturated zone in the bedrock in this area is not able to buffer the groundwater table from storm event inputs. The observed increased hydraulic conductivity in the riparian zone and ephemeral hollows (likely a weathering feedback) caused a more pronounced decline in water tables during dry periods. This drove a spatially variable heterogeneous but structured groundwater drainage

pattern that was correlated to wetter convergent regions of the catchment with greater groundwater mobility.

2.6.2 The bedrock groundwater domain: gradients, age and streamflow contributions

Identifying the groundwater flow domain within small headwater catchments is often complex due to bedrock heterogeneity and considerable topographic relief that drives small-scale spatially variable flow paths (*Kosugi et al., 2011; Salve et al., 2012; Fujimoto et al., 2014; Katsura et al., 2014; Masaoka et al., 2016; Oshun et al., 2016*). Previous catchment studies have shown the value of combined hydrometric and tracer analyses to constrain mechanistic runoff processes and develop conceptual hydrologic models that are both parsimonious and consistent with multiple data sets (*Clark et al., 2011*). Our extensive soil and bedrock well network provided the ability to independently identify the groundwater flow domain through hydrometric analysis (i.e. groundwater flow gradients) and tritium-based MTT via groundwater isochrones (Figure 2.4 and 2.5). The two data sets identified spatially consistent groundwater recharge and discharge zones within the catchment confirming contributions of bedrock groundwater to catchment runoff.

2.6.2.1 Vertical bedrock groundwater gradients

Vertical groundwater head gradients across all hillslope positions were downward and indicated no bedrock groundwater discharge along the catchment hillslopes, consistent with previous studies at M8 (*Gabrielli et al., 2012*) and many hillslope bedrock groundwater observations elsewhere (*Kosugi et al., 2011; Salve et al., 2012; Katsura et al., 2014*). Interestingly, downward groundwater gradients within most of the wetted riparian corridor, including the ephemeral hollow, indicated that for the majority of the observed study period the stream channel acted as a groundwater recharge source (as opposed to sink) for bedrock groundwater. Although losing streams are common across many landscapes (*Sophocleous, 2002*), they are much less common in humid headwater regions where the riparian corridor is generally viewed as the discharge zone for deeper hillslope derived flowpaths (*Voltz et al., 2013*). This presents new implications for land use management at M8 and other similar riparian recharged headwater catchments, where hillslope or shallow riparian derived contaminants may be transported to depth more easily in these locations.

Upward groundwater gradients were observed at the base of the ephemeral hollow during the peak hours of storm events under high antecedent conditions. The specific discharge calculated using observed bedrock aquifer hydraulic conductivity and the well head gradient was a mere 0.5 l/h/m². Even assuming uniform discharge across the entire riparian corridor (~5% of catchment area), bedrock groundwater contributions to catchment runoff of this rate would only deliver 0.00025 mm/h (assuming direct connection to the stream channel), a rate too small to be measured or appreciably shift hydrometric or hydrochemical characteristics during event runoff periods.

Similar event-based discharge gradients were also noted at the most downstream riparian transect, but likewise were too small to measurably influence storm runoff characteristics. However, discharging bedrock groundwater at this same location was found to appreciably contribute to catchment discharge under extremely low baseflow conditions in the absence of recent rainfall input to the stream channel. The effect of this deeper bedrock groundwater contributions to the stream channel on streamwater MTT is discussed in detail below.

2.6.2.2 Bedrock groundwater MTT

Recharge and discharge zones represent the initiation and endpoints of groundwater flowlines (*Salvucci and Entekhabi, 1995*) thus, spatial patterns of groundwater MTT should mirror spatial patterns of the groundwater flow domain. Indeed, we found younger waters in recharge zones and correspondingly older water in discharge zones (i.e. the most downstream riparian transect). Bedrock groundwater samples extracted from the recharging upper riparian corridor were among the youngest waters in the catchment, indicative of recent recharge from young overlying stream and soil water. In the lower riparian zone, older bedrock groundwater was co-located with discharging gradients suggesting streamwater should reflect contributions from these older sources. Indeed, we found streamwater to be 2.5 y, having increased in age from a computed 0.3 y only 120 m upstream. The independent agreement of groundwater head gradients with spatial groundwater age patterns not only provides direct source-area evidence of bedrock groundwater contribution to streamflow, but better informs process understanding of the catchment groundwater flow domain and surface water–groundwater interactions.

The lack of correlation between groundwater age and spatial and depth metrics is likely a result of the inability of one or two dimensional landscape derived metrics to fully capture the complex three dimensional groundwater flow structure and storage volume that sets groundwater MTT. This inability for simple topographic parameters to capture the groundwater age at Maimai may hint at why many other studies have also failed to find simple landscape derived scaling metrics that accurately capture stream water MTT (*Tetzlaff et al.*, 2009). In humid catchments, storage volume is critical in setting the age of discharge, and the degree to which any metric acts as a proxy for this storage volume likely controls the strength of its correlation to catchment MTT (*McNamara et al.*, 2011). In steep humid topographically driven catchments with low permeability bedrock, shallow flowpaths dominate and storage is small. Single or composite metrics such as flowpath length or gradient tend to scale with catchment MTT since landscape form acts as a sufficient proxy for subsurface mixing volume (*McGlynn et al.*, 2003; *McGuire et al.*, 2005). However, as bedrock permeability increases and the active mixing zone deepens, storage likewise increases and simple topographic metrics no longer capture this, now much larger, storage volume that controls catchment MTT. Instead, metrics that are a better proxy for the increased subsurface storage are more suited. *Hale and McDonnell* (2016) compared catchments with similar rainfall-runoff regimes but with different underlying bedrock permeability. Less permeable younger catchments scaled with topographic characteristics, while older and more permeable catchments not only failed to scale with topographic characteristics but instead scaled to catchment area, indeed, a better proxy for the increased storage. This elegantly captured the control of bedrock permeability, and thus storage, on catchment streamwater age and the required shift in metrics to accurately reflect the increase in storage depth. In a further example, *Asano and Uchida* (2012) found that bedrock flowpath depth controlled baseflow MTT in 8 nested granite catchments. Geologic properties was similar across all catchments, so that the volume of bedrock storage per unit area was set by the flowpath depth. Accordingly, flowpath depth accurately scaled with subsurface storage volume and thus catchment MTT between catchments.

At Maimai, bedrock groundwater MTT was not captured by topographic metrics likely because these metrics failed to capture the larger 3-dimensional flow domain and storage volume that controlled groundwater MTT. However, it should be pointed out that Maimai streamflow is dominated by shallow subsurface flowpaths, thus simple landscape derived metrics should scale

to streamwater MTT at this site. Indeed, this was found in earlier studies at Maimai by *McGlynn et al.* (2003). In general, as catchments shift from shallower to deeper flowpath dominance, the metrics that capture discharge MTT should equally shift to capture the increasing volume of storage, which acts as a primary control on setting mean catchment age (*Pfister et al.*, 2017).

2.6.3 Time-varying streamwater transit time

Our silica-based MTT estimates demonstrate the time-varying nature of streamwater MTT at M8. This highlights the intricate connection between catchment wetness condition, discharge rate and transit time. Antecedent conditions and event precipitation drive spatially distributed landscape scale connectivity that controls the release of differentially aged water from differentially stored subsurface units to the stream channel. The integration of these varying runoff sources through time and space form the single time-varying mean runoff age observed at the catchment outlet (*Soulsby et al.*, 2015). The bi-modal nature of streamwater MTT at M8 reflects seasonal shifts in environmental forcing factors, primarily precipitation and evapotranspiration, which drive landscape scale shifts in hydrologic connectivity (Figure 2.7). The Maimai remained under high antecedent wetness conditions for nearly 8 months of the year from March through October, and correspondingly, young shallow subsurface flow dominated runoff. Streamwater MTT remained near 4 months, an age that corresponds to soil-water storage residence times observed by *Stewart and McDonnell* (1991). During this extended wet period, MTT was relatively stable and age fluctuations were minimal despite order-of-magnitude changes in catchment discharge. Perhaps most significant was the persistence of young streamwater between storm events while the catchment drained. Elevated baseflow discharge, sourced primarily from younger soil water storage, dominated runoff and diluted the older bedrock groundwater discharge signal.

During summer months, when precipitation inputs dropped slightly and evapotranspiration rates increased significantly, baseflow discharge decreased by almost 3 orders of magnitude compared to the wet season. Antecedent wetness was low and spatial connectivity of shallow soil stores to the stream channel declined. Streamwater MTT became highly variable. Transient connectivity of younger shallow flowpaths during and immediately following rain events would temporarily drive streamwater to much younger MTTs. But between events MTT increased considerably, reflecting

the contraction of younger flowpaths and the reduction of discharge volume to levels where contributions from older bedrock groundwater were proportionately more significant.

Birkel et al. (2015) similarly found antecedent conditions drove hydrologic connectivity at a Scottish Highlands catchment, which in turn also controlled the time-varying nature of streamwater MTT. Interestingly, their MTT time series, established using a tracer-aided model, showed an almost reverse bi-modal trend from what we found at M8 (*Soulsby et al., 2015*). MTT was stable at low discharge rates and highly dynamic (and young) at high discharge rates. This contrast from Maimai perhaps offers end-member examples of differences in catchment MTT dynamics that result from differences in shallow-versus-deep proportioning of subsurface water in humid catchments. Greater volumes of catchment precipitation are distributed to deeper storage at the ‘more permeable’ Scottish catchment (with its glacial drift deposits and deep soils), and accordingly, runoff generation is sourced from greater contributions of this storage unit across all flow conditions. During low flow, deep storage acts as the primary source of runoff generation and streamwater MTT reflects the age of this single storage unit, and is thus stable. At higher flows, although younger flowpaths are activated, they do not completely inundate the dominant deeper groundwater signal and the catchment MTT is controlled by the proportional mixing of the two (or more) storage units. This creates a highly flow dependent and highly variable streamwater MTT at higher flows. Whereas at Maimai, the same dynamics are observed, however, in reverse. That is, streamwater MTT is stable at high flow and highly variable at low flow. Redistribution of moisture to deep groundwater storage is minimal at Maimai and catchment runoff is predominantly sourced by young shallow flowpaths. At higher discharge, these shallow young flowpaths effectively “drown out” the bedrock groundwater signal and MTT is thus stable, reflecting only the single young shallow storage unit. During low flow periods bedrock groundwater contributions are proportionately significant and streamwater MTT becomes highly flow dependent and highly variable. Although streamwater MTT is also controlled by the proportional mixing of the two main catchment storage units at Maimai, as in the Scottish catchments, the conditions under which these controls dominate are opposite.

2.6.4 An evolving perceptual model of Maimai hydrology

So why have previous studies at Maimai not seen bedrock groundwater? Simply put, bedrock groundwater contributions to streamflow at Maimai are extremely limited. Figure 2.8 shows our conceptual model of the primary groundwater flowpaths and general groundwater flow domain. The lack of fractured bedrock, low bedrock conductivity and predominately downward hydraulic gradients result in a relatively isolated groundwater body that has limited connectivity to the stream channel. Further, the sharp permeability contrast at the soil-bedrock interface causes most infiltrating water to shed laterally downslope at this boundary instead of continuing vertically into the bedrock. This, combined with shallow soils, minimal available soil-storage and long periods of high antecedent wetness means that the majority of precipitation is filtered only through the soil profile en route to the stream channel resulting in the now well-observed high runoff ratios, large volumes of quickflow and young runoff observed at Maimai (*Mosley, 1979; Pearce et al., 1986; McDonnell, 1990*).

Although bedrock groundwater storage (based on porosity and volume of saturated bedrock) is large at M8, the low bedrock hydraulic conductivity results in minimal groundwater flux within the headwater aquifer. This has the effect of driving up bedrock groundwater MTT, while simultaneously reducing contributions to the stream channel. So although the potential of bedrock groundwater to influence streamwater MTT is high because its age is much greater than that of other shallower storages, this is offset by the low total bedrock discharge volume – too small to considerably alter streamwater MTT under most runoff conditions. This dichotomy establishes what is effectively a two-storage compartmentalized hydrologic system with a young, shallow and dominant upper domain and a much deeper and relatively isolated older groundwater body beneath. If bedrock groundwater contributions were to increase, say through weathering-induced increases in permeability, this would reduce groundwater MTT through greater flux. Interestingly, this *drop* in bedrock groundwater MTT would result in an *increase* in catchment MTT, as the greater contribution of bedrock groundwater to runoff would increase the overall age of streamwater.

Lastly, it is necessary to address the conflicting hillslope versus catchment runoff ratios that initially led to the notion of a hillslope bedrock underflow runoff mechanism. Upon further inspection, the 110 day hillslope monitoring period conducted by *Woods and Rowe* (1996) at Maimai occurred during the summer months when high evapotranspiration budgets and reduced precipitation had dried up the catchment. This had the effect of increasing the necessary precipitation input to surpass hillslope runoff generation thresholds, and thus, many small storms produced no hillslope runoff. This caused the hillslope runoff ratio during this period to dramatically deviate from the annually averaged total catchment runoff ratio.

Although event-scale water table dynamics were observed within the bedrock aquifer both during our study and previously (*Gabrielli et al.*, 2012), they are likely an integrated response to changes in barometric pressure (*Van der Kamp and Gale*, 1983), precipitation-induced pressure propagation (*Rasmussen*, 2001), and small amounts of direct recharge to the water table. In the steep landscape at Maimai, increases in water table height over both storm and seasonal time scales do not equate to large changes in groundwater hydraulic head. For example, a mid-slope water table may rise 0.2 m during a large storm event, however, if this position were 30 m above the riparian zone, the resulting hydraulic gradient change would be only 0.7%. In unfractured low conductivity bedrock this would not alter considerably the groundwater flow structure, and no measurable increase in bedrock groundwater discharge would likely occur. Although, small rises in water table can produce large volumes of hillslope discharge in shallow soils due to a transmissivity feedback mechanism (*Bishop et al.*, 2004), we do not expect this phenomena to occur within the deeper bedrock underlying Maimai.

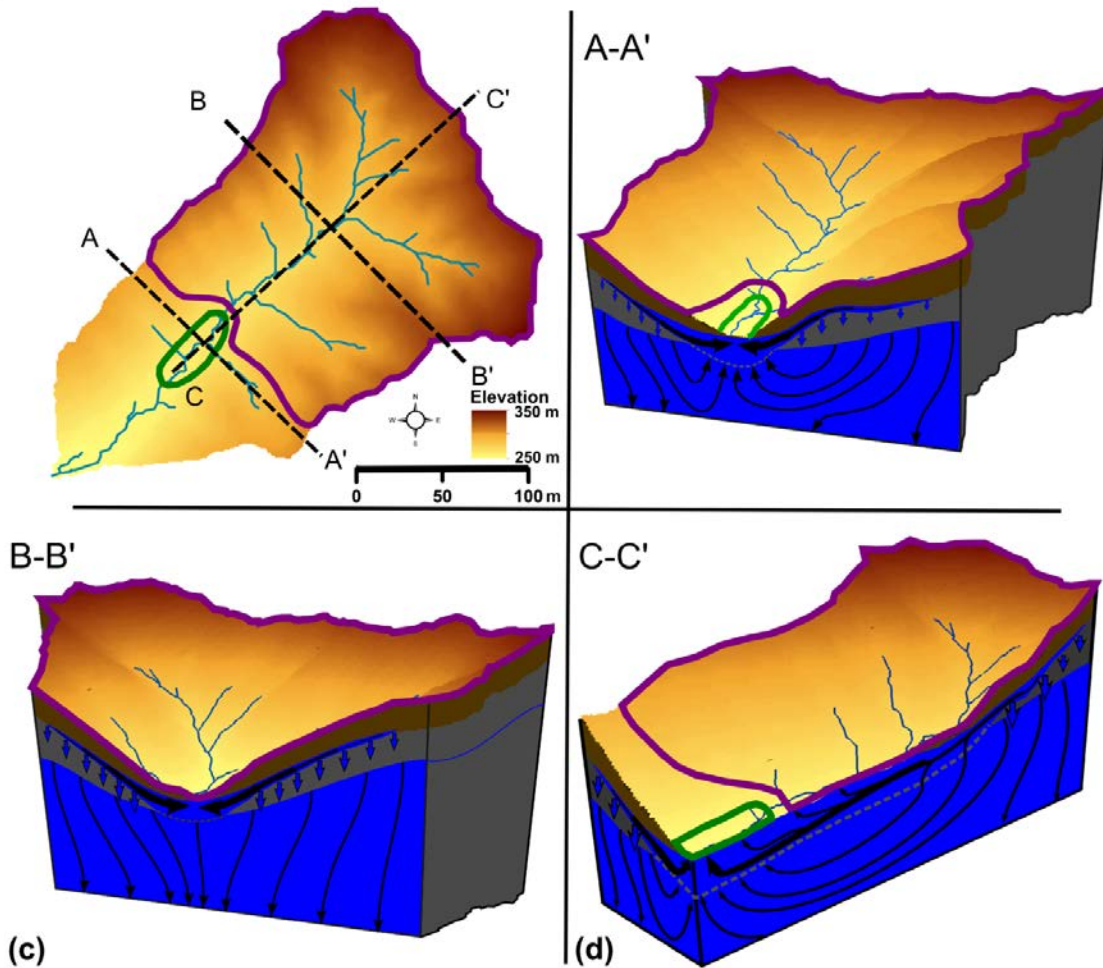


Figure 2.8 Conceptual model of the bedrock groundwater flow domain through various cross sections of the M8 catchment. (a) shows the location of cross sections, as well as the approximate area of observed bedrock groundwater recharge within the magenta outline and the approximate area of observed bedrock groundwater discharge within the green outline. All cross sections show the accumulation of soil water at the soil-bedrock interface with increasing distance downslope which functions as the primary source of young streamflow for the catchment outlet. Cross section A-A' (b) shows deeper and older contributions of bedrock groundwater discharge to the lower reach of the stream channel with some portion of hillslope recharge being lost to the larger regional groundwater system. Cross section B-B' (c) shows only groundwater recharge occurring across all landscape positions in the upper portion of the catchment, and cross section C-C' (d) displays the longitudinally split view of the catchment length. Here, upper reaches of the riparian zone contribute soil water to bedrock groundwater recharge and to stream discharge, while the lower reach of the riparian zone contributes both hillslope derived soil water and bedrock groundwater to the stream.

Early water balance estimates at Maimai by *Pearce et al.* (1977) calculated approximately 100 mm/y loss to deeper groundwater. In a system which receives 2600 mm of rainfall annually and

has minimal groundwater flux, small uncertainties inherent in precipitation, discharge and evapotranspiration measurements can be equal to the total estimated loss to deeper groundwater. We are therefore cautious to place an exact value on bedrock groundwater recharge and discharge amounts. However, our new analysis suggests that approximately 200 mm/y is recharged to the bedrock aquifer, half of which is discharged back into the catchment above the M8 weir and thus contributes to runoff generation processes, while the other half likely subsidizes flows at larger catchment scales down valley from the upper M8 headwaters (the subject of active ongoing work).

2.7 Conclusion

Our findings showed that despite a relatively shallow bedrock groundwater aquifer that displayed both event and seasonal scale water table fluctuations, bedrock groundwater contributions to catchment discharge at Maimai were minimal. The unfractured low-conductivity bedrock provided no opportunity to move considerable volumes of excess soil moisture to depth over short periods of time, and therefore, bedrock groundwater infiltration was controlled we hypothesize by the permeability of the bedrock matrix, occurring as flow through the primary porosity of the conglomerate bedrock. Although bedrock groundwater storage itself was considerable, the low recharge rate combined with stable hillslope water tables drove an annually constant discharge to the riparian corridor. With the exception of some transient event-scale switches in vertical groundwater gradient at two well locations, general gradient direction remained temporally and spatially constant throughout all wetness conditions. We observed all hillslope locations and mid and upper reaches of the riparian zone to be groundwater sinks, while a small zone of upwelling bedrock groundwater was identified near the catchment outlet.

We noted a shift in the control on streamwater MTT from soil storage effusion during the 8-month wet season to a combined soil and bedrock storage effusion during the drier summer months. During the wet season, large volumes of young soil water controlled the streamwater MTT signal and maintained a relatively stable and young streamwater age even during inter-storm periods. During drier months, bedrock groundwater contributions to runoff became proportionally large enough to exert some control on streamwater MTT. During these intervals, stream age fluctuates

significantly between young and old conditions corresponding to storm and inter-storm periods and reflected the mixing of the two main catchment storage units.

This work reinforces the need to maintain large-scale field-based investigations to provide new data sets that inform the next generation of catchment and regional scale hydrologic modeling (*Burt and McDonnell, 2015*), especially regarding differences in celerity and velocity (*McDonnell and Beven, 2014*) which differentially control the hydrograph response and transit time distributions. Our work highlights the control of bedrock characteristics, specifically permeability in controlling catchment runoff process and in setting streamwater MTT.

2.8 Transition statement

Chapter 2 established the general hydrogeologic characteristics of the Old Man Gravel bedrock at the Maimai watershed. This chapter linked bedrock properties with the bedrock groundwater flow domain to identify the groundwater-surface water linkages responsible for the time-varying nature of streamwater discharge. It also identified general understanding of groundwater flow, storage and age distribution within the catchment, providing the foundational understanding of the underlying headwater aquifer. This understanding was then built upon in Chapter 3, which sought to identify the geologic control of bedrock on the timing of deep groundwater recharge. While bedrock permeability was identified as a critical component controlling groundwater age and movement in Chapter 2, Chapter 3 showed that it was also a key factor for mediating bedrock groundwater recharge timing.

2.9 Acknowledgments

This work was supported through funding by NSERC Discovery grant to J.J. McDonnell and the Horton Hydrology Research Grant from the American Geophysical Union to Christopher Gabrielli. We thank John Payne at Landcare Research, Matt Taylor, Christie Thomson, Emma and Bob Noonan, and Shaun McCracken for their invaluable assistance and support in the field and throughout the extended field campaign in New Zealand.

2.10 Author contributions

CPG and JJM conceived the rationale for the study, while CPG carried out all field work and data analysis. UM and MS conducted the tritium analysis and offered interpretation of results. CPG wrote the paper and JJM, UM and MS provided comments and contributed to the text.

2.11 References

Asano, Y. and T. Uchida (2012), Flow path depth is the main controller of mean base flow transit times in a mountainous catchment, *Water Resour. Res.*, 48(3), W03512. 10.1029/2011WR010906.

Beven, K.J. and M.J. Kirkby (1979), A physically based, variable contributing area model of basin hydrology, *Hydrological Sciences Bulletin*, 24(1), 43-69. 10.1080/02626667909491834.

Birkel, C., C. Soulsby and D. Tetzlaff (2015), Conceptual modelling to assess how the interplay of hydrological connectivity, catchment storage and tracer dynamics controls nonstationary water age estimates, *Hydrol. Processes*, 29(13), 2956-2969. 10.1002/hyp.10414.

Bishop, K., J. Seibert, S. Köhler and H. Laudon (2004), Resolving the double paradox of rapidly mobilized old water with highly variable responses in runoff chemistry, *Hydrol. Processes*, 18(1), 185-189. 10.1002/hyp.5209

Bowen, F. (1967), Early pleistocene glacial and associated deposits of the west coast of the south island, new zealand, *New Zealand journal of geology and geophysics*, 10(1), 164-181.

Burns, D.A., L.N. Plummer, J.J. McDonnell, E. Busenberg, G.C. Casile, C. Kendall, R.P. Hooper, J.E. Freer, N.E. Peters, K.J. Beven and P. Schlosser (2003), The geochemical evolution of riparian ground water in a forested piedmont catchment, *Ground Water*, 41(7), 913-925. 10.1111/j.1745-6584.2003.tb02434.x.

Burt, T.P. and J.J. McDonnell (2015), Whither field hydrology? The need for discovery science and outrageous hydrological hypotheses, *Water Resour. Res.*, 51(8), 5919-5928. 10.1002/2014WR016839.

Clark, M.P., D. Kavetski and F. Fenicia (2011), Pursuing the method of multiple working hypotheses for hydrological modeling, *Water Resour. Res.*, 47(9). 10.1029/2010WR009827.

Ebel, B.A. and K. Loague (2006), Physics-based hydrologic-response simulation: Seeing through the fog of equifinality, *Hydrol. Processes*, 20(13), 2887-2900. 10.1002/hyp.6388.

Edmunds, W. and P. Smedley (2000), Residence time indicators in groundwater: The east midlands triassic sandstone aquifer, *Appl. Geochem.*, 15(6), 737-752. 10.1016/S0883-2927(99)00079-7.

Fetter, C.W. (2000), Applied hydrogeology, Prentice hall.

Freeze, R.A. and J.A. Cherry (1979), Groundwater, Prentice-Hall, Englewood Cliffs, NJ.

Frisbee, M.D., F.M. Phillips, A.R. Campbell, F. Liu and S.A. Sanchez (2011), Streamflow generation in a large, alpine watershed in the southern rocky mountains of colorado: Is streamflow generation simply the aggregation of hillslope runoff responses?, *Water Resour. Res.*, 47(6). 10.1029/2010WR009391.

Fujimoto, M., K.I. Kosugi, M. Tani, N. Banba and R. Fukagawa (2014), Evaluation of bedrock groundwater movement in a weathered granite hillslope using tracer methods, *International Journal of Erosion Control Engineering*, 7(1), 32-40. 10.13101/ijece.7.32.

Gabrielli, C.P. and J.J. McDonnell (2012), An inexpensive and portable drill rig for bedrock groundwater studies in headwater catchments, *Hydrol. Processes*, 26(4), 622-632. 10.1002/hyp.8212.

Gabrielli, C.P., J.J. McDonnell and W.T. Jarvis (2012), The role of bedrock groundwater in rainfall-runoff response at hillslope and catchment scales, *J. Hydrol.*, 450, 117-133. 10.1016/j.jhydrol.2012.05.023.

Gleeson, T. and A.H. Manning (2008), Regional groundwater flow in mountainous terrain: Three-dimensional simulations of topographic and hydrogeologic controls, *Water Resour. Res.*, 44(10), W10403. 10.1029/2008WR006848.

Gleeson, T., K. Novakowski and T. Kurt Kyser (2009), Extremely rapid and localized recharge to a fractured rock aquifer, *J. Hydrol.*, 376(3-4), 496-509. 10.1016/j.jhydrol.2009.07.056.

Graham, C.B., R.A. Woods and J.J. McDonnell (2010), Hillslope threshold response to rainfall: (1) a field based forensic approach, *J. Hydrol.*, 393(1-2), 65-76. 10.1016/j.jhydrol.2009.12.015.

Haitjema, H.M. and S. Mitchell-Bruker (2005), Are water tables a subdued replica of the topography?, *Ground Water*, 43(6), 781-786. 10.1111/j.1745-6584.2005.00090.x.

Hale, V.C. and J.J. McDonnell (2016), Effect of bedrock permeability on stream base flow mean transit time scaling relations: 1. A multiscale catchment intercomparison, *Water Resour. Res.*, 52(2), 1358-1374. 10.1002/2014WR016124.

Hale, V.C., J.J. McDonnell, M.K. Stewart, D.K. Solomon, J. Doolittle, G.G. Ice and R.T. Pack (2016), Effect of bedrock permeability on stream base flow mean transit time scaling relationships: 2. Process study of storage and release, *Water Resour. Res.*, 52(2), 1375-1397. 10.1002/2015WR017660.

Haria, A.H. and P. Shand (2004), Evidence for deep sub-surface flow routing in forested upland wales: Implications for contaminant transport and stream flow generation, *Hydrology and Earth System Sciences Discussions*, 8(3), 334-344. hal-00304922.

Harr, R.D. (1977), Water flux in soil and subsoil on a steep forested slope, *J. Hydrol.*, 33, 37-58. 10.1016/0022-1694(77)90097-X.

Hewlett, J.D. and A.R. Hibbert (1967), Forest hydrology. Sopper, W.E. and Lull, H.W. (eds), pp. 275-291, Pergamon Press, New York.

Hvorslev, M.J. (1951), Time lag and soil permeability in ground-water observations.

Iwagami, S., M. Tsujimura, Y. Onda, J. Shimada and T. Tanaka (2010), Role of bedrock groundwater in the rainfall–runoff process in a small headwater catchment underlain by volcanic rock, *Hydrol. Processes*, 24(19), 2771-2783. 10.1002/hyp.7690.

Iwasaki, K., M. Katsuyama and M. Tani (2014), Contributions of bedrock groundwater to the upscaling of storm-runoff generation processes in weathered granitic headwater catchments, *Hydrol. Processes*, 29(6), 1535–1548. 10.1002/hyp.10279.

Jamieson, G.R. and R.A. Freeze (1982), Determining hydraulic conductivity distributions in a mountainous area using mathematical modeling, *Ground Water*, 20(2), 168-177. 10.1111/j.1745-6584.1982.tb02745.x.

Katsura, S.Y., K.I. Kosugi, T. Mizutani, S. Okunaka and T. Mizuyama (2008), Effects of bedrock groundwater on spatial and temporal variations in soil mantle groundwater in a steep granitic headwater catchment, *Water Resour. Res.*, 44(9), W09430. 10.1029/2007WR006610.

Katsura, S.Y., K.I. Kosugi, Y. Yamakawa and T. Mizuyama (2014), Field evidence of groundwater ridging in a slope of a granite watershed without the capillary fringe effect, *J. Hydrol.*, 511. 10.1016/j.jhydrol.2014.02.021.

Katsuyama, M., N. Ohte and N. Kabeya (2005), Effects of bedrock permeability on hillslope and riparian groundwater dynamics in a weathered granite catchment, *Water Resour. Res.*, 41(1), W01010. 10.1029/2004WR003275.

Katz, B.G., A.R. Chelette and T.R. Pratt (2004), Use of chemical and isotopic tracers to assess nitrate contamination and ground-water age, woodville karst plain, USA, *J. Hydrol.*, 289(1-4), 36-61. 10.1016/j.jhydrol.2003.11.001.

Kazemi, G.A., J.H. Lehr and P. Perrochet (2006), Groundwater age, John Wiley & Sons.

Kosugi, K.I., S.Y. Katsura, M. Katsuyama and T. Mizuyama (2006), Water flow processes in weathered granitic bedrock and their effects on runoff generation in a small headwater catchment, *Water Resour. Res.*, 42(2), W02414. 10.1029/2005WR004275.

Kosugi, K.I., M. Fujimoto, S.Y. Katsura, H. Kato, Y. Sando and T. Mizuyama (2011), Localized bedrock aquifer distribution explains discharge from a headwater catchment, *Water Resour. Res.*, 47(7). 10.1029/2010WR009884.

Maloszewski, P. and A. Zuber (1982), Determining the turnover time of groundwater systems with the aid of environmental tracers. 1. Models and their applicability, *J. Hydrol.*, 57, 207-231. 10.1016/0022-1694(82)90147-0.

Masaoka, N., K.I. Kosugi, Y. Yamakawa and D. Tsutsumi (2016), Processes of bedrock groundwater seepage and their effects on soil water fluxes in a foot slope area, *J. Hydrol.*, 535, 160-172. 10.1016/j.jhydrol.2016.01.081.

Maxwell, R.M. and L.E. Condon (2016), Connections between groundwater flow and transpiration partitioning, *Science*, 353(6297), 377-380. 10.1126/science.aaf7891.

Mcdonnell, J.J. (1990), A rationale for old water discharge through macropores in a steep, humid catchment, *Water Resour. Res.*, 26(11), 2821-2832. 0.1029/WR026i011p02821.

Mcdonnell, J.J. and K. Beven (2014), Debates—the future of hydrological sciences: A (common) path forward? A call to action aimed at understanding velocities, celerities and residence time distributions of the headwater hydrograph, *Water Resour. Res.*, 50(6), 5342-5350. 10.1002/2013WR015141.

Mcglynn, B., J. Mcdonnell, M. Stewart and J. Seibert (2003), On the relationships between catchment scale and streamwater mean residence time, *Hydrol. Processes*, 17(1), 175-181. 10.1002/hyp.5085.

Mcglynn, B.L., J.J. Mcdonnell and D.D. Brammer (2002), A review of the evolving perceptual model of hillslope flowpaths at the maimai catchments, new zealand, *J. Hydrol.*, 257, 1-26. 10.1016/S0022-1694(01)00559-5.

Mcglynn, B.L. and J.J. Mcdonnell (2003), Role of discrete landscape units in controlling catchment dissolved organic carbon dynamics, *Water Resour. Res.*, 39(4), SWC31-SWC318. 10.1029/2002WR001525.

Mcglynn, B.L., J.J. Mcdonnell, J. Seibert and C. Kendall (2004), Scale effects on headwater catchment runoff timing, flow sources, and groundwater-streamflow relations, *Water Resour. Res.*, 40(7), W07504. 10.1029/2003WR002494.

Mcguire, K.J., J.J. Mcdonnell, M. Weiler, C. Kendall, B.L. McGlynn, J.M. Welker and J. Seibert (2005), The role of topography on catchment-scale water residence time, *Water Resour. Res.*, 41(5). 10.1029/2004WR003657.

Mckie, D. (1978), A study of soil variability within the blackball hill soils, reefton, new zealand, Lincoln College, University of Canterbury.

Mcnamara, J.P., D. Tetzlaff, K. Bishop, C. Soulsby, M. Seyfried, N.E. Peters, B.T. Aulenbach and R. Hooper (2011), Storage as a metric of catchment comparison, *Hydrol. Processes*, 25(21), 3364-3371. 10.1002/hyp.8113.

Montgomery, D.R., W.E. Dietrich, R. Torres, S.P. Anderson, J.T. Heffner and K. Loague (1997), Hydrologic response of a steep, unchanneled valley to natural and applied rainfall, *Water Resour. Res.*, 33(1), 91-109. 10.1029/96WR02985.

Morgenstern, U. and C.B. Taylor (2009), Ultra low-level tritium measurement using electrolytic enrichment and lsc, *Isotopes in environmental and health studies*, 45(2), 96-117. 10.1080/10256010902931194.

Morgenstern, U., M.K. Stewart and R. Stenger (2010), Dating of streamwater using tritium in a post nuclear bomb pulse world: Continuous variation of mean transit time with streamflow, *Hydrol. Earth Syst. Sci.*, 14(11), 2289-2301. 10.5194/hess-14-2289-2010.

Mortimer, N., R. Sutherland and S. Nathan (2001), Torlesse greywacke and haast schist source for pliocene conglomerates near reefton, new zealand, *New Zealand Journal of Geology and Geophysics*, 44(1), 105-111. 10.1080/00288306.2001.9514927.

Mosley, M.P. (1979), Streamflow generation in a forested watershed, *Water Resour. Res.*, 15, 795-806. 10.1029/WR015i004p00795.

Nathan, S., H.J. Anderson, R.A. Cook, R. Herzer, R. Hoskins, J. Raine and D. Smale (1986), Cretaceous and cenozoic sedimentary basins of the west coast region, south island, new zealand, Science Information Pub. Centre, DSIR, for the New Zealand Geological Survey.

O'loughlin, C.L., L.K. Rowe and A.J. Pearce (1978), Sediment yields from small forested catchments, north westland-nelson, new zealand, *J. Hydrol. (NZ)*, 17(1), 1-15.

Oshun, J., W.E. Dietrich, T.E. Dawson and I. Fung (2016), Dynamic, structured heterogeneity of water isotopes inside hillslopes, *Water Resour. Res.*, 52(1), 164-189. 10.1002/2015WR017485.

Pearce, A.J., C.L. O'loughlin and L.K. Rowe (1977), Hydrologic regime of small, undisturbed beech forest catchments, north westland, *Inf Ser NZ Dep Sci Ind Res*.

Pearce, A.J. and L.K. Rowe (1979), Forest management effects on interception, evaporation, and water yield, *J. Hydrol.*, 18(2), 73-87.

Pearce, A.J., M.K. Stewart and M.G. Sklash (1986), Storm runoff generation in humid headwater catchments: 1. Where does the water come from?, *Water Resour. Res.*, 22, 1263-1272. 10.1029/WR022i008p01263.

Peters, N.E., D.A. Burns and B.T. Aulenbach (2014), Evaluation of high-frequency mean streamwater transit-time estimates using groundwater age and dissolved silica concentrations in a small forested watershed, *Aquatic geochemistry*, 20(2-3), 183-202.

Pfister, L., N. Martínez-Carreras, C. Hissler, J. Klaus, G.E. Carrer, M.K. Stewart and J.J. McDonnell (2017), Bedrock geology controls on catchment storage, mixing and release: A comparative analysis of 16 nested catchments, *Hydrol. Processes*, 31(10), 1828-1845. 10.1002/hyp.11134.

Praamsma, T., K. Novakowski, K. Kyser and K. Hall (2009), Using stable isotopes and hydraulic head data to investigate groundwater recharge and discharge in a fractured rock aquifer, *J. Hydrol.*, 366(1), 35-45.

Rantz, S.E. (1982), Measurement and computation of streamflow: Volume 2, computation of discharge, USGPO.

Rasmussen, T.C. (2001), Flow and transport through unsaturated fractured rock, pp. 45-52, American Geophysical Union.

Rowe, L. and A. Pearce (1994), Hydrology and related changes after harvesting native forest catchments and establishing pinus radiata plantations. Part 2. The native forest water balance and changes in streamflow after harvesting, *Hydrol. Processes*, 8(4), 281-297. 10.1002/hyp.3360080402.

Salve, R., D.M. Rempe and W.E. Dietrich (2012), Rain, rock moisture dynamics, and the rapid response of perched groundwater in weathered, fractured argillite underlying a steep hillslope, *Water Resour. Res.*, 48(11). 10.1029/2012WR012583.

Salvucci, G.D. and D. Entekhabi (1995), Hillslope and climatic controls on hydrologic fluxes, *Water Resour. Res.*, 31(7), 1725-1739. 10.1029/95WR00057.

Sanford, W. (2002), Recharge and groundwater models: An overview, *Hydrogeol. J.*, 10(1), 110-120. 10.1007/s10040-001-0173-5.

Sayama, T. and J.J. McDonnell (2009), A new time-space accounting scheme to predict stream water residence time and hydrograph source components at the watershed scale, *Water Resour. Res.*, 45(7). 10.1029/2008WR007549.

Seibert, J. and J.J. McDonnell (2003), The quest for an improved dialog between modeler and experimentalist, *Water Science and Applications*, 6, 301-316. 10.1029.006WS22.

Seibert, J., A. Rodhe and K. Bishop (2003), Simulating interactions between saturated and unsaturated storage in a conceptual runoff model, *Hydrol. Processes*, 17(2), 379-390. 10.1002/hyp.1130.

Sklash, M.G., M.K. Stewart and A.J. Pearce (1986), Storm runoff generation in humid headwater catchments: 2. A case study of hillslope and low-order stream response, *Water Resour. Res.*, 22(8), 1273-1282. 10.1029/WR022i008p01273.

Sophocleous, M. (2002), Interactions between groundwater and surface water: The state of the science, *Hydrogeol. J.*, 10(1), 52-67. 10.1007.2Fs10040-001-0170-8.

Soulsby, C., C. Birkel, J. Geris, J. Dick, C. Tunaley and D. Tetzlaff (2015), Stream water age distributions controlled by storage dynamics and nonlinear hydrologic connectivity: Modeling with high-resolution isotope data, *Water Resour. Res.*, 51(9), 7759-7776. 10.1002/2015WR017888.

Stewart, M.K. and J.J. McDonnell (1991), Modeling base flow soil water residence times from deuterium concentrations, *Water Resour. Res.*, 27(10), 2681-2693. 10.1029/91WR01569.

Stewart, M.K., J. Mehlhorn and S. Elliott (2007), Hydrometric and natural tracer (oxygen-18, silica, tritium and sulphur hexafluoride) evidence for a dominant groundwater contribution to pukemanga stream, New Zealand, *Hydrol. Processes*, 21(24), 3340-3356. 10.1002/hyp.6557.

Tague, C. and G.E. Grant (2004), A geological framework for interpreting the low-flow regimes of cascade streams, willamette river basin, oregon, *Water Resour. Res.*, 40, W04303. 10.1029/2003WR002629.

Tetzlaff, D., J. Seibert, K.J. McGuire, H. Laudon, D.A. Burns, S.M. Dunn and C. Soulsby (2009), How does landscape structure influence catchment transit time across different geomorphic provinces?, *Hydrol. Processes*, 23(6), 945-953. 10.1002/hyp.7240.

Todd, D.K. (1956), Ground-water flow in relation to a flooding stream, pp. 1-20, ASCE.

Vaché, K.B. and J.J. McDonnell (2006), A process-based rejectionist framework for evaluating catchment runoff model structure, *Water Resour. Res.*, 42(2). 10.1029/2005WR004247.

Van Der Kamp, G. and J. Gale (1983), Theory of earth tide and barometric effects in porous formations with compressible grains, *Water Resour. Res.*, 19(2), 538-544. 10.1029/WR019i002p00538.

Voltz, T., M. Gooseff, A.S. Ward, K. Singha, M. Fitzgerald and T. Wagener (2013), Riparian hydraulic gradient and stream-groundwater exchange dynamics in steep headwater valleys, *Journal of Geophysical Research: Earth Surface*, 118(2), 953-969. 10.1002/jgrf.20074.

Ward, A.S., R.A. Payn, M.N. Gooseff, B.L. Mcglynn, K.E. Bencala, C.A. Kelleher, S.M. Wondzell and T. Wagener (2013), Variations in surface water-ground water interactions along a headwater mountain stream: Comparisons between transient storage and water balance analyses, *Water Resour. Res.*, 3359–3374. 10.1002/wrcr.20148.

Weiler, M., B.L. Mcglynn, K.J. McGuire and J.J. McDonnell (2003), How does rainfall become runoff? A combined tracer and runoff transfer function approach, *Water Resour. Res.*, 39(11), 1315, doi:1310.1029/2003WR002331.

Weiler, M. and J. McDonnell (2004), Virtual experiments: A new approach for improving process conceptualization in hillslope hydrology, *J. Hydrol.*, 285(1-4), 3-18. 10.1016/S0022-1694(03)00271-3.

Weiler, M. and J.J. McDonnell (2007), Conceptualizing lateral preferential flow and flow networks and simulating the effects on gauged and ungauged hillslopes, *Water Resour. Res.*, 43(3). 10.1029/2006WR004867.

Winter, T.C., D.O. Rosenberry and J.W. Labaugh (2003), Where does the ground water in small watersheds come from?, *Ground Water*, 41(7), 989-1000. 10.1111/j.1745-6584.2003.tb02440.x.

Woods, R. and L. Rowe (1996), The changing spatial variability of subsurface flow across a hillside, *Journal of Hydrology New Zealand*, 35(1), 51-86.

CHAPTER 3

GEOLOGIC CONTROL ON THE SEASONALITY OF RECHARGE IN THE CRITICAL ZONE

Status: Submitted September 2017

Citation: Gabrielli, C.P., J.J. McDonnell (2017), Geologic control on the seasonality of recharge in the critical zone. *Water Resources Research*, in review.

3.1 Abstract

The mechanisms and processes controlling the timing and magnitude of recharge to headwater aquifers are not fully understood. Here we study the controls of geology on the mechanisms of bedrock groundwater recharge and examine specifically how bedrock characteristics mediate seasonal patterns of deep groundwater recharge in the well-studied steep and wet Maimai headwater catchment in New Zealand. We found extreme seasonality in the timing of bedrock recharge despite almost no seasonality in annual precipitation and little seasonality in catchment runoff. Isotopic analysis and noble gas measurements of bedrock groundwater revealed that recharge occurs almost exclusively during the cold winter months. We developed a simple empirical recharge model that showed nearly 60% of annual recharge was produced from only 25% of annual precipitation during the 3 peak winter recharge months. In contrast, during the 3 peak summer months only 2.4% of annual recharge was produced from almost the same volume of precipitation – resulting in a 24-fold difference in recharge efficiency between peak summer and winter months. A comprehensive bedrock characterization of 40 bedrock wells and a new plot-scale sprinkler and tracer experiment identified a distinct lack of bedrock fractures. The absence of fractures forced all bedrock recharge to occur through the low permeability bedrock matrix. We found that during winter months recharge was geologically mediated by the ability of the bedrock to transfer water to depth. During the summer period, we hypothesize that the well-documented

hillslope-scale preferential flow networks allow quick shedding of stormflow from the catchment accounting for high runoff ratios despite minimal recharge. The increased summer evapotranspiration flux depletes between-storm soil moisture, largely negating summer bedrock recharge. We found no correlation between monthly, seasonal or annual precipitation and recharge. This work shows that a simple and temporally stable rainfall-runoff relation can mask a highly seasonal and geologically controlled recharge regime. It is a cautionary tale for predictions of recharge scenarios based solely on precipitation and/or runoff dynamics, even in wet regions.

3.2 Introduction

Groundwater recharge in steep wet headwater catchments is often poorly studied and poorly described in the hillslope hydrology literature. That is because most of the work in the field to date has focused on event-scale runoff dynamics (i.e. lateral flow) through the often thin veneer of soil covering steep, wet hillslopes (*Hewlett and Hibbert, 1967; Harr, 1977; Mosley, 1979; Sklash and Farvolden, 1979*). In the past two decades, process studies have begun to explore storage and runoff mechanisms extending much deeper into the critical zone to include saprolite and bedrock that underlie steep slopes (*Kosugi et al., 2006*). New flowpath insights (*Anderson et al., 1997*), new runoff generating mechanisms (*Katsura et al., 2014*), new storage release processes (*Sayama et al., 2011*) and new understanding of the time-varying controls on streamwater mean transit time (*Katsuyama et al., 2010; Asano and Uchida, 2012; Hale and McDonnell, 2016*) have all evolved from this consideration of the deeper system within headwaters.

But despite the now considerable body of literature on catchment storage release and drainage of the headwater aquifer (*Brutsaert and Nieber, 1977; Tallaksen, 1995; Kirchner, 2009; Price, 2011*), there is comparatively little work focused on the processes and mechanisms that control recharge to this aquifer (e.g. *Wilson and Guan (2004)*). This is in part due to the extreme difficulty and time-consuming nature of such characterization. Measuring the spatial patterns of soil depth, the characteristics of the soil-bedrock interface and the nature of below-soil saprolite, weathered and unweathered bedrock on steep hillslopes is a major challenge. And only a few studies have done this (*Anderson et al., 1997; Kosugi et al., 2008*). Additionally, precisely measuring and quantifying recharge can be complex, convoluted and contain large uncertainties (*Scanlon et al., 2002*). All of

this explains why estimates of groundwater recharge in headwater catchments have often used hydrograph dynamics and water balance measurements as a proxy for water that does or does not infiltrate into the deeper system (*Lee et al.*, 2006; *Kirchner*, 2009; *Price*, 2011), or why many studies focus solely on the timing or magnitude of recharge, but lack process-based insights to the internal mechanisms controlling observed dynamics (*Winograd et al.*, 1998; *Gleeson and Manning*, 2008; *Smerdon et al.*, 2009; *Welch et al.*, 2012; *Taylor et al.*, 2013a). Consequently, our understanding of groundwater in steep, wet headwaters is skewed heavily toward general hydrograph-derived metrics of storage and release (*Eckhardt*, 2005; *Hammond and Han*, 2006; *Wagner et al.*, 2007) with relatively few insights into the fundamental controls on groundwater infiltration and recharge, its spatial and temporal dynamics, the hierarchy of these controls and how they link to storage and release of the underlying headwater aquifer.

Groundwater recharge in headwater catchments is vital to maintaining groundwater resources in lower lying areas (*Winter et al.*, 1998), as recharge in the headwaters is often greater than lower relief portions of the landscape (*Jasechko et al.*, 2016). Catchment scale modeling exercises have provided valuable insight into headwater recharge processes. *Gleeson and Manning* (2008) illustrated landscape scale controls on the headwater aquifer by revealing how complex interactions between topography, hydraulic conductivity, and recharge control partitioning of flow between local and regional groundwater systems. At the hillslope scale, bedrock surface topography, combined with soil depth and storm size, have been shown to control the formation and location of fill and spill features at the soil-bedrock interface (e.g. *Tromp-van Meerveld and McDonnell* (2006)). These zones of transient saturation can act as locations of preferential deep recharge when they overlap regions of higher bedrock permeability (*Hopp and McDonnell*, 2009).

Recent hillslope-scale irrigation experiments have begun to further elucidate the controls and characteristics of hillslope-scale groundwater recharge dynamics (*Brooks et al.*, 2004; *Tromp-van Meerveld et al.*, 2007; *Graham et al.*, 2010a; *Jackson et al.*, 2016; *van Verseveld et al.*, 2017). These studies have shown generally that bedrock properties influence subsurface stormflow dynamics and the hillslope and catchment scale water balance; but how bedrock characteristics influence the mechanisms controlling the proportion of deep recharge is still poorly understood.

Fracture networks within hillslope bedrock have been highlighted as important transport pathways capable of carrying large volumes of soil water to depth over short time intervals (*Montgomery et al.*, 1997; *McGuire and McDonnell*, 2010). These preferential flowpaths can provide rapid and localized recharge to the underlying aquifer, controlling seasonal variations in recharge (*Abbott et al.*, 2000), groundwater isotopic signatures (*Gleeson et al.*, 2009) and catchment water balance (*Iwasaki et al.*, 2014). *Appels et al.* (2015) showed, however, that although fractures (represented as zones of higher bedrock permeability) were critical to modeled recharge dynamics when event-based saturation existed at the soil-bedrock interface, slower more persistent unsaturated vertical flux contributed greater total volume to annual deep recharge at the hillslope scale – revealing the complex nature of bedrock interactions on recharge.

Although it is clear that the soil-bedrock interface characteristics and soil moisture patterns are critical to recharge, many questions remain: What conditions are required to initiate bedrock groundwater recharge in the headwaters? What are the spatial and temporal patterns of these conditions? How do soil and bedrock characteristics work in concert (or in opposition) for deep recharge? And, how is total recharge magnitude and timing set by hydroclimatic, colluvial and geologic interactions?

Here we seek answers to these questions through a coupled field and modelling based approach using data from the well-studied Maimai, M8 watershed in New Zealand. We remove the hillslope soil mantle to determine bedrock characteristics and to determine its role in redistributing water to depth, and we drill the critical zone down to 9 m at 40 locations across our 4.5 ha catchment to explore the depth and hydraulic characteristics of the unsaturated bedrock above the water table and below the soil-bedrock interface. Recent work by *Gabrielli et al.* (2017) has shown that the spatial extent, dynamics, and age of underlying bedrock aquifer, as well as its contribution to streamflow and influence of streamwater age, are controlled by bedrock permeability. We leverage new noble gas recharge temperature data, groundwater isotopic composition and long term climatic and runoff data to explore directly the hillslope-scale groundwater recharge processes at this steep wet site. In so doing, we connect independent data sets to establish a coherent and parsimonious description of catchment scale subsurface hydrologic partitioning, and further build

upon the long Maimai legacy and its critical role in long-term hydrologic monitoring and discovery. Finally, we examine the connections between seasonal climate patterns and groundwater hydrochemistry, age, and storage dynamics to specifically ask:

- i. How do bedrock characteristics control recharge mechanisms?
- ii. When does groundwater recharge occur on the steep hillslopes?
- iii. How does the soil mantle affect the recharge process?
- iv. How does Maimai compare to other sites?

3.3 Study site

The Maimai is located approximately 15 km inland from the northwest coast of the South Island of New Zealand (Figure 3.1; 42°05'S 171°47'E). The highly dissected landscape is defined by its short steep slopes, thin soils and high runoff ratios. Hillslope lengths average less than 50 m and average slope angle is 34° with short sections nearing 55°.

The wet temperate coastal environment produces, on average, 2600 mm of rainfall annually with nearly 150 rain-days per year. Frontal systems moving in from the Tasman Sea produce long duration low intensity storms, with average rainfall intensities of ~1.2 mm/h, although storms have produced intensities upwards of 30 mm/h and it is not uncommon for total rainfall to exceed 100 mm for single events. There is a slight seasonality in the rainfall regime with the mid-winter months (Jul-Aug) being the wettest and mid-summer (Jan-Feb) being the driest. The low catchment elevation and proximity to the coast result in only 1-2 snow days each year which melt within hours to days.

The constant rainfall results in persistently high antecedent conditions and a soil mantle that remains within 10% of saturation for most of the year (*McGlynn et al.*, 2002). The catchment is defined by its highly responsive and flashy storm hydrograph. An annual runoff ratio of ~60% is among the highest of any research catchment reported in literature (*Anderson and McDonnell*, 2005). Approximately 1000 mm (65%) of the 1550 mm of average annual runoff leaves the

catchment as quickflow, as defined by the *Hewlett and Hibbert (1967)* separation method (*McDonnell, 1990*).

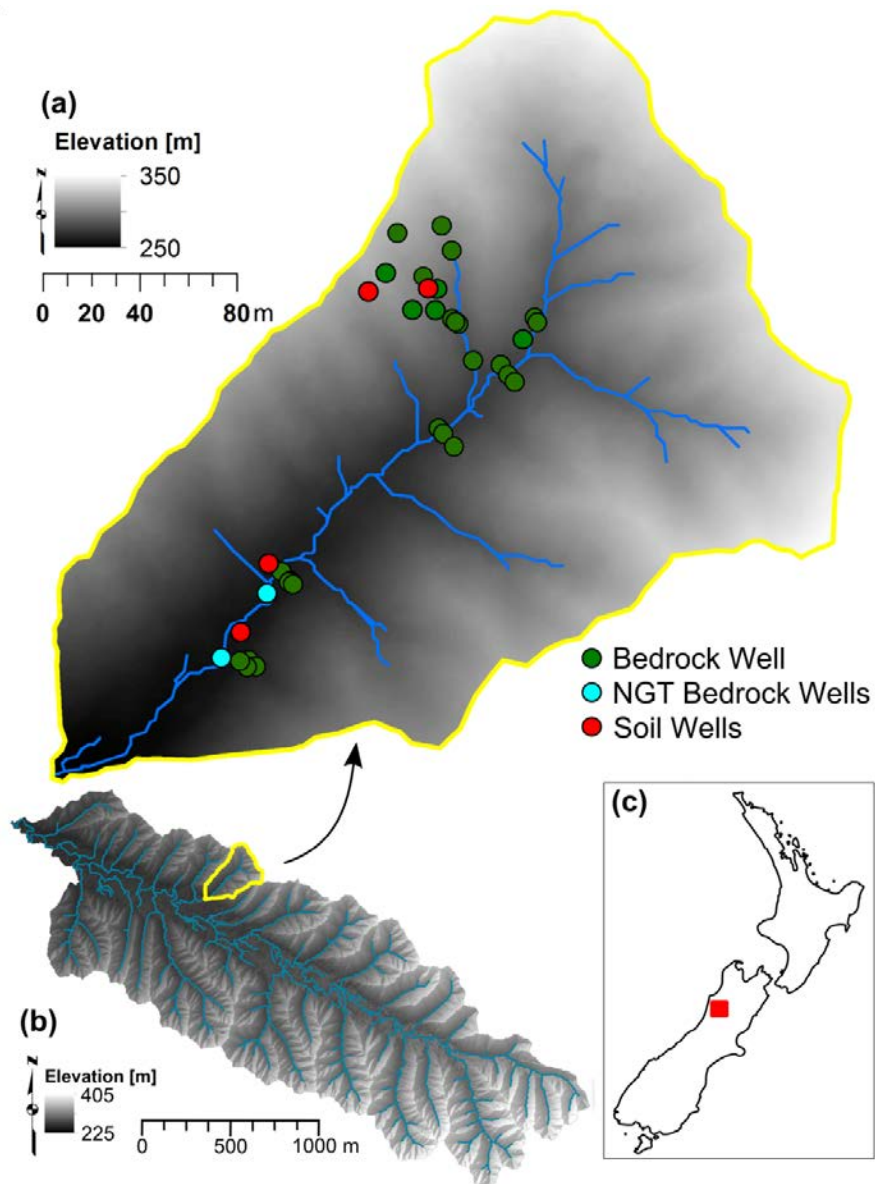


Figure 3.1 M8 sub-catchment with location of bedrock and soil wells (a) Maimai Experimental Watershed (b) and New Zealand locational inset (c). NGT wells are those sampled for noble gas recharge temperature (NGT) measurements.

Soils are thin (range: 0.1 - 1.8 m, average: 0.6 m) and broadly classified as Blackball Hill soils (*McDonnell, 1990*). They are characterized as podsolized to mottled yellow-brown earths along the hillslopes and ridges and gley soils within the poorly drained hollows and riparian zones.

Infiltration capacity in the top 170 mm humic horizon is as great as 6100 mm/hr and average hydraulic conductivity of the upper mineral soil is on the order of 250 mm/h (*McDonnell*, 1990).

The bedrock underlying the catchment is known as Old Man Gravel (OMG) belonging to a larger formation known as the Old Man Group (*Bowen*, 1967) which was laid down in the early Pleistocene as a thick (> 400 m) layer of glacial outwash during an erosional sequence in the formation of the Southern Alps (*Mortimer et al.*, 2001). The bedrock is a conglomerate composed primarily of sandstone clasts (greywacke) with small additions of schist and granite in a compact weakly cemented sandy-clay matrix. The rounded clasts range in size from 10 to 500 mm in diameter, but are predominantly less than 200 mm in diameter (*Mortimer et al.*, 2001).

This research is focused primarily in the 4.5 ha M8 sub-catchment (Figure 1) within the Maimai. Landscape structure, geology, soil and runoff characteristics in the M8 are similar to that of the other sub-catchments within the larger Maimai Experimental Watershed (*McGlynn et al.*, 2004). Total catchment relief in M8 is approximately 100 m with elevations ranging from 250 to 350 m.a.s.l. For review of previous research at M8, see *McGlynn et al.* (2002).

3.4 Data and methods

Our study approach starts by defining bedrock characteristics and the mechanism of bedrock groundwater recharge through borehole testing and a plot-scale sprinkler experiment. Seasonality in bedrock recharge is then identified through groundwater measurements of noble gas and stable isotopes of water. Armed with the understanding of bedrock infiltration processes we quantify seasonal fluctuations in hydroclimatic forcing that drive catchment wetness conditions which control temporal recharge patterns. We construct a simple empirical recharge model constrained by known mean annual recharge magnitude and temperature to explore intra and inter-annual patterns of bedrock recharge timing and volume over a 13-year period. Our findings are related to seasonality of various hydroclimatic metrics. We finish by running the model for an additional 1 year period and compare results to daily soil water data to further identify linkages between

catchment wetness patterns, soil water dynamics, runoff characteristics, geology and the seasonality of recharge.

3.4.1 Bedrock characteristics and recharge mechanisms

3.4.1.1 Hydraulic conductivity

Average bedrock saturated hydraulic conductivity (K_{sat}) was determined for 4 major landscapes units within the catchment: the riparian zone, toe-slopes, hillslopes and ephemeral hollows. Forty bedrock wells were drilled within these landscape positions and K_{sat} was calculated following the *Hvorslev* (1951) approach using falling-head slug test data, as outlined in *Gabrielli et al.* (2017).

3.4.1.2 Sprinkler Experiment: Bedrock infiltration rate and mechanisms of recharge

We conducted a plot scale sprinkler experiment on an exposed section of bedrock to identify the flow mechanisms associated with bedrock groundwater recharge and to test plot-scale bedrock infiltration rates. We specifically sought to distinguish between recharge by bedrock fracture flow and recharge by diffuse matrix flow. Fracture flow in steep headwater catchments has been shown to move subsurface storm flow rapidly to depth on time scales of individual storm events (*Montgomery et al.*, 1997), while diffuse porous media flow is governed by the primary porosity of the bedrock matrix and occurs over much greater time scales. We expected these different mechanisms of bedrock recharge to be associated with different catchment wetness conditions and different hydroclimatic temporal patterns.

The sprinkler experiment was conducted on a previously trenched and instrumented planer hillslope just downstream of the main M8 catchment weir (*Woods and Rowe*, 1996; *Graham et al.*, 2010b). A small landslide occurred in 2013 on the hillslope removing the overlying colluvium down to the soil-bedrock interface over an area of approximately 300 m² (30 m upslope by 10 m across slope). We constructed a 150 mm tall cement perimeter around the landslide scar to isolate and collect surface runoff from within the landslide area.

Water was pumped from a 200 L stilling basin through a sprinkler system onto the open bedrock surface. Surface runoff was collected and routed back to the stilling basin creating a closed loop system. Once the initial bedrock surface storage was filled, bedrock infiltration and surface evaporation represented the only withdrawal of water from the system. To isolate bedrock infiltration from evaporative loss, we assumed no evaporation between the hours of 22:00 and 06:00. A capacitance-type water level logger (Odyssey®), recording at 10 minute intervals, measured the drop in water level within the stilling basin. Using the surface area of the stilling basin, the drop in water level was converted to a volumetric loss rate equal to the rate of water lost to the bedrock. We operated the sprinkler continuously for 96 hours, providing 4 nights of measurements. In traditional sprinkler experiments where prescribed rainfall rates rarely exceed the soil infiltration capacity, large volumes of input water are required along with precise control of pumping and sprinkler rates. These requirements have historically made field-based sprinkler experiments logistically difficult to perform. However, our sites' absence of soil, low bedrock infiltration rates, and the collection of applied sprinkler water allowed for a simple and novel permutation of the traditional sprinkler experiment. Because the rainfall application rate was much greater than bedrock infiltration, excess surface water was always present at the bedrock surface. This condition made it possible to relax the need for exact control or knowledge of sprinkling rates, considerably simplifying the field design.

Bedrock infiltration was determined by fitting a linear regression to stilling basin water level measurements for each night. The slope of the line (m/h) multiplied by the surface area of the stilling basin (m^2) equaled the volumetric loss rate of water from the system (m^3/h). We averaged the slopes from the 4 nights to create a master slope. Finally, this average volumetric loss rate was divided by the wetted bedrock area ($\sim 10 \text{ m}^2$) to determine the plot-scale bedrock infiltration rate.

We additionally conducted tracer and hydrometric analysis to identify bedrock flow paths and distinguish between fracture and matrix flow. We recorded water table elevation in two bedrock wells, one located within the wetted area and one located just downslope, to capture rapid infiltration of sprinkler water to the water table. Brilliant blue dye and a salt slug (concentration of 200 mg/L) were added to the pumped water at hour 48. We monitored bedrock groundwater

electrical conductivity prior to, during, and for 120 hours after the sprinkler experiment concluded, to identify the breakthrough curve of infiltrating water. Finally, we destructively analyzed the bedrock surface at the end of the experiment to identify bedrock flowpaths. Visual observations were taken to quantify depth of dye penetration and degree of bedrock fracturing.

3.4.2 Recharge seasonality

3.4.2.1 Noble gas measurements

Atmospheric gases are taken into solution by rainfall and soil water at concentrations proportional to the local environmental temperature (*Lindsay, 1979*), and concentrations of dissolved noble gases remain fixed once soil water intercepts the saturated zone. By measuring noble gas concentration in groundwater samples – and correcting for measured excess gas – the environmental temperature under which groundwater was recharged can be determined (*Burnard, 2013*). This technique, known as the noble gas recharge temperature (NGT), has traditionally been employed in sedimentary systems for paleoclimatology studies where NGT values reflect local mean annual air temperature (MAAT) at the base of the vadose zone (*Stute et al., 1992*). However, recent work in two separate fractured bedrock systems has shown that NGTs can vary greatly from MAAT (*Warrier et al., 2012; Niu et al., 2017*). In these situations, NGT instead reflects environmental conditions during seasonally focused recharge periods and provides a means to directly identify seasonally selective patterns in groundwater recharge by matching NGT values to seasonal environmental temperature variations.

We analyzed gas concentrations in groundwater samples taken from two bedrock wells located in the toe-slope and riparian zone within the lower part of the M8 catchment (Figure 3.1). Samples were collected under deep baseflow conditions and 3 well volumes were evacuated from each well prior to sampling. Dissolved Argon (Ar) and Nitrogen (N₂) were measured in both samples at the GNS Science Stable Isotope Laboratory (Lower Hutt, New Zealand) and NGT was determined using the standard graphical method (*Heaton and Vogel, 1981; Bohlke and Krantz, 2003*).

3.4.2.1 Stable isotope measurements

We used the possible existence of a seasonal contrast in isotopic composition between soil and bedrock groundwater to further test for seasonally selective bedrock groundwater recharge. Soil water mean transit time was previously established at less than 4 months for the M8 catchment (*Stewart and McDonnell, 1991*). Late summer soil-water was therefore expected to heavily reflect the isotopic composition of summer precipitation. Due to simple temperature driven fractionation, bedrock groundwater was expected to have an isotopic composition distinctly more depleted than late summer soil water if recharged was sourced primarily from colder winter soil water (*Kendall and McDonnell, 2012*).

We collected soil, surface and bedrock groundwater samples for isotope analysis over 3 sampling periods all under summer low flow conditions. Specific sampling dates were: Jan 16, 2015, Feb 1, 2015 and Feb 24, 2015. Streamwater was collected at the catchment weir during each sampling period, and different soil and bedrock wells were sampled for each of the three periods. Samples collected during the first two periods were stored in 30 ml glass scintillation vials and sealed with para-film. Samples were analyzed at the Watershed Hydrology Lab at the University of Saskatchewan using a Los Gatos Research liquid water isotope analyzer that utilizes high-resolution laser absorption spectroscopy. Analytical precision was ± 0.2 ‰ for O18 and ± 1.0 ‰ for 2H. Samples from Feb 24, 2015 were analyzed at the GNS Science Stable Isotope Laboratory (Lower Hutt, New Zealand). Samples were analyzed using a GVI Isoprime mass spectrometer coupled with a PyrOH elemental analyzer. Analytical precision was ± 0.1 ‰ for O18 and ± 1.0 ‰ for 2H.

3.4.3 Climatic and hydrologic seasonality

To identify seasonality in climate and hydrologic metrics, we used long term rainfall-runoff records from the M8 subcatchment within Maimai, as well as publically available data from a meteorological station maintained by the New Zealand National Institute of Water and Atmospheric Research located in the township of Reefton, 5 km west of Maimai (Lat: -42.11578, Long:171.86014).

Daily rainfall (P) and catchment discharge (Q_{tot}) were measured at M8 from 1975-1987. Rainfall was recorded using a tipping bucket rain gauge located 500 m from the M8 outlet, and M8 discharge was recorded with a 90° v-notch weir located within M8. We also calculated baseflow (Q_{base}) using a recursive digital filter on 1-hour discharge data via the WHAT hydrograph analysis tool (*Lim et al.*, 2005). Direct runoff (Q_{dir}) was also calculated as total runoff minus baseflow ($Q_{\text{tot}} - Q_{\text{base}}$). We used daily temperature records (T) from the Reefton met station to calculate potential evapotranspiration (PET) from 1975-87 using the *Thornthwaite* (1948) approach. Monthly averaged T , P , Q_{tot} , Q_{base} , Q_{dir} and PET over the 13-year monitoring period were used to identify intra and inter annual seasonal trends.

3.4.4 Bedrock groundwater recharge model

We constructed a simple empirical recharge model combined with a temperature-based energy balance to explore temporal patterns of bedrock groundwater recharge over the 13-year period from 1975-1987. We used inverse modeling to identify the best fitting parameter set that constrained model output to known observations of annual bedrock groundwater recharge depth and temperature, and compared the resulting temporal pattern of recharge to hydroclimatic variables. Finally, we modeled bedrock groundwater recharge for the year 2015 using the previously established parameter set and compared model output to daily soil water data to further elucidate the temporal linkages between catchment storage conditions, soil water states and bedrock recharge.

We used this simple modeling exercise not to identify or capture exact physical processes of groundwater recharge or bedrock infiltration, but instead to identify how seasonal patterns of recharge associated with seasonal climate, storage and wetness conditions and to understand how bedrock characteristics may shape these associations.

3.4.4.1 The model

We assumed that bedrock groundwater recharge was primarily controlled by catchment wetness conditions. We therefore used a simple water balance approach focusing on dynamic storage

(DS(t)) as a proxy for catchment wetness and as the single input variable to the model. DS(t) was calculated as:

$$DS(t) = P(t) - Q(t) - PET(t) \quad (\text{Eq. 3.1})$$

Where P is precipitation, Q is streamflow and PET is potential evapotranspiration as described above. DS(t) was calculated on a daily time step from 1975-1987.

Bedrock recharge, I(t), was then calculated on a daily time step using a simple 3 parameter model, such that:

$$I(t) = \left\{ \begin{array}{ll} 0 & \text{if } DS(t) < 0 \\ Ksat * \alpha_1 & \text{if } 0 < DS(t) < \beta \\ Ksat * \alpha_2 & \text{if } DS(t) > \beta \end{array} \right\} \quad (\text{Eq. 3.2})$$

Where Ksat is equal to the sprinkler experiment derived bedrock infiltration rate, α_1 and α_2 are scaling factors such that $\alpha_1 < \alpha_2$ and $0 \leq [\alpha_1, \alpha_2] \leq 1$, and β is a threshold value delimiting between lower and higher rates of recharge. This simple empirical model allowed for 3 rates of bedrock recharge based on different catchment wetness conditions providing a limited amount of flexibility to more realistically capture differential rates of recharge associated with changes in catchment wetness conditions. All infiltration into the bedrock was assumed to reach the bedrock groundwater table.

Since the focus of this modeling exercise was to identify temporal trends in bedrock infiltration we included a temperature-based energy balance to constrain the timing of recharge determined by equation 3.2. That is, it is possible that modeled recharge from equation 3.2 could equal the observed annual recharge depth, but timing of recharge would not match observation. Including a temperature-based weighting of infiltration ensured both timing and magnitude of recharge were

captured. To accomplish this, we calculated the mean weighted annual recharge temperature, T_I , as:

$$T_I = \sum_{i=1}^t \frac{I_i * T_i}{y * I_{tot}} \quad (\text{Eq. 3.3})$$

Where I_i is daily infiltration as calculated in equation 3.2, T_i is daily air temperature based on records from the Reefton met station, I_{tot} is the total infiltration over the full time series, and y is the number of years modeled. This approach weighted daily recharge by the daily air temperature, providing a means to calculate the mean annual temperature of modeled bedrock recharge. Using the parameter identification processes described below, we then constrained the model output to known annual bedrock recharge depth and temperature.

3.4.4.2 Parameter identification and model input filtering

Parameter identification was conducted by varying α_1 and α_2 from 0 to 1.0 in 0.001 increments, and β from 0.1 to the maximum value of DS(t) on an interval that produced 50 equally spaced steps. Model output was compared to target values of annual bedrock groundwater recharge and temperature. Bedrock groundwater recharge at Maimai has been reported between 100 mm (*Pearce and McKerchar, 1979*) and 200 mm annually (*Gabrielli et al., 2017*). We used 150 mm as the model target. Target mean annual groundwater recharge temperature was based on the mean of the two NGT values as described above.

We evaluated the goodness of fit for each parameter set using the least squares method as our objective function. The least squares method minimizes residuals between modeled and target values. A final best-fitting parameter set was identified and seasonal variability in modeled recharge and hydroclimatic variables were compared.

As an additional step in the modeling process we applied a wavelet-based low pass filter to the daily DS(t) time series. Temporal patterns of groundwater recharge have been commonly observed to follow seasonal trends across a range of geologic and climatic settings (*Gee and Hillel, 1988*;

O'Driscoll et al., 2005; Scanlon et al., 2006; Dripps and Bradbury, 2007; Jasechko et al., 2014). These longer-term seasonal trends are generally associated with subtle seasonal shifts in climate forcing that are embedded within the higher frequency daily or weekly climate patterns. In order to explore if longer-term patterns of recharge were driven by longer-term patterns of catchment wetness conditions we applied the low pass filter to the DS(t) input function using 10 different filter lengths to extract embedded lower frequency signals. The filtered DS(t) signal reflects changes in catchment wetness associated with the length of the applied filter, so that a 0-day filter equals the unfiltered daily DS(t) signal, while a 30-day filter corresponds to monthly variations in DS(t), and a 180-day filter corresponds to summer-winter seasonal variations. We specifically tested filter lengths of 0, 3, 6, 13, 25, 50, 100, 200, 400, and 800 days to examine how shifts in catchment wetness control shifts in bedrock recharge on time scales from daily, to weekly, to monthly to seasonally to inter-annually.

3.4.4.3 Soil water comparison

Finally, daily water table depth was monitored in 4 soil wells located in the riparian zone, toe-slope, hillslope hollow and upper hillslope positions within the M8 catchment for the 2015 calendar year. We compared soil water depth with calculated 2015 DS(t) and bedrock groundwater recharge to identify how patterns in catchment wetness linked to soil water storage and modeled recharge.

3.5 Results

3.5.1 Mode of recharge: Bedrock sprinkler experiment and bedrock characterization

3.5.1.1 Bedrock Characterization

Spatial patterns of saturated bedrock hydraulic conductivity largely followed the main geomorphic landscape units within the catchment. Although considerable variability existed within each landscape unit, mean hydraulic conductivity increased from hillslope to hollow to toe-slope to the riparian zone. Mean values, respectively, were 5.5×10^{-8} m/s, 7.5×10^{-7} m/s, 7.2×10^{-6} m/s and 1.6×10^{-5} m/s (Table 3.1).

Table 3.1 Landscape position and mean saturated hydraulic conductivity (Ksat) values for the 40 bedrock wells tested through falling-head slug tests.

Landscape unit	Number of wells	Mean Ksat, m/s	± 1 standard deviation, m/s
Hillslope	13	5.5×10^{-8}	8.8×10^{-8}
Hollow	10	7.5×10^{-7}	1.2×10^{-6}
Toe-slope	6	7.2×10^{-6}	8.0×10^{-6}
Riparian	11	1.6×10^{-5}	2.0×10^{-5}

3.5.1.2 Sprinkler Experiment

During the 96-hour sprinkler experiment an equivalent rainfall depth of 4950 mm, or approximately 2 years of rainfall, was applied to the 10.5 m² open bedrock surface. Figure 3.2 shows the water elevation time series from the stilling basin during the sprinkler experiment. Linear regression models fit well to water table drawdown data for each night (R^2 : 0.99, 0.97, 0.99, 0.98 for nights 1-4, respectively), indicating a relatively constant rate of bedrock infiltration through each evening. Water loss from the stilling basin ranged from 0.70 to 3.97 l/h and averaged 2.2 ± 1.17 l/h, corresponding to an average bedrock infiltration rate of $5.69\text{E-}08 \pm 3.09\text{E-}8$ m/s. The sprinkler-based mean bedrock infiltration rate corresponded well to the mean saturated hydraulic conductivity of hillslope bedrock wells tested via slug tests (Table 3.1) and also to both previous measurements at the site (*Graham et al.*, 2010b; *Gabrielli et al.*, 2012).

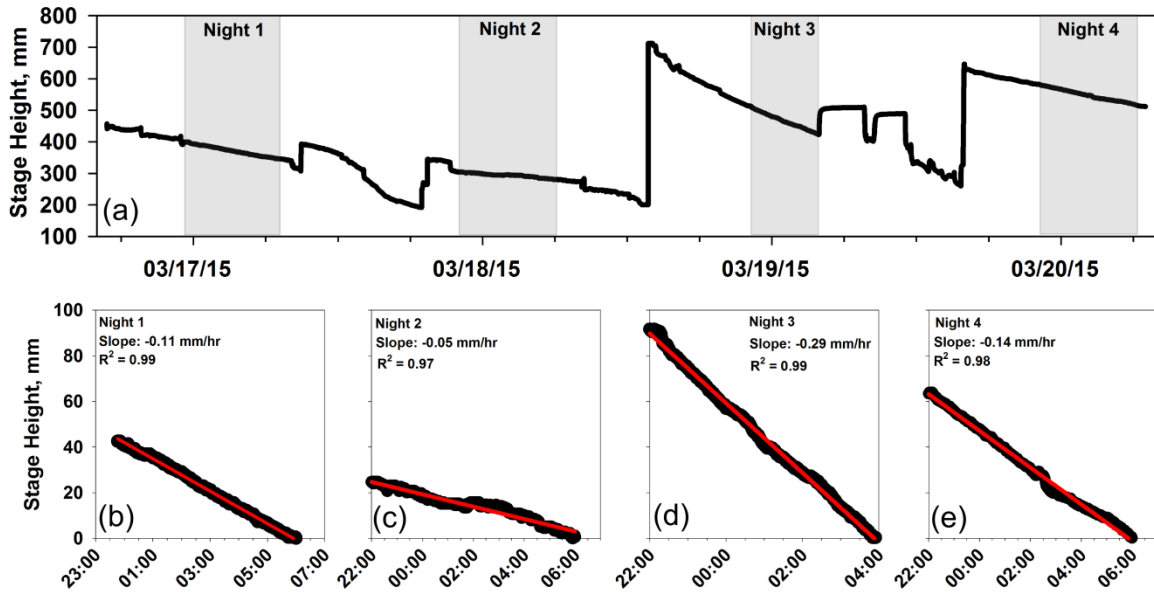


Figure 3.2 Stage height time series of sprinkler stilling basin with highlighted sections showing selected data from each night (a), selected stage data with fitted linear regression (b, c, d and e).

Destructive analysis of the bedrock surface revealed no evidence of fracture pathways within the upper zone of the bedrock across the wetted and dyed area (Figure 3.3a). Dye infiltration was minimal overall, but did show a tendency (visually) towards preferential flow between the clast-matrix boundaries. The embedded and isolated nature of most clasts within the matrix, however, prevented these preferential flowpaths from connecting to deeper zones and these flowpaths occurred only for clasts found within the surface layer of the bedrock (Figure 3.3b). No vertical penetration of dye beyond 5-10 mm was noted within the matrix of the bedrock. This is consistent with the 0.2 mm/h infiltration rate calculated during the experiment. Multiple surface clasts were split immediately after the experiment to see if any blue dye could be detected. After examining 30 pieces from 10 sites on the slope, no visual dye penetration was observed in any sample (Figure 3.3c). Taken together, these observations all suggest a general lack of fracturing or fracture flowpaths within the bedrock, inferring that bedrock recharge likely occurs exclusively as porous media flow through the bedrock matrix.

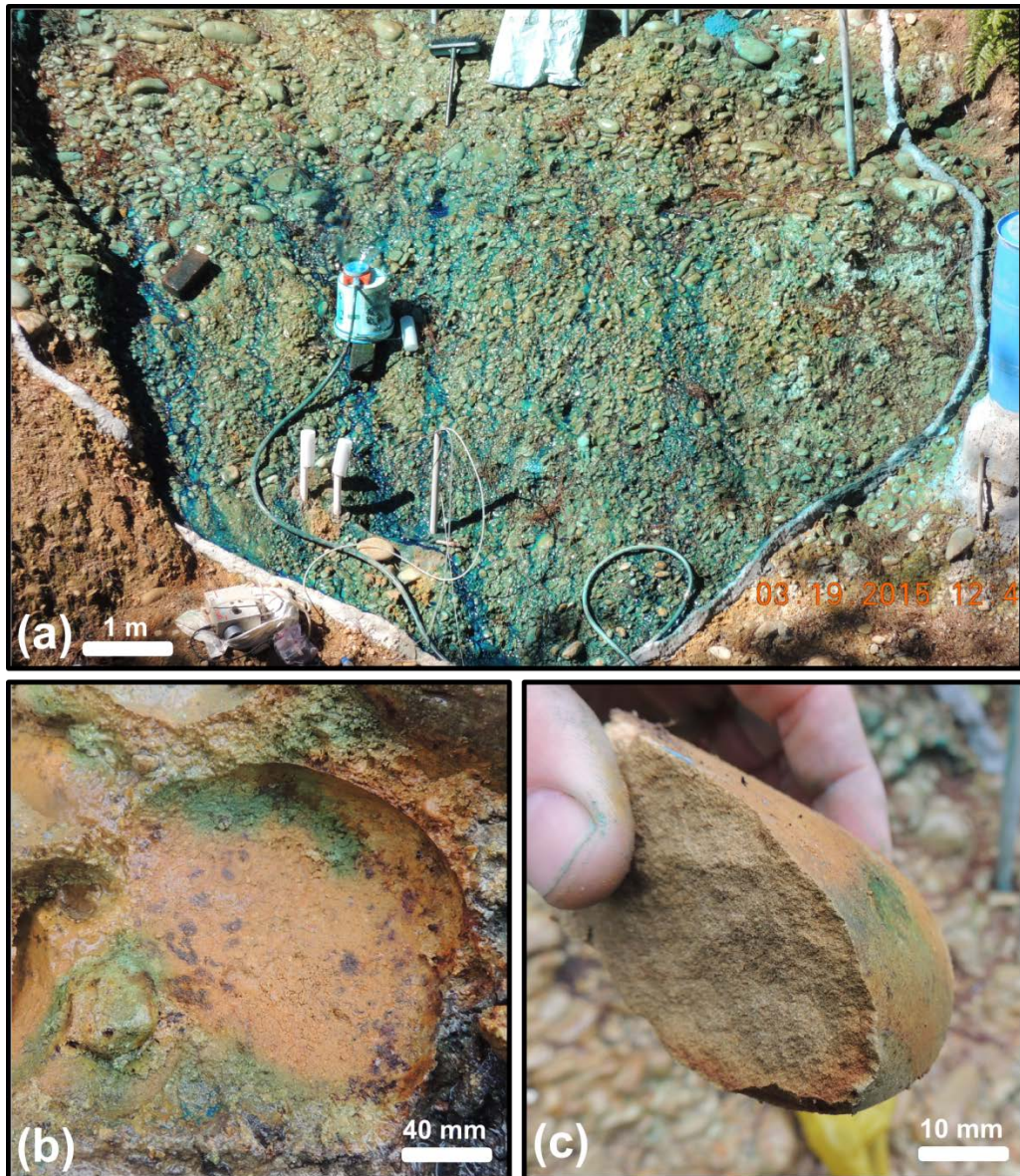


Figure 3.3 Bedrock sprinkler experiment showing brilliant blue dye staining of the bedrock surface and the extent of the sprinkler plot (a). Destructive testing of the bedrock surface post sprinkler experiment revealing minimal matrix penetration and limited preferential flow between the clast-matrix boundary for the surface clasts, this preferential flow did not extend beyond the depth of surface clasts (b). A surface clast freshly split revealing no dye penetration within the clast (c).

Bedrock water table dynamics and electrical conductivity in observation wells remained unchanged during and for 120 hours post-experiment (data not shown), further confirming a general absence of rapid flowpaths through the bedrock. The lack of deviation in the water table and electrical conductivity values also indicated no direct recharge reached the underlying bedrock

water table during the observation period via matrix flow or otherwise, consistent with the measured Ksat and time length of the experiment.

3.5.2 Bedrock groundwater recharge seasonality

We identified groundwater recharge temperatures of 7.6 ± 1.5 °C for bedrock well 1, and 7.2 ± 1.8 °C for well 2 (Figure 3.4a). These NGTs represent the mean volume-weighted annual recharge temperature of the sampled water. Under conditions of uniform monthly recharge, NGT would equal local MAAT, however, local MAAT at Maimai was 11.3 °C, nearly 4 °C warmer than observed recharge temperatures. What's more, mean summer temperature from November through April was 14.8 °C, and mean winter temperature from May through October was 7.8 °C. The significantly colder NGT values that match well to mean winter air temperatures reveal a strong seasonal bias in bedrock groundwater recharge towards colder months indicating bedrock groundwater recharge is sourced primarily from cold season precipitation.

Isotopic composition of the sampled summer stream, soil and bedrock groundwater ranged from -6.61 to 4.53 ‰ $\delta^{18}\text{O}$ and -36.85 to -23.25 ‰ δD (Figure 3.4b). A cluster of bedrock groundwater samples from deep upper-hillslope wells and from identified groundwater discharge zones within the lower riparian corridor showed distinctly depleted isotopic compositions compared to all other streamwater, soil water and shallow bedrock groundwater samples. The distinct isotopic signature of the deeper bedrock groundwater in comparison to other catchment waters provides evidence of recharge to the bedrock aquifer from waters associated with precipitation *outside* of the summer season. The relative depletion of the isotopic signature further supports cold-season precipitation as the source of bedrock groundwater recharge.

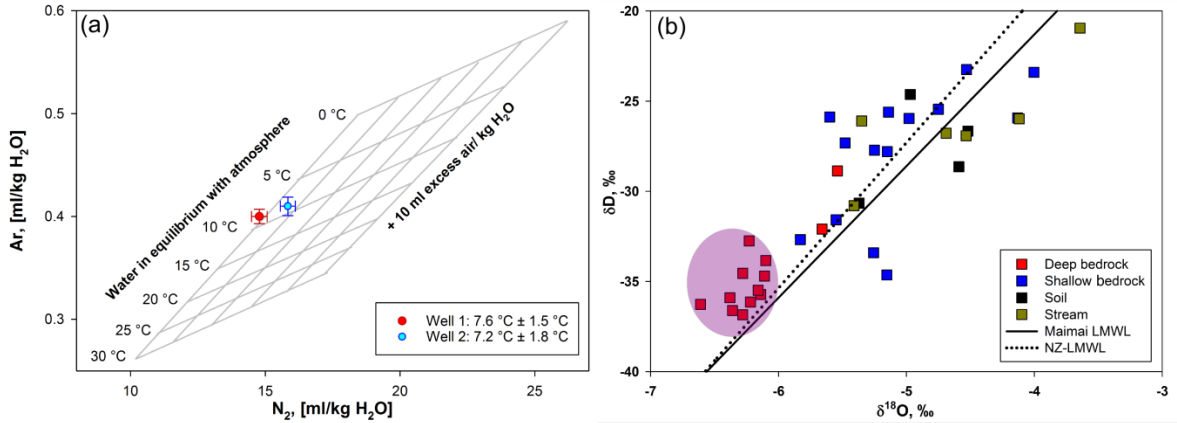


Figure 3.4 Dissolved nitrogen and argon concentrations of well samples overlaid on grid showing atmospheric equilibrium concentration and in the presence of excess air (a), figure style as seen in (*Heaton and Vogel, 1981*). Dual isotope plot of groundwater samples from deep bedrock, shallow bedrock and soil wells in addition to streamwater samples and Maimai and New Zealand local meteoric water lines (LMWL) (b). The shaded region shows the distinctly more negative isotopic signature of the deep bedrock wells, suggesting bedrock groundwater recharge from cold-season precipitation

3.5.3 Bedrock groundwater recharge model

3.5.3.1 DS(t) filter and Parameter Identification

The parameter space for the recharge model is shown in Figure 3.5 for all filter lengths of DS(t). A total of 50,000 parameter sets were tested for each filter length. The 100 and 200-day filtered DS(t) signal were the only two filter lengths, including the unfiltered DS(t) signal, which produced results within ± 50 mm of the target recharge depth (i.e. 150 mm) and within ± 0.5 °C of the target recharge temperature (i.e. 7.4 °C). All other parameter sets under all other filter lengths produced recharge temperatures higher than target values, and most parameter sets and filter lengths produced recharge depths greater than the target recharge depth.

The best-fitting parameter set, associated with the 200-day filter, was identified with $\alpha_1 = 0.03$, $\alpha_2 = 0.33$ and $\beta = 1.22$ mm. Model output for this parameter set obtained a mean annual recharge of 150 mm, and a mean annual recharge temperature of 7.4 °C averaged over the 13-year modeling period.

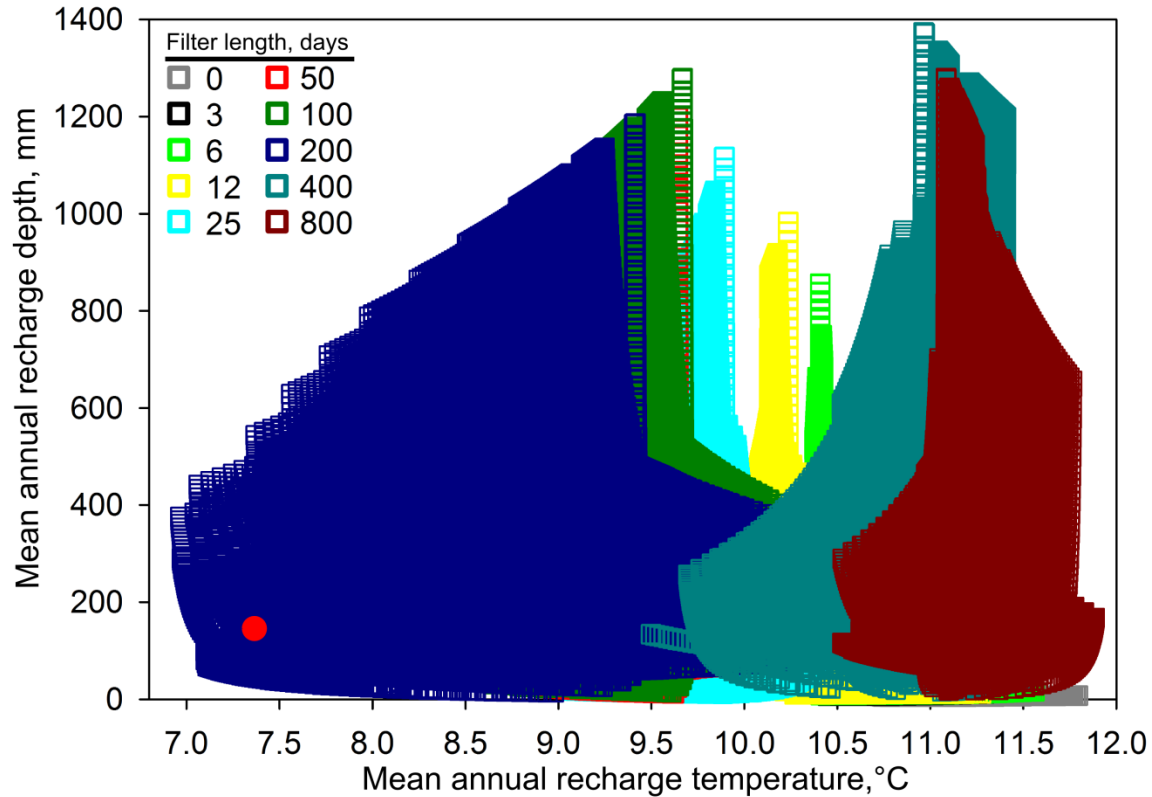


Figure 3.5 Mean annual recharge temperature and mean annual recharge magnitude for each tested parameter set for all filter lengths. Only the 200-day filter length produced parameter sets that captured target recharge depth and temperature (150 mm and 7.4 °C, respectively) as indicated in the figure by the red circle. The final parameter set was chosen using a least-squares approach.

Figure 3.6 shows the filtered DS(t) signal for each of the 10 filter lengths, as well as the modeled daily recharge calculated with the best-fitting parameter set. Although model output was rejected for each filter length other than the 200-day filter, we display all filter lengths in Figure 3.6 to highlight how changing filter lengths changed the temporal pattern of the DS(t) input signal which resulted in shifted temporal patterns of recharge. Figure 3.6 also shows how the low pass filter reduced variability and smoothed the DS(t) signal to a greater extent with increasing filter length. As the input signal smoothed, so too did the corresponding modeled recharge, shifting the temporal pattern of recharge from individual storm events or weekly wet periods (Figure 3.6a-d) to longer sustained monthly or seasonal episodes (Figure 3.6e-h), to inter-annual patterns (Figure 3.6i-j). Variability in the unfiltered DS(t) signal (Figure 3.6a) was primarily controlled by precipitation events, which at Maimai occur on average every 2 days. The minimal seasonality in precipitation

at the site translated to minimal seasonality in DS(t) and ultimately minimal seasonality in recharge for the unfiltered (Figure 3.6a), as well the short filtered (Figure 3.6c-d) outputs. The lack of seasonality resulted in the inclusion of warmer summer recharge to the annual recharge budget, leading to the modeled annual recharge temperature being above the target value for all filters less than 200 days.

Filter lengths greater than 200 days over-smoothed the input signal, resulting in sporadic interannual recharge over the modeling period and mean annual recharge depth and temperature that were lower and higher than target values, respectively (Figure 3.6i and 3.6j). The 200-day filter produced a mean annual recharge depth and temperature that aligned with target values, as expected with the applied inverse modeling approach and results from this model output are discussed below (Figure 3.6h).

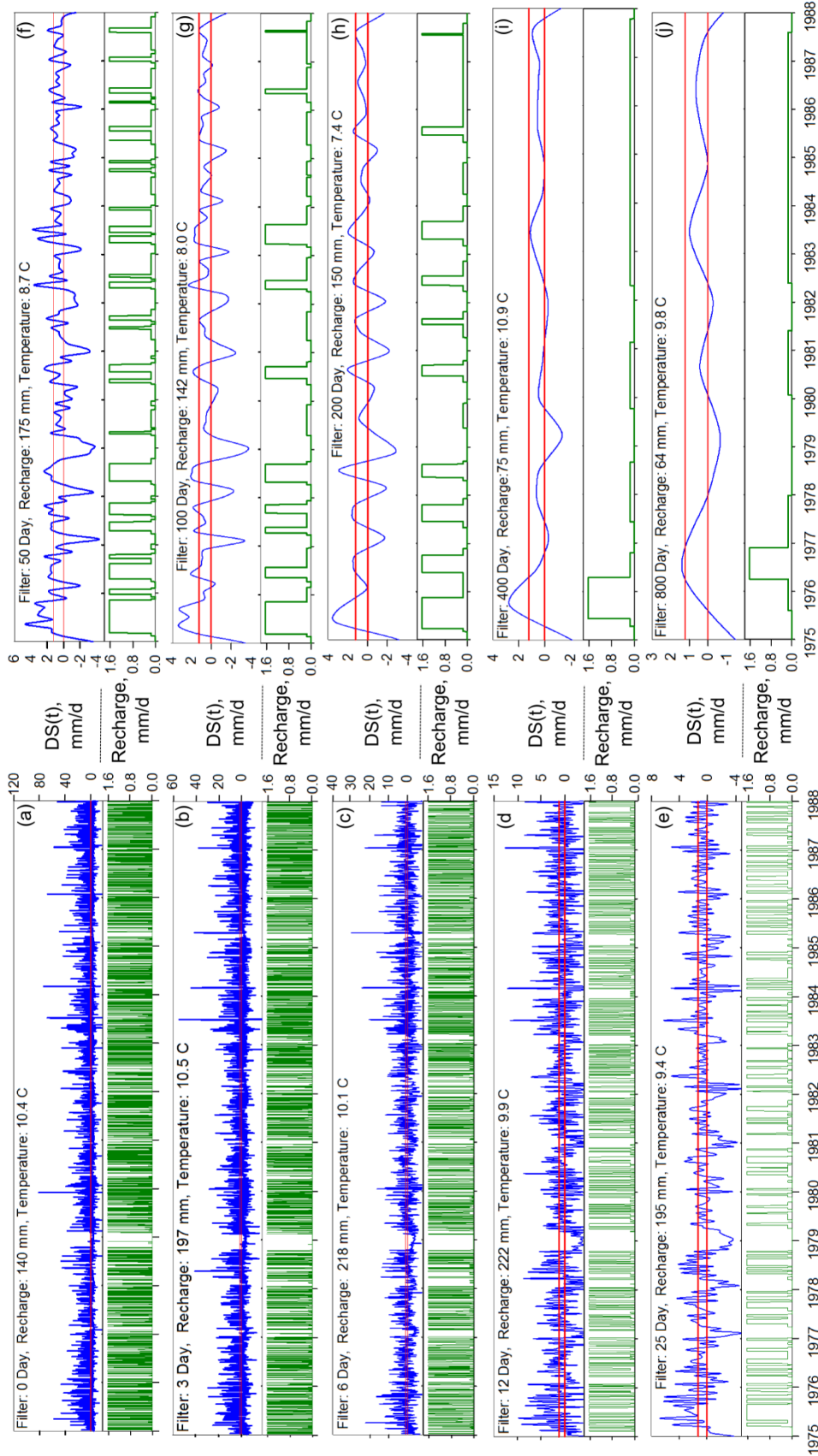


Figure 3.6 Filtered DS(t) signal (blue lines) and modeled bedrock groundwater recharge (green lines) for the 13-year modeling period for each filter length. The two horizontal red lines in each DS(t) plot represent threshold values (i.e. zero and β), which determined the recharge rate. Y-axis labels for all charts are in the center of the figure, and x-axis labels for all charts are at the bottom of the figure.

3.5.3.2 Intra-annual and inter-annual recharge patterns

Mean monthly recharge using the 200-day filter and the identified optimal parameter set is displayed in Figure 3.7, along with long term mean monthly P, Q_{tot} and PET from 1975-1987. Values are additionally presented in Table 3.2. Recharge followed a clear seasonal trend peaking at nearly 34 mm/month in July during mid-winter and dropping to near zero throughout most of the summer. PET followed a similar but inverse seasonal pattern, peaking during the summer and declining considerably during the colder winter months. Precipitation and runoff dipped slightly from February to April, but showed little seasonality otherwise. Sixty percent of annual recharge occurred during the months of June, July and August, produced from only 25% of the annual precipitation, and nearly 90% of annual recharge occurred during the 6 month period from May through October, during which 55% of annual precipitation fell.

Interestingly, although bedrock recharge during the warm-season months accounted for only 11% of the annual recharge, catchment runoff from November through April (i.e. summer months) accounted for 38% of yearly runoff and runoff ratios for this same period were high – 53%. So while the catchment continued to efficiently convert rainfall to runoff during the summer period, almost no recharge was produced during this period, highlighting a complex seasonally shifting internal redistribution process.

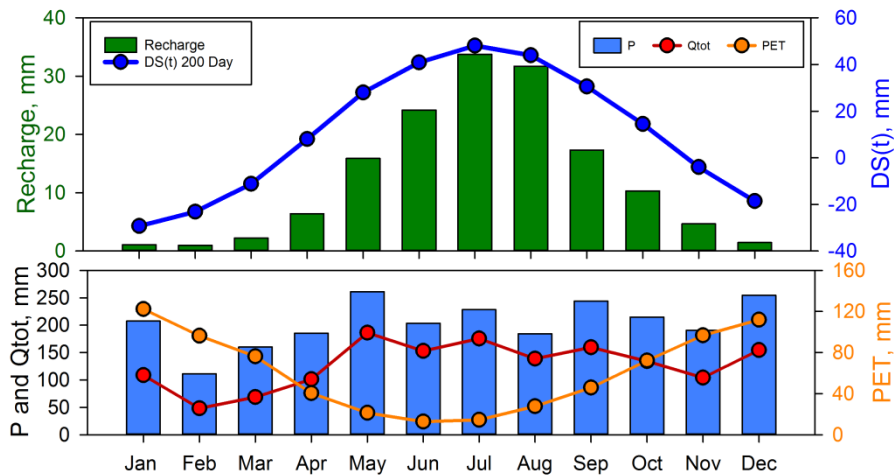


Figure 3.7 Mean monthly bedrock groundwater recharge and the 200-day filtered DS(t) input signal (a), as well as mean monthly precipitation (P), total catchment discharge (Q_{tot}) and potential evapotranspiration (PET) (b). All monthly values are averaged from daily values between 1975 and 1987.

Table 3.2 Mean monthly hydroclimatic variables and modeled bedrock groundwater recharge, as well as annual total and seasonal statistics for each variable where appropriate.

	Jan	Feb	Mar	Apr	May	Jun	Jul	Aug	Sep	Oct	Nov	Dec	Annual total or mean	^c Winter total or mean	^d Summer total or mean	Ratio of winter to annual total	Ratio of summer to annual total
^a Mean temp, °C	16.8	16.9	15	11.8	8.3	5.6	5.1	6.9	9.3	11.3	13.3	15.3	11.3	7.8	14.8	-	-
^b Rainfall, mm	207	111	160	185	261	203	228	184	244	215	190	255	2445	1336	1109	0.55	0.45
^b Runoff, mm	109	48	69	101	186	153	175	139	159	134	104	154	1531	947	585	0.62	0.38
^b Baseflow, mm	21	9	14	23	45	36	43	36	39	30	23	34	354	229	124	0.65	0.35
^b Direct runoff, mm	87	39	55	78	141	117	132	103	120	104	81	120	1178	718	460	0.61	0.39
^a PET, mm	122	96	76	40	21	13	14	28	46	72	97	112	738	194	544	0.26	0.74
Runoff ratio, %	52	43	43	55	71	75	77	75	65	62	55	61	63	71	53	-	-
Recharge, mm	1	1	2	6	16	24	34	32	17	10	5	1	150	133	17	0.89	0.11

^aReefton Met Station 1960-2010, ^b1975-1987 rainfall-runoff at Maimai, ^cWinter represents May through October, ^dSummer represents November through April

Figure 3.8 shows scatter plots of monthly averaged recharge versus monthly averaged P, Q_{tot} , Q_{dir} , Q_{base} , and PET, as well as the relationship between P and Q_{tot} again for the period from 1975-1987. As expected, P and Q_{tot} were highly correlated ($R^2 = 0.81$), however, there was little relationship between P and recharge ($R^2 = 0.09$), indicating that mean monthly rainfall totals were a poor predictor of monthly recharge. Monthly recharge was only moderately correlated to the different monthly flow statistics with an R^2 of 0.43, 0.38 and 0.54 for Q_{tot} , Q_{dir} and Q_{base} , respectively. Q_{base} likely had the strongest relation to recharge as it best captured the general seasonal wetness trends of the catchment. Monthly recharge, however, was much more strongly correlated to monthly PET ($R^2 = 0.72$), suggesting that seasonal patterns in recharge track well with seasonal patterns of catchment evaporation.

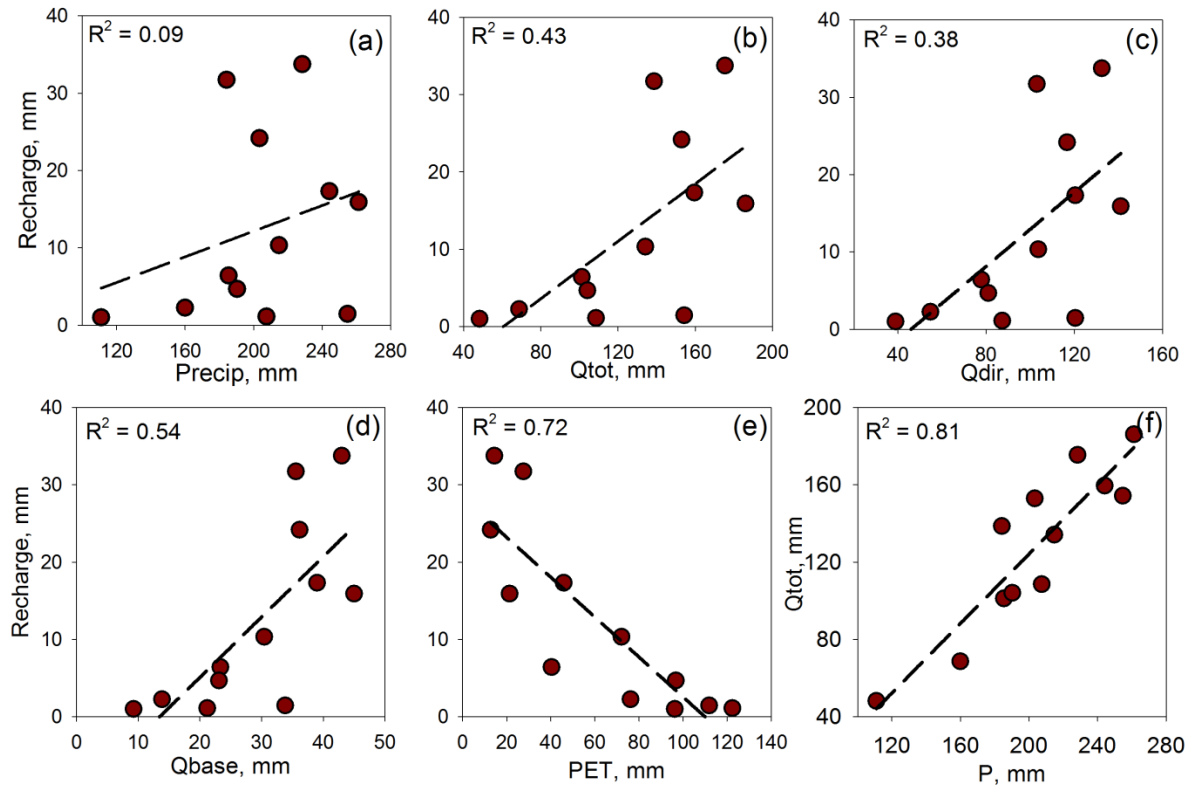


Figure 3.8 Mean monthly recharge versus P, Q_{tot} , Q_{dir} , Q_{base} , PET (a-e), and rainfall versus runoff (f). All monthly values are averaged from daily values between 1975 and 1987.

Figure 9 shows annual recharge totals from 1975-1987 plotted against annual rainfall, Q_{tot} , Q_{dir} , Q_{base} and PET and DS(t) for the same period. Figure 3.9a shows that annual rainfall totals from 1975 to 1987 were poorly correlated to annual recharge totals during the same period ($R^2 = 0.22$), further supporting the lack of connection between precipitation and bedrock groundwater recharge. In fact, annual recharge totals lacked significant correlation with annual Q_{tot} , Q_{dir} , Q_{base} and PET during this same period ($R^2 = 0.08$, 0.06 , 0.12 , and 0.06 , respectively – Figure 3.9b-e), and were only moderately correlated with annual DS(t) ($R^2 = 0.44$ – Figure 3.9f). This reveals that simple annually averaged hydroclimatic metrics do not capture the annual trends of bedrock recharge at Maimai.

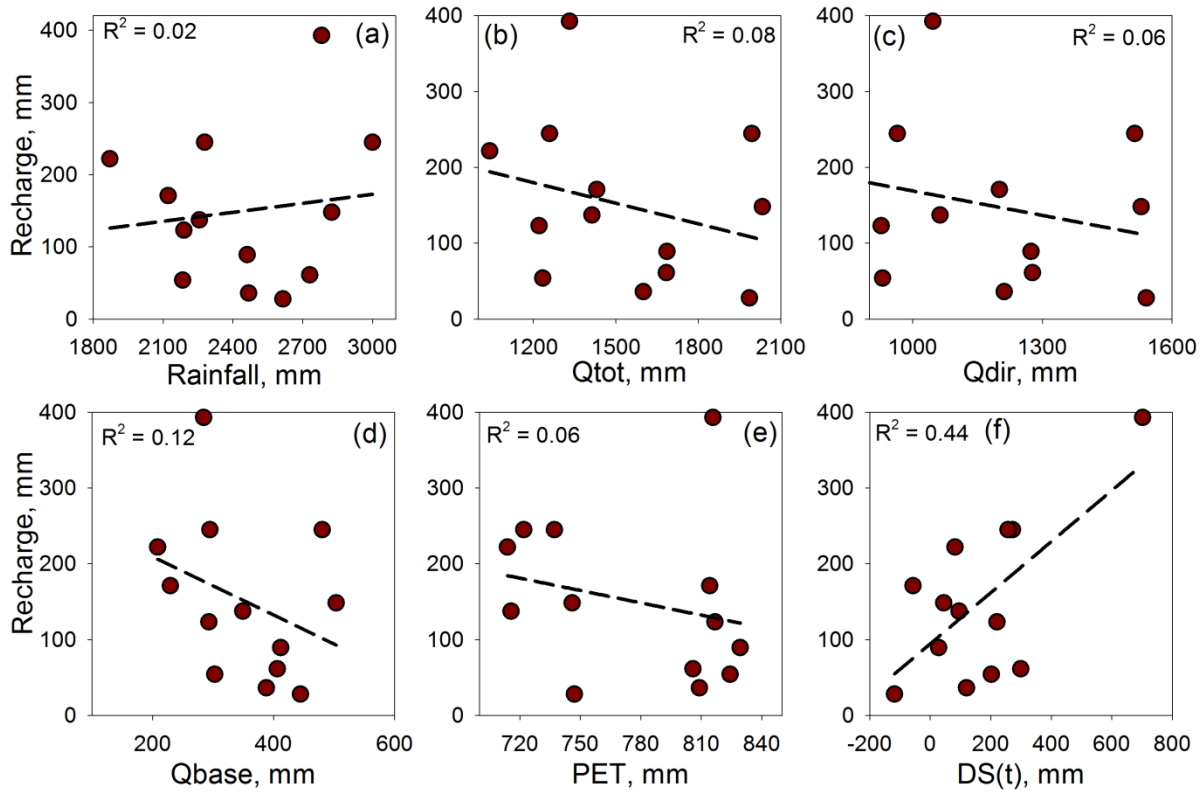


Figure 3.9 Modeled yearly recharge totals between 1975 and 1987 compared against yearly total P, Q_{tot} , Q_{dir} , Q_{base} , PET and DS(t) 0-day for the same time period.

3.5.3.3 Soil water comparison

Figure 3.10a shows the 2015 time series of daily mean water table depth above the soil bedrock interface for each of the 4 monitored soil wells. The riparian, toe-slope and hollow wells were

perennially saturated but showed a distinct and sustained water table rise during the winter season. The hillslope well had a transient water table that occurred with greater consistency during the winter months but which also existed during larger storms throughout the summer season. Figure 3.10b displays the scatter plot of mean monthly water table depth for each well compared to the 2015 modeled mean monthly bedrock recharge depths. A strong threshold-like relationship was observed such that below a well-specific mean water table depth little to no recharge occurred, but above that threshold monthly recharge increased to and sustained a constant rate, suggesting that the strong seasonal shift in soil water dynamics were also linked to seasonal recharge timing.

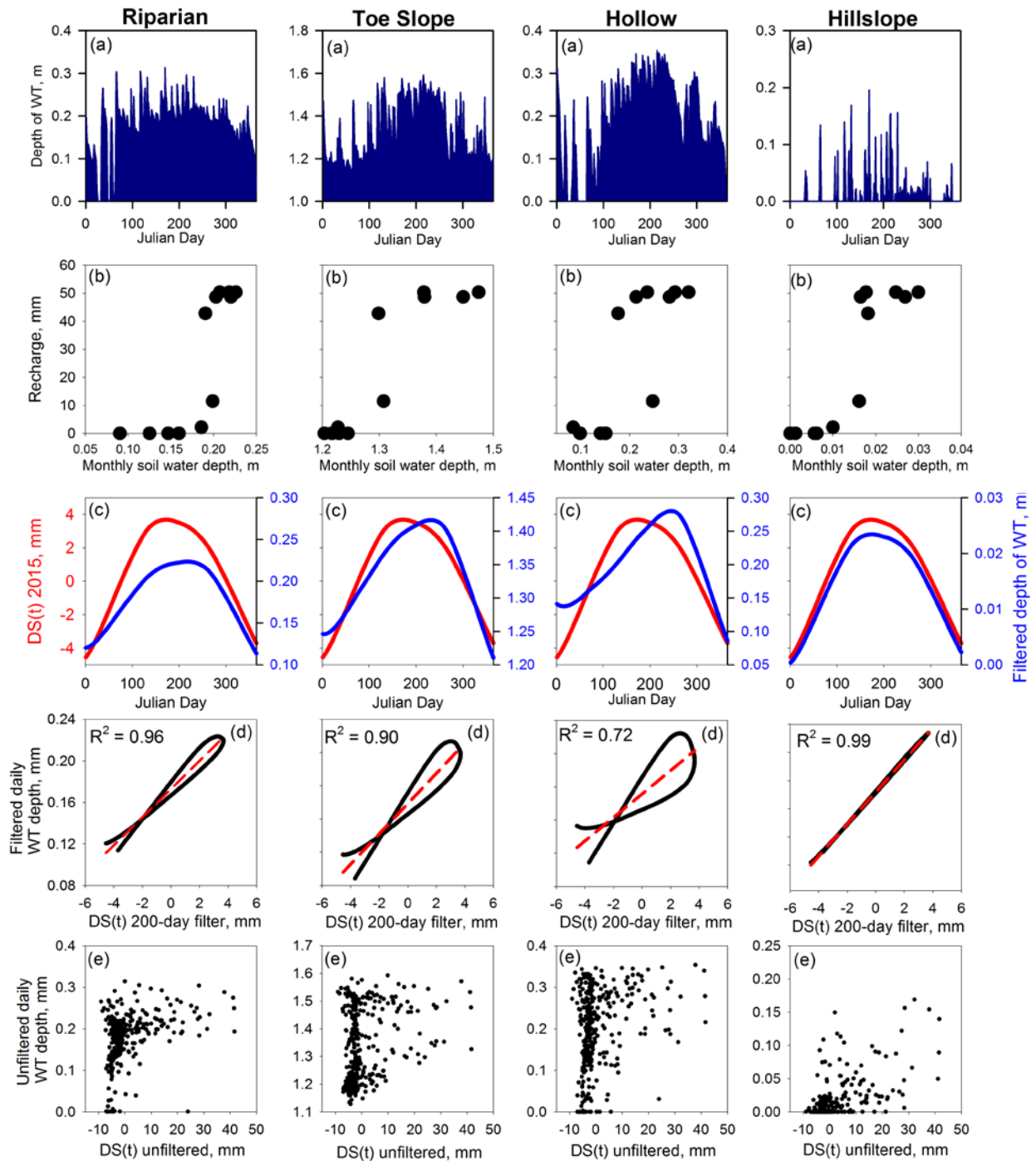


Figure 3.10 Depth of water table above the soil-bedrock interface for 4 wells located in riparian, toe-slope, hollow and hillslope positions (a). Modeled bedrock groundwater recharge compared to monthly mean depth of water table for each soil well (b). DS(t) for year 2015 and 2015 daily soil water table time series both filtered with the 200-day low pass filter to compare seasonal patterns (c). 200-day filtered 2015 DS(t) versus filtered soil water time series (d). Unfiltered daily 2015 DS(t) versus unfiltered daily soil time series.

We passed the soil water time series for each well through the 200-day filter and compared results to the filtered 200-day DS(t) signal to compare seasonal patterns of soil water with seasonal patterns of DS(t). This comparison acted as a measure to validate if indeed, DS(t) was a good proxy for temporal patterns of catchment wetness. The two signals shared similar temporal patterns (Figure 3.10c) and were highly correlated (Figure 3.10d), indicating the same seasonal variability observed in catchment wetness (i.e. DS(t)) was also present in the observed catchment soil water dynamics. Interestingly, the unfiltered (i.e. 0-day filter) daily water table depths for all wells were poorly correlated with the unfiltered DS(t) signal (Figure 3.10e), implying that on daily time scales, dynamic storage was a poor indicator of soil water dynamics, further impressing on the fact that not daily or weekly fluctuations, but rather summer-winter seasonality, imparts critical control on the timing of recharge.

3.6 Discussion

3.6.1 Geologic control on groundwater recharge

Our results suggest complex interactions between bedrock characteristics, soil storage and seasonal climatic conditions at Maimai that control bedrock groundwater recharge timing and magnitude. Slug tests and the sprinkler experiment revealed low permeability hillslope bedrock void of major fracture pathways, inferring that the bedrock structure lacks significant secondary porosity. This fracture-free state is critical to recharge processes as all recharge must occur through the primary porosity only. Although the conductivity of the intact bedrock is relatively high compared to other intact bedrock formations (e.g. unfractured metamorphic and igneous rock: 1×10^{-12} m/s (Freeze and Cherry, 1979)), the mechanism of recharge is still one of diffuse porous flow – orders of magnitude slower than would be the case via preferential fracture flow.

Previous sprinkler experiments in other headwater catchments have noted the critical role of fracture flow in transporting water both downslope to supplement storm runoff (Montgomery *et al.*, 1997) and to-depth to recharge deeper aquifer systems (Tromp-van Meerveld *et al.*, 2007; Graham *et al.*, 2010a). The effective permeability of these tested hillslopes was likely controlled by the size, distribution and interconnectedness of the fracture network (Gerke and Genuchten,

1993). *Appels et al.* (2015) noted the role of fractures as local recharge ‘hotspots’ during event runoff in modeled bedrock recharge at the Panola Mountain Research Watershed in Georgia, USA. Observations in other fractured headwater settings have shown large rises in bedrock water tables from both rainfall and snowmelt inputs on time scales of minutes to hours, further reinforcing fracture flow as a major mechanism of headwater recharge (*Sukhija et al.*, 2003).

At Maimai, the distinct lack of fractured bedrock offers another end member of headwater recharge processes and illustrates a clear example of the interactions between geology, overlying colluvium and water balance components in controlling the timing and magnitude of headwater recharge. At Maimai, since bedrock recharge only occurs slowly through the primary porosity of the bedrock matrix long durations of favorable recharge conditions must exist (i.e. high catchment wetness) in order for appreciable bedrock groundwater recharge to occur. These favorable recharge conditions are in turn, seasonally controlled by long term fluctuations in climate forcing, creating a geologically mediated groundwater recharge system with temporal patterns that link to seasonality in hydroclimatic forcing.

Gabrielli et al. (2017) identified bedrock permeability at Maimai as a first order control on bedrock groundwater age and on the time-varying nature of streamwater mean transit time. Bedrock permeability has also been identified as a key characteristic controlling the time and length scales over which catchments store, mix and release their waters elsewhere (*Tague et al.*, 2008; *Hale et al.*, 2016; *Pfister et al.*, 2017). Perhaps it is no surprise then that the geologic characteristics of the bedrock underlying Maimai were found, in part, to control the seasonal timing of moisture redistribution to depth. Permeability continues to be identified as a critical distinguishing characteristic influencing rainfall-runoff processes in complex ways in the headwaters.

3.6.2 Summer runoff but no summer recharge: Seasonality is crucial

Noble gas tracer measurements representing the larger bedrock groundwater domain revealed recharge temperatures nearly 4°C lower than the local mean annual air temperature. This indicated seasonally specific recharge during colder winter months, an observation further supported by the distinctly more-depleted stable isotope composition of bedrock groundwater compared to other

catchment waters (e.g. soil water and streamflow). Although seasonality of recharge is a widely observed phenomena (*Jasechko et al.*, 2014), it has been most often associated with strong intra-annual patterns in precipitation (*Descloitres et al.*, 2008), or in regions where late autumn rainfall and early spring snow melt occur concurrently with low ET demands (*Abbott et al.*, 2000; *O'Driscoll et al.*, 2005; *Jasechko et al.*, 2017). Strong seasonality in recharge, however, has been rarely observed in rain dominated hydrologic systems that lack seasonal precipitation variability as we report here for Maimai.

At Maimai, rainfall occurs on average every 2 days. The 2450 mm annual rainfall is distributed roughly evenly between winter – 55%, and summer – 45%, yet 89% of annual bedrock recharge takes place during the winter period from May through October, and 60% of annual recharge results from only 25% of the annual rainfall during peak recharge months of June, July and August. In contrast, during the peak summer months of December, January and February, nearly the same volume of precipitation produces only 2.4% of annual recharge. This results in a recharge efficiency (calculated as depth of recharge divided by depth of rainfall) that is nearly 24-fold higher in peak winter months compared to peak summer months.

Although the magnitude and timing of precipitation has been widely shown to control groundwater recharge (*Winograd et al.*, 1998; *Lee et al.*, 1999; *Keese et al.*, 2005; *O'Driscoll et al.*, 2005; *Scanlon et al.*, 2006; *Mileham et al.*, 2009; *Owor et al.*, 2009), at Maimai we found no such correlation. In fact, recharge was found to be uncorrelated to monthly precipitation, wet season precipitation, and annual precipitation totals. Instead the control of recharge shifts seasonally from geologic properties to PET.

During winter months, excess moisture is abundant within the catchment, but the low permeability bedrock limits infiltration rates, as is commonly observed in other humid regions (*Sanford*, 2002). Although saturation at the soil-bedrock interface is frequent at Maimai, infiltration rates of the low permeability bedrock are quickly exceeded and a form of infiltration-excess subsurface flow occurs over the bedrock surface but within the soil mantle (as reported in many early studies at the site by *Mosley* (1979). Further additions of moisture are either driven laterally downslope to the

stream channel or fulfil unrequited soil storage (*McDonnell, 1990*). It is precisely because bedrock infiltration rates are so readily exceeded by the large quantities of rainfall that no correlation exists between rainfall and recharge, either monthly, seasonally or annually. Thus, in the winter the magnitude of recharge is limited not by the availability of water but by the ability of the geologic formation to transfer water to depth.

In summer months, much greater PET rates are aligned with slightly lower rainfall totals. Under these conditions, the distribution of subsurface moisture shifts such that the bedrock groundwater recharge budget is now used up to meet ET demands, essentially eliminating bedrock groundwater recharge during these summer months. Although this is seen in more seasonally diverse locations (*Scanlon et al., 2006; Jasechko et al., 2014; Jasechko et al., 2017*), this was not expected at the Maimai where for decades it was believed that the catchment stays perpetually “wet” (*McGlynn et al., 2002*) and where “soils remain within 10% of saturation for most of the hydrologic year” (*Mosley, 1979*) and where it was believed that all rainfall events resulted in some groundwater recharge (*Stewart and McDonnell, 1991; Vaché and McDonnell, 2006*).

The lack of correlation between recharge magnitude and precipitation is important as most large-scale recharge models used to inform groundwater sustainability have shown trends in recharge that widely track future changes in precipitation (both positively and negatively, due to competing feedbacks) (*Taylor et al., 2013a*). We show here, however, that geologic properties and seasonal trends in evaporation instead act as the primary control on recharge. Thus, future changes in precipitation at Maimai will likely have little effect on changes in groundwater recharge.

So how can there be summer runoff but no summer recharge? Isn't runoff an indicator of excess water in the catchment? Rainfall-runoff processes at Maimai directly reflect the minimal soil storage capacity (*Stewart and McDonnell, 1991*), low bedrock permeability (*Gabrielli et al., 2012*) and large quantities of annual rainfall (*Pearce et al., 1977*). As a result, the catchment is dominated by a highly efficient and extensive preferential flow system capable of delivering large quantities of subsurface stormflow to the stream channel over short periods of time (*Mosley, 1982; McDonnell, 1990; Weiler et al., 2003; Graham et al., 2010b*). Indeed, the Maimai is defined by

rainfall-runoff ratios that exceed nearly every studied headwater in the literature (*Mosley, 1979; Pearce et al., 1986*).

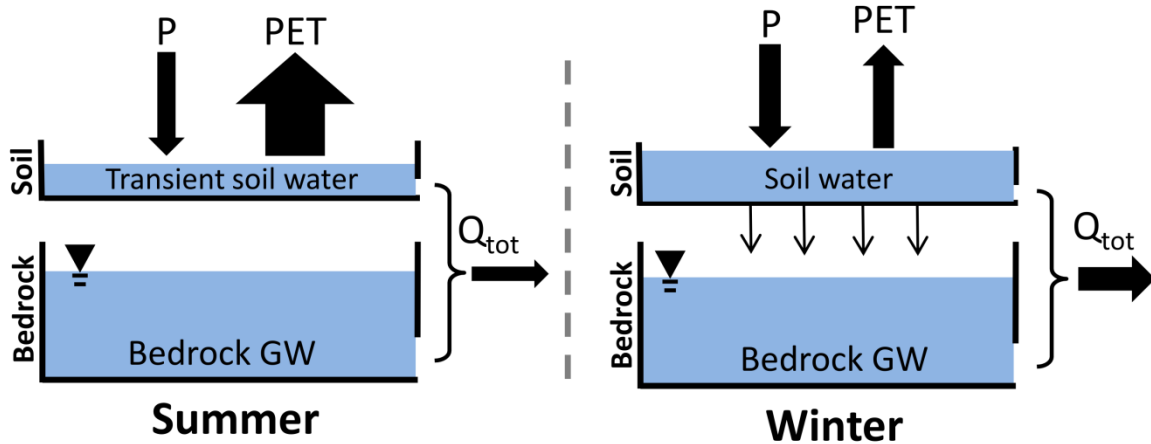


Figure 3.11 Conceptual model of seasonal catchment water balance fluxes. The width of the black arrows represent the magnitude of the seasonal flux compared to annual flux for each metric (P , PET and Q_{tot}), allowing for easy visual comparison of the difference between summer and winter water balance components.

Figure 3.11 shows our conceptual model of seasonal recharge and the water balance flux components at Maimai. In the summer, rainfall-runoff ratios – while lower than winter ratios – are still high, 53%. This is somewhat paradoxical as high runoff ratios generally indicate abundant excess moisture. Yet our soil water observations show marked decline in catchment wetness conditions. We hypothesize that summer rainfall events activate the preferential flow network (just as they do in winter) on storm event time scales, thus removing most of the precipitation input from the catchment and limiting the degree to which soil matrix storage is replenished, contrary to the apparent capacity of available soil-water storage. *Stewart and McDonnell (1991)* specifically noted that rainfall bypasses the soil matrix through preferential flowpaths and recharge of the soil matrix occurs more slowly through diffusive processes. The increase in storage that does occur within the soil matrix during events is quickly depleted between events by the much greater summer ET rates, and soil water that would otherwise go to bedrock recharge is lost instead to evaporative processes. Under this scenario, the catchment experiences episodic high wetness conditions. But, critically, the long periods of extended wetness needed for recharge are not attained and thus bedrock recharge rates fall to near zero during the warmer summer season.

3.6.3 Review of the groundwater recharge model

Our simple modeling approach to understand the timing and magnitude of recharge provided a coarse empirical approximation of what is otherwise an extremely complex process (*Scanlon et al.*, 2002). But its simplicity too, provides valuable insight to the importance of seasonality in a system which for decades at Maimai was believed to be minimal. Although the model design was unable to discern exact catchment conditions that lead to recharge initiation and thus the exact timing during which these events occurred, it was able to identify broad seasonal patterns including the wet-up and dry-down transitions between summer and winter seasons. It is likely that even during summer runoff events a small degree of recharge occurs. In addition, recharge during the winter months does not occur as a continuous single-rate steady-state process but instead likely fluctuates in concert with storm events. More complex 3-dimensional physics-based coupled models currently exist (e.g. *Ebel and Loague* (2006), *Maxwell and Kollet* (2008)) that would likely be able to capture the precise catchment conditions under which recharge occurs, providing higher resolution of the seasonality of recharge and a more refined conceptual model to identify the driving forces that control recharge timing and magnitude.

Our model input function, $DS(t)$, has previously been used in different model formulations to identify total catchment storage and seasonal storage thresholds (*Sayama et al.*, 2011) and to identify trends in catchment mean transit time and functional relationships between $DS(t)$ and catchment runoff characteristic (*Buttle*, 2016). We used $DS(t)$ as a daily water balance record to measure the general catchment wetness conditions and trends. Our modeling results revealed, however, the need to filter the $DS(t)$ signal in order to achieve model fits that met observed criteria for recharge depth and temperature. The unfiltered daily $DS(t)$ signal contained considerable variability and the simplicity of our empirical model could not differentiate between the high winter $DS(t)$ values that drove recharge and the high summer $DS(t)$ values that did not. Variability in the unfiltered $DS(t)$ signal was primarily controlled by rainfall events, thus the unfiltered $DS(t)$ signal lacked seasonality. In headwater catchments where fracture flow plays a more considerable role in recharge processes, we would expect recharge to more closely follow precipitation patterns since any storm event that created saturation at the soil-bedrock interface would likely contribute

materially to the bedrock water table. Thus, an unfiltered DS(t) signal may prove viable to model seasonal recharge patterns in fractured systems.

Although modeled monthly recharge estimates were highly correlated to monthly PET values, we also tested PET and filtered-PET as a potential input signal for the model. Despite the same parameter identification scheme, we were not able to achieve target recharge temperatures or depths. This suggests that although PET is highly correlated with recharge, the secondary processes associated with catchment storage and release that are captured in the DS(t) signal were critical to accurately capture the temporal characteristics of bedrock recharge. Indeed, available soil storage plays a role in moderating the rainfall-runoff response, and is inherently embedded in the DS(t) signal through its relationship with Q_{tot} , which is not otherwise captured in the PET signal.

3.6.4 What is the role of soil for groundwater recharge at Maimai?

The thin veneer of soil at Maimai and at other headwater catchments acts to buffer rainfall inputs, both damping the immediate streamflow response and providing a storage compartment to retain moisture between events (*Hopp and McDonnell, 2009*). Generally, one thinks of this buffering capacity as a positive contribution to groundwater recharge: soils inhibit flashy runoff, allowing retained soil moisture to trickle charge to depth over time. Indeed, *Appels et al. (2015)* found that 60% of the annual bedrock groundwater recharge budget at the Panola Mountain Research Watershed was derived from unsaturated flow within the soil horizon. But what if the soil were removed? Would bedrock recharge decrease as expected? We ask this simple question because of our work on the open bedrock plot within the Maimai watershed where soil was indeed removed and where we did see flashy runoff during storm events.

Our results from this soil-free area, however, suggest that the soil layer may in fact impede bedrock groundwater recharge at Maimai. If hourly rainfall rates are examined from 1975-1987 and we remove from this data the equivalent hourly rate of bedrock infiltration (equal to hillslope K_{sat} with an assumed unit gradient), the total depth of water removed is equivalent to the depth of water theoretically recharged to the bedrock. We found this value averaged 385 mm/y, or 185-285 mm/y greater than observed bedrock recharge with the soil mantle intact. All other things being equal,

rather than promoting bedrock groundwater recharge, the soil mantle at Maimai appears to inhibit it.

There are two factors that might conspire to explain this response. First, the low-intensity, very long-duration storms experienced at Maimai provide long periods of favorable recharge conditions which aggregate to large volumes of annual recharge. We would not expect the same result if rainfall episodes were concentrated to shorter time scales and higher intensities, as less bedrock infiltration would result from the same total rainfall. Second, observed annual recharge is less than what was calculated in this simple theoretical analysis because in reality, unrequited summer soil storage must first be replenished before excess moisture is available for recharge. The water held in storage within the soil mantle is then available for evaporative extraction, a factor not present when the soil is removed and summer rainfall would otherwise directly recharge into the bedrock.

This simple theoretical analysis places our process-based work into a longer time series context and reveals the critical and complex interactions between soil storage, rainfall distribution and seasonal fluctuations in ET – that all conspire to induce selective seasonal recharge at the Maimai.

3.7 Conclusion

We showed the combined importance of geologic properties and seasonal fluctuations in PET on the seasonal timing of bedrock groundwater recharge. We found that the hydrologic system at Maimai, where little apparent seasonality in the precipitation or catchment runoff ratios exists, masks extreme seasonality in bedrock groundwater recharge. Our analysis of bedrock groundwater isotopic signatures and noble gas temperatures revealed a seasonally selective groundwater recharge regime that is based almost entirely on cold-season winter recharge. A simple empirical recharge model and extensive bedrock characterization associated with an on-bedrock sprinkler experiment supported the finding of the linkage between the seasonality of bedrock groundwater recharge and the geologic controls imposed by the bedrock structure. Our work suggests that low bedrock permeability directly controls the timing of bedrock recharge by regulating winter

recharge amounts during large excess water conditions in winter, and by inhibiting significant recharge during transient event-based high wetness conditions in the summer months.

With recent work highlighting the importance of headwaters as focal recharge zones for downslope aquifers (*Jasechko et al.*, 2016), our work helps to understand how hydroclimatic and geologic variables combine to control the nature of groundwater recharge. While future projections of groundwater recharge under various climate change scenarios are largely associated with changes in precipitation (*Taylor et al.*, 2013a) and that precipitation intensity and magnitude control recharge timing and rates (*Owor et al.*, 2009; *Allen et al.*, 2010; *Taylor et al.*, 2013b), our work is something of a cautionary tale. For such studies using precipitation to directly estimate recharge, the Maimai is a clear example of a headwater aquifer that shows no relationship to precipitation amount or timing, despite catchment runoff dynamics that indicate a clear abundance of excess moisture in the system year-round.

3.8 Transition statement

Chapter 3 built upon the bedrock aquifer characterization that was conducted and outlined in Chapter 2. I found that bedrock characteristics, specifically bedrock permeability and the absence of large fracture networks, drove a bedrock groundwater recharge situation where long durations of high catchment wetness were needed in order for significant bedrock groundwater recharge to occur. This condition was only achieved during cold winter months when precipitation was high and also, when evapotranspiration rates were low. This led to a seasonally-focused recharge pattern that was unexpected for a catchment that showed little seasonality in either precipitation input or catchment discharge output. The geologically mediated recharge identified in Chapter 3, and the geologically mediated time-varying streamwater transit times identified in Chapter 2 both supported the construction of a new catchment scale geology and landform index in Chapter 4. This new index aimed to capture the controls of bedrock permeability and catchment topographic structure on the timescales over which landscapes store and release their water.

3.9 Acknowledgements

This work was supported through funding by NSERC Discovery grant to Jeffrey McDonnell and the Horton Hydrology Research Grant from the American Geophysical Union to Chris Gabrielli. We thank Uwe Morgenstern for the noble gas analysis and for useful discussions along the way. We also thank Garth Vanderkamp, Lee Barbour and Andrew Ireson for useful comments on various aspects of this work along the way. We thank John Payne at Landcare Research, and Matt Taylor and Christie Thomson for their invaluable assistance and support in the field and throughout the extended field campaign in New Zealand.

3.10 Author contributions

CPG and JJM brainstormed the manuscript outline. CPG carried out all fieldwork, data collection, analyses and general writing of the manuscript, while JJM contributed to editing, feedback and final text.

3.11 References

Abbott, M., A. Lini and P. Bierman (2000), $\Delta 18\text{O}$, δd and 3 h measurements constrain groundwater recharge patterns in an upland fractured bedrock aquifer, Vermont, USA, *J. Hydrol.*, 228(1), 101-112. 10.1016/S0022-1694(00)00149-9.

Allen, D., P. Whitfield and A. Werner (2010), Groundwater level responses in temperate mountainous terrain: Regime classification, and linkages to climate and streamflow, *Hydrol. Processes*, 24(23), 3392-3412. 10.1002/hyp.7757.

Anderson, M.G. and J.J. McDonnell (2005), *Encyclopedia of hydrological sciences*, John Wiley & Sons, Hoboken, N.J.

Anderson, S.P., W.E. Dietrich, D.R. Montgomery, R. Torres, M.E. Conrad and K. Loague (1997), Subsurface flow paths in a steep, unchanneled catchment., *Water Resour. Res.*, 33(12), 2637-2653. 10.1029/97WR02595.

Appels, W.M., C.B. Graham, J.E. Freer and J.J. McDonnell (2015), Factors affecting the spatial pattern of bedrock groundwater recharge at the hillslope scale, *Hydrol. Processes*, 29(21), 4594-4610. 10.1002/hyp.10481.

Asano, Y. and T. Uchida (2012), Flow path depth is the main controller of mean base flow transit times in a mountainous catchment, *Water Resour. Res.*, 48(3), W03512. 10.1029/2011WR010906.

Bohlke, J. and D.E. Krantz (2003), Isotope geochemistry and chronology of offshore groundwater beneath Indian River Bay, Delaware, US Department of the Interior, US Geological Survey.

Bowen, F. (1967), Early Pleistocene glacial and associated deposits of the west coast of the South Island, New Zealand, *New Zealand Journal of Geology and Geophysics*, 10(1), 164-181.

Brooks, E.S., J. Boll and P.A. Mcdaniel (2004), A hillslope-scale experiment to measure lateral saturated hydraulic conductivity, *Water Resour. Res.*, 40, W04208. 10.1029/2003WR002858.

Brutsaert, W. and J.L. Nieber (1977), Regionalized drought flow hydrographs from a mature glaciated plateau, *Water Resour. Res.*, 13(3), 637-643. 10.1029/WR013i003p00637.

Burnard, P. (2013), *The noble gases as geochemical tracers*, Springer.

Buttle, J.M. (2016), Dynamic storage: A potential metric of inter-basin differences in storage properties, *Hydrol. Processes*, 30(24), 4644-4653. 10.1002/hyp.10931.

Descloitres, M., L. Ruiz, M. Sekhar, A. Legchenko, J.J. Braun, M. Kumar and S. Subramanian (2008), Characterization of seasonal local recharge using electrical resistivity tomography and magnetic resonance sounding, *Hydrol. Processes*, 22(3), 384-394. 10.1002/hyp.6608.

Dripps, W.R. and K.R. Bradbury (2007), A simple daily soil–water balance model for estimating the spatial and temporal distribution of groundwater recharge in temperate humid areas, *Hydrogeol. J.*, 15(3), 433-444. 10.1007/s10040-007-0160-6.

Ebel, B.A. and K. Loague (2006), Physics-based hydrologic-response simulation: Seeing through the fog of equifinality, *Hydrol. Processes*, 20(13), 2887-2900. 10.1002/hyp.6388.

Eckhardt, K. (2005), How to construct recursive digital filters for baseflow separation, *Hydrol. Processes*, 19(2), 507-515. 10.1002/hyp.5675.

Freeze, R.A. and J.A. Cherry (1979), *Groundwater*, Prentice-Hall, Englewood Cliffs, NJ.

Gabrielli, C.P., J.J. McDonnell and W.T. Jarvis (2012), The role of bedrock groundwater in rainfall–runoff response at hillslope and catchment scales, *J. Hydrol.*, 450, 117-133. 10.1016/j.jhydrol.2012.05.023.

Gabrielli, C.P., J.J. McDonnell, U. Morgenstern and M. Stewart (2017), Bedrock groundwater age, water table dynamics and time-varying transit time at the maimai watershed *Water Resour. Res.*, In Review.

Gee, G.W. and D. Hillel (1988), Groundwater recharge in arid regions: Review and critique of estimation methods, *Hydrol. Processes*, 2(3), 255-266. 10.1002/hyp.3360020306.

Gerke, H. and M.V. Genuchten (1993), A dual-porosity model for simulating the preferential movement of water and solutes in structured porous media, *Water Resour. Res.*, 29(2), 305-319. 10.1029/92WR02339.

Gleeson, T. and A.H. Manning (2008), Regional groundwater flow in mountainous terrain: Three-dimensional simulations of topographic and hydrogeologic controls, *Water Resour. Res.*, 44(10), W10403. 10.1029/2008WR006848.

Gleeson, T., K. Novakowski and T. Kurt Kyser (2009), Extremely rapid and localized recharge to a fractured rock aquifer, *J. Hydrol.*, 376(3–4), 496-509. 10.1016/j.jhydrol.2009.07.056.

Graham, C.B., W. Van Verseveld, H.R. Barnard and J.J. McDonnell (2010a), Estimating the deep seepage component of the hillslope and catchment water balance within a measurement uncertainty framework, *Hydrol. Processes*, 24(25), 3631-3647. 10.1002/hyp.7788.

Graham, C.B., R.A. Woods and J.J. McDonnell (2010b), Hillslope threshold response to rainfall: (1) a field based forensic approach, *J. Hydrol.*, 393(1-2), 65-76. 10.1016/j.jhydrol.2009.12.015.

Hale, V.C. and J.J. McDonnell (2016), Effect of bedrock permeability on stream base flow mean transit time scaling relations: 1. A multiscale catchment intercomparison, *Water Resour. Res.*, 52(2), 1358-1374. 10.1002/2014WR016124.

Hale, V.C., J.J. McDonnell, M.K. Stewart, D.K. Solomon, J. Doolittle, G.G. Ice and R.T. Pack (2016), Effect of bedrock permeability on stream base flow mean transit time scaling relationships: 2. Process study of storage and release, *Water Resour. Res.*, 52(2), 1375-1397. 10.1002/2015WR017660.

Hammond, M. and D. Han (2006), Recession curve estimation for storm event separations, *J. Hydrol.*, 330(3), 573-585. 10.1016/j.jhydrol.2006.04.027.

Harr, R.D. (1977), Water flux in soil and subsoil on a steep forested slope, *J. Hydrol.*, 33, 37-58. 10.1016/0022-1694(77)90097-X.

Heaton, T.H.E. and J.C. Vogel (1981), "Excess air" in groundwater, *J. Hydrol.*, 50, 201-216. 10.1016/0022-1694(81)90070-6.

Hewlett, J.D. and A.R. Hibbert (1967), Forest hydrology. Sopper, W.E. and Lull, H.W. (eds), pp. 275-291, Pergamon Press, New York.

Hopp, L. and J.J. McDonnell (2009), Connectivity at the hillslope scale: Identifying interactions between storm size, bedrock permeability, slope angle and soil depth, *J. Hydrol.*, 376(3-4), 378-391. 10.1016/j.jhydrol.2009.07.047.

Hvorslev, M.J. (1951), Time lag and soil permeability in ground-water observations.

Iwasaki, K., M. Katsuyama and M. Tani (2014), Contributions of bedrock groundwater to the upscaling of storm-runoff generation processes in weathered granitic headwater catchments, *Hydrol. Processes*, 29(6), 1535–1548. 10.1002/hyp.10279.

Jackson, C.R., E. Du, J. Klaus, N.A. Griffiths, M. Bitew and J.J. McDonnell (2016), Interactions among hydraulic conductivity distributions, subsurface topography, and transport thresholds revealed by a multitracer hillslope irrigation experiment, *Water Resour. Res.*, 52(8), 6186-6206. 10.1002/2015WR018364.

Jasechko, S., S.J. Birks, T. Gleeson, Y. Wada, P.J. Fawcett, Z.D. Sharp, J.J. McDonnell and J.M. Welker (2014), The pronounced seasonality of global groundwater recharge, *Water Resour. Res.*, 50(11), 8845-8867. 10.1002/2014WR015809.

Jasechko, S., J.W. Kirchner, J.M. Welker and J.J. McDonnell (2016), Substantial proportion of global streamflow less than three months old, *Nature Geosci*, 9(2), 126-129. 10.1038/ngeo2636.

Jasechko, S., L.I. Wassenaar and B. Mayer (2017), Isotopic evidence for widespread cold-season-biased groundwater recharge and young streamflow across central Canada, *Hydrol. Processes*, 31(12), 2196–2209. 10.1002/hyp.11175.

Katsura, S.Y., K.I. Kosugi, Y. Yamakawa and T. Mizuyama (2014), Field evidence of groundwater ridging in a slope of a granite watershed without the capillary fringe effect, *J. Hydrol.*, 511. 10.1016/j.jhydrol.2014.02.021.

Katsuyama, M., M. Tani and S. Nishimoto (2010), Connection between streamwater mean residence time and bedrock groundwater recharge/discharge dynamics in weathered granite catchments, *Hydrol. Processes*, 24(16), 2287-2299. 10.1002/hyp.7741.

Keese, K.E., B.R. Scanlon and R.C. Reedy (2005), Assessing controls on diffuse groundwater recharge using unsaturated flow modeling, *Water Resour. Res.*, 41(6), n/a-n/a. 10.1029/2004WR003841.

Kendall, C. and J.J. McDonnell (2012), *Isotope tracers in catchment hydrology*, Elsevier.

Kirchner, J.W. (2009), Catchments as simple dynamical systems: Catchment characterization, rainfall-runoff modeling, and doing hydrology backward, *Water Resour. Res.*, 45(2), W02429. 10.1029/2008WR006912.

Kosugi, K.I., S.Y. Katsura, M. Katsuyama and T. Mizuyama (2006), Water flow processes in weathered granitic bedrock and their effects on runoff generation in a small headwater catchment, *Water Resour. Res.*, 42(2), W02414. 10.1029/2005WR004275.

Kosugi, K.I., S.Y. Katsura, T. Mizuyama, S. Okunaka and T. Mizutani (2008), Anomalous behavior of soil mantle groundwater demonstrates the major effects of bedrock groundwater on surface hydrological processes, *Water Resour. Res.*, 44(1). 10.1029/2006WR005859.

Lee, C.-H., W.-P. Chen and R.-H. Lee (2006), Estimation of groundwater recharge using water balance coupled with base-flow-record estimation and stable-base-flow analysis, *Environmental Geology*, 51(1), 73-82. 10.1007/s00254-006-0305-2.

Lee, K.-S., D.B. Wenner and I. Lee (1999), Using h-and o-isotopic data for estimating the relative contributions of rainy and dry season precipitation to groundwater: Example from cheju island, korea, *J. Hydrol.*, 222(1), 65-74. 10.1016/S0022-1694(99)00099-2.

Lim, K.J., B.A. Engel, Z. Tang, J. Choi, K.S. Kim, S. Muthukrishnan and D. Tripathy (2005), Automated web gis based hydrograph analysis tool, what, *JAWRA Journal of the American Water Resources Association*, 41(6), 1407-1416. 10.1111/j.1752-1688.2005.tb03808.x.

Lindsay, W.L. (1979), *Chemical equilibria in soils*, John Wiley and Sons Ltd.

Maxwell, R.M. and S.J. Kollet (2008), Quantifying the effects of three-dimensional subsurface heterogeneity on hortonian runoff processes using a coupled numerical, stochastic approach, *Adv. Water Resour.*, 31(5), 807-817. 10.1016/j.advwatres.2008.01.020.

Mcdonnell, J.J. (1990), A rationale for old water discharge through macropores in a steep, humid catchment, *Water Resour. Res.*, 26(11), 2821-2832. 0.1029/WR026i011p02821.

Mcglynn, B.L., J.J. Mcdonnell and D.D. Brammer (2002), A review of the evolving perceptual model of hillslope flowpaths at the maimai catchments, new zealand, *J. Hydrol.*, 257(1-4), 1-26. 10.1016/S0022-1694(01)00559-5.

Mcglynn, B.L., J.J. Mcdonnell, J. Seibert and C. Kendall (2004), Scale effects on headwater catchment runoff timing, flow sources, and groundwater-streamflow relations, *Water Resour. Res.*, 40(7), W07504. 10.1029/2003WR002494.

Mcguire, K.J. and J.J. Mcdonnell (2010), Hydrological connectivity of hillslopes and streams: Characteristic time scales and nonlinearities, *Water Resour. Res.*, 46(10). 10.1029/2010WR009341.

Mileham, L., R.G. Taylor, M. Todd, C. Tindimugaya and J. Thompson (2009), The impact of climate change on groundwater recharge and runoff in a humid, equatorial catchment: Sensitivity of projections to rainfall intensity, *Hydrological sciences journal*, 54(4), 727-738.

Montgomery, D.R., W.E. Dietrich, R. Torres, S.P. Anderson, J.T. Heffner and K. Loague (1997), Hydrologic response of a steep, unchanneled valley to natural and applied rainfall, *Water Resour. Res.*, 33(1), 91-109. 10.1029/96WR02985.

Mortimer, N., R. Sutherland and S. Nathan (2001), Torlesse greywacke and haast schist source for pliocene conglomerates near reefton, new zealand, *New Zealand Journal of Geology and Geophysics*, 44(1), 105-111. 10.1080/00288306.2001.9514927.

Mosley, M.P. (1979), Streamflow generation in a forested watershed, *Water Resour. Res.*, 15, 795-806. 10.1029/WR015i004p00795.

Mosley, M.P. (1982), Subsurface flow velocities through selected forest soils, south island, new zealand, *J. Hydrol.*, 55, 65-92. 10.1016/0022-1694(82)90121-4.

Niu, Y., M.C. Castro, C.M. Hall, S.B. Gingerich, M.A. Scholl and R.B. Warrier (2017), Noble gas signatures in the island of maui, hawaii: Characterizing groundwater sources in fractured systems, *Water Resour. Res.*, 53(5), 3599–3614. 10.1002/2016WR020172.

O'Driscoll, M., D. Dewalle, K. Mcguire and W. Gburek (2005), Seasonal 18 o variations and groundwater recharge for three landscape types in central pennsylvania, USA, *J. Hydrol.*, 303(1), 108-124. 10.1016/j.jhydrol.2004.08.020.

Owor, M., R. Taylor, C. Tindimugaya and D. Mwesigwa (2009), Rainfall intensity and groundwater recharge: Empirical evidence from the upper Nile basin, *Environmental Research Letters*, 4(3), 035009.

Pearce, A.J., C.L. O'loughlin and L.K. Rowe (1977), Hydrologic regime of small, undisturbed beech forest catchments, north westland, *Inf Ser NZ Dep Sci Ind Res*.

Pearce, A.J. and A.I. Mckerchar (1979), Physical hydrology, new zealand experience. Murray, D.L. and Ackroyd, P. (eds), pp. 165-192, N.Z. Hydrological Society, Wellington.

Pearce, A.J., M.K. Stewart and M.G. Sklash (1986), Storm runoff generation in humid headwater catchments: 1. Where does the water come from?, *Water Resour. Res.*, 22, 1263-1272. 10.1029/WR022i008p01263.

Pfister, L., N. Martínez-Carreras, C. Hissler, J. Klaus, G.E. Carrer, M.K. Stewart and J.J. McDonnell (2017), Bedrock geology controls on catchment storage, mixing and release: A comparative analysis of 16 nested catchments, *Hydrol. Processes*, 31(10), 1828-1845. 10.1002/hyp.11134.

Price (2011), Effects of watershed topography, soils, land use, and climate on baseflow hydrology in humid regions: A review, *Progress in Physical Geography*, 35(4), 465-492. 10.1177/0309133311402714.

Sanford, W. (2002), Recharge and groundwater models: An overview, *Hydrogeol. J.*, 10(1), 110-120. 10.1007/s10040-001-0173-5.

Sayama, T., J.J. McDonnell, A. Dhakal and K. Sullivan (2011), How much water can a watershed store?, *Hydrol. Processes*, 25, 3899-3908. 10.1002/hyp.8288.

Scanlon, B.R., R.W. Healy and P.G. Cook (2002), Choosing appropriate techniques for quantifying groundwater recharge, *Hydrogeol. J.*, 10(1), 18-39. 10.1007/2Fs10040-001-0176-2.

Scanlon, B.R., K.E. Keese, A.L. Flint, L.E. Flint, C.B. Gaye, W.M. Edmunds and I. Simmers (2006), Global synthesis of groundwater recharge in semiarid and arid regions, *Hydrol. Processes*, 20(15), 3335-3370. 10.1002/hyp.6335.

Sklash, M.G. and R.N. Farvolden (1979), The role of groundwater in storm runoff, *J. Hydrol.*, 43, 45-65. 10.1016/0022-1694(79)90164-1

Smerdon, B., D. Allen, S. Grasby and M. Berg (2009), An approach for predicting groundwater recharge in mountainous watersheds, *J. Hydrol.*, 365(3), 156-172. 10.1016/j.jhydrol.2008.11.023.

Stewart, M.K. and J.J. McDonnell (1991), Modeling base flow soil water residence times from deuterium concentrations, *Water Resour. Res.*, 27(10), 2681-2693. 10.1029/91WR01569.

Stute, M., P. Schlosser, J.F. Clark and W.S. Broecker (1992), Paleotemperatures in the southwestern united states derived from noble gases in ground water, *Science*, 256(5059), 1000-1003.

Sukhija, B., D. Reddy, P. Nagabhushanam and S. Hussain (2003), Recharge processes: Piston flow vs preferential flow in semi-arid aquifers of india, *Hydrogeol. J.*, 11(3), 387-395. 10.1007/s10040-002-0243-3.

Tague, C., G. Grant, M. Farrell, J. Choate and A. Jefferson (2008), Deep groundwater mediates streamflow response to climate warming in the oregon cascades, *Climatic Change*, 86(1), 189-210. 10.1007.2Fs10584-007-9294-8.

Tallaksen, L. (1995), A review of baseflow recession analysis, *J. Hydrol.*, 165(1), 349-370. 10.1016/0022-1694(94)02540-R.

Taylor, R.G., B. Scanlon, P. Döll, M. Rodell, R. Van Beek, Y. Wada, L. Longuevergne, M. Leblanc, J.S. Famiglietti and M. Edmunds (2013a), Ground water and climate change, *Nature Climate Change*, 3(4), 322-329. 10.1038/nclimate1744.

Taylor, R.G., M.C. Todd, L. Kongola, L. Maurice, E. Nahozya, H. Sanga and A.M. Macdonald (2013b), Evidence of the dependence of groundwater resources on extreme rainfall in east africa, *Nature Climate Change*, 3(4), 374-378.

Thornthwaite, C.W. (1948), An approach toward a rational classification of climate, *Geographical review*, 38(1), 55-94.

Tromp-Van Meerveld, H. and J. McDonnell (2006), Threshold relations in subsurface stormflow: 2. The fill and spill hypothesis, *Water Resour. Res.*, 42(2). 10.1029/2004WR003800.

Tromp-Van Meerveld, H., N. Peters and J. McDonnell (2007), Effect of bedrock permeability on subsurface stormflow and the water balance of a trenched hillslope at the panola mountain research watershed, georgia, USA, *Hydrol. Processes*, 21(6), 750-769. 10.1002/hyp.6265.

Vaché, K.B. and J.J. McDonnell (2006), A process-based rejectionist framework for evaluating catchment runoff model structure, *Water Resour. Res.*, 42(2). 10.1029/2005WR004247.

Van Verseveld, W.J., H.R. Barnard, C.B. Graham, J.J. McDonnell, J.R. Brooks and M. Weiler (2017), A sprinkling experiment to quantify celerity-velocity differences at the hillslope scale, *Hydrol. Earth Syst. Sci. Discuss.*, 2017, 1-39. 10.5194/hess-2017-125.

Wagener, T., M. Sivapalan, P. Troch and R. Woods (2007), Catchment classification and hydrologic similarity, *Geography Compass*, 1(4), 901-931. 10.1111/j.1749-8198.2007.00039.x.

Warrier, R.B., M.C. Castro and C.M. Hall (2012), Recharge and source-water insights from the galapagos islands using noble gases and stable isotopes, *Water Resour. Res.*, 48(3), W03508. 10.1029/2011WR010954.

Weiler, M., B.L. McGlynn, K.J. McGuire and J.J. McDonnell (2003), How does rainfall become runoff? A combined tracer and runoff transfer function approach, *Water Resour. Res.*, 39(11), SWC41-SWC413. 10.1029/2003WR002331.

Welch, L.a.A., D.M.M. Allen and H.J. Van Meerveld (2012), Topographic controls on deep groundwater contributions to mountain headwater streams and sensitivity to available recharge, *Canadian Water Resources Journal / Revue canadienne des ressources hydriques*, 37(4), 349-371. 10.4296/cwrj2011-907.

Wilson, J.L. and H. Guan (2004), Mountain-block hydrology and mountain-front recharge, *Water Science and Application*, 9, 113-137. 10.1029/009WSA08.

Winograd, I.J., A.C. Riggs and T.B. Coplen (1998), The relative contributions of summer and cool-season precipitation to groundwater recharge, spring mountains, nevada, USA, *Hydrogeol. J.*, 6(1), 77-93. 10.1007.2Fs100400050135.

Winter, T.C., J.W. Harvey, O.L. Franke and W.M. Alley (1998), Ground water and surface water a single resource, p. 79, United States Geological Survey, Denver, CO.

Woods, R. and L. Rowe (1996), The changing spatial variability of subsurface flow across a hillside, *Journal of Hydrology New Zealand*, 35(1), 51-86.

CHAPTER 4

A LANDSCAPE ANISOTROPY INDEX TO QUANTIFY THE RELATIONSHIP BETWEEN GEOLOGY, LANDSCAPE STRUCTURE AND WATER TRANSIT TIME THROUGH CATCHMENTS

4.1 Abstract

The relationship between streamwater mean transit time (MTT), catchment geology and landscape structure is still poorly characterized. In catchments underlain by poorly permeable bedrock, the permeability contrast at the soil bedrock interface can play a key role in shunting young water laterally downslope towards the stream channel. In such situations MTT has been shown to relate to topographic metrics of slope length and inverse slope angle. In permeable bedrock situations, streamwater MTT has been observed to scale not with topographic parameters but with catchment area – where larger watersheds have older streamwater than the smaller catchments that comprise them. Here we present a new simple index that focuses specifically on permeability contrasts at the soil-bedrock interface and DEM-based physical flowpath measurements to identify broad landscape trends of moisture redistribution in the subsurface. We use this index to explore the relationship between geology, landscape structure and water transit time through the lens of landscape anisotropy (here defined as the relative partitioning between lateral flow and vertical percolation). We hypothesize that catchments with a greater tendency to shed water laterally will correlate with younger stream water MTT and catchments with a greater tendency to infiltrate water vertically will correlate with older streamwater MTT. We tested the new index at 8 geologically diverse Pacific Rim catchments in Oregon, Japan and New Zealand. The new index explained 77% of the variability in measured streamwater MTT across these varied sites. These findings suggest that landscape anisotropy and catchment form are first-order controls on the time scales over which catchments store and release their water and that a simple index may usefully capture this relationship.

4.2 Introduction

In its most basic form, the turnover time for water in a catchment follows the simple steady state equation $T = S/Q$, where T is the turnover time, S is the catchment storage and Q is catchment discharge (*Maloszewski and Zuber, 1982; McGuire and McDonnell, 2006; Staudinger et al., 2017*). The time varying nature of catchment conditions combined with the non-linear and often hysteretic activation and deactivation of subsurface storage units and flowpaths, however, results in a much more complex and time varying turnover time (*Duffy, 2010; Heidbüchel et al., 2012*). This complex storage-release interaction and catchment turnover time variation in space and time has been the subject of recent active theoretical research (*Hrachowitz et al., 2010; Botter et al., 2011; Birkel et al., 2012; Heidbüchel et al., 2012*). Contemporary particle tracking work (*Davies et al., 2013; Ameli et al., 2017*) and new complex storage selection functions (*Harman, 2015; Rinaldo et al., 2015*) aim to define the nonstationary nature of catchment discharge age across all catchment conditions. Indeed, the field has gone down a very detailed path into complex theory and mathematics.

But while much uncertainty still remains in terms of how fundamental catchment properties such as geology, topography, vegetation cover and seasonality in climate forcing control the age of water leaving a catchment (*McNamara et al., 2011; Heidbüchel et al., 2013; Hale and McDonnell, 2016; Stewart et al., 2016*), few studies have explored the value of simple metrics in illuminating the control of subsurface architecture on catchment transit times. Here, we ask if there is a parallel, simple track perhaps worth exploring – a search for a basic catchment scale metric that might capture some of the overarching controls on catchment transit time? And in so doing, convey insights into how landscape form and subsurface structure influences the internal catchment mixing dynamics that drive catchment storage-release processes. We base this on our recent work in geologically diverse catchments in Oregon, where *McGuire et al. (2005)* found landscape organization, specifically median flowpath length divided by slope gradient, controlled catchment mean transit time (MTT) – defined as the average time water spends transiting the subsurface before entering the stream network – in 7 nested catchments within the Oregon Cascade volcanics. *Hale and McDonnell (2016)* then tested this relationship in the Oregon Coast Range where more permeable meta-sedimentary bedrock resulted in no relation to topographic metrics, but instead

MTT was controlled by catchment area (where MTT increased as catchment area increased). These findings suggest that landscape-scale subsurface anisotropy appears to be a first-order control on how catchments store and release their water between catchments of varying geologies. *Hale et al.* (2016) further expanded on the role of bedrock permeability in setting catchment scale storage-release patterns, identifying it as a critical catchment characteristic in setting the age distribution of water exiting catchments in the Oregon Coast Range.

So how might this knowledge be incorporated into a simple index when so many model and theoretical approaches have been so complex? If we assume MTT as a proxy for T and start with the most basic form where $MTT = S/Q$, then decreases in S or increases in Q drive shorter MTT, and vice versa. Though this simplistic view is bedeviled by the complexity of interactions between inherent catchment properties, many field observations still come back to this ratio of storage and flux as a first approximation of MTT (*Stewart et al.*, 2007). For example, catchment flux is directly controlled by precipitation or landscape gradient. Indeed, in different geologic and climatic settings both *Hrachowitz et al.* (2009b) and *Heidbüchel et al.* (2013) observed that increased annual precipitation amount led to shorter MTT, and in high relief landscapes, steep flow gradients have been found to be highly correlated with catchment transit times (*Tetzlaff et al.*, 2009b). Alternatively, differences in catchment storage, predominantly manifested as differences in soil thickness or bedrock permeability, have also been found to control catchment MTT. Deeper more freely draining soils (*Tetzlaff et al.*, 2009a; *Tetzlaff et al.*, 2014) and greater percentages of more permeable bedrock (*Pfister et al.*, 2017) both increase storage and result in longer catchment MTT.

Many efforts have been made with varying success to find simple scaling relationships between terrain-based indices and catchment transit times in order to shed light on the underlying storage-release relationship (*McGlynn et al.*, 2003; *McGuire et al.*, 2005; *McNamara et al.*, 2011; *Soulsby et al.*, 2011; *Heidbüchel et al.*, 2013; *Hale et al.*, 2016). Yet, most studies have lacked expansion of observation beyond their single study site or region, and none yet have found a simple terrain-based index that encapsulates both landscape form and geologic properties and their combined control on storage-release processes that can explain variations in the mean age of water discharged from headwaters in different regions. Although *Hale and McDonnell* (2016) and *Hale et al.* (2016)

came close, their work stopped short of any index development. It appears that geologic anisotropy (defined here as permeability contrast at the soil-bedrock interface) may be the key general factor for setting MTT and MTT scaling relationships. Indeed, it has been observed for some time that strong subsurface permeability contrasts are key to the initiation of lateral subsurface flow (*Hopp and McDonnell, 2009*), a flow mechanism that drastically shifts moisture redistribution from vertically downward, and thus through deeper more tortuous flowpaths, to laterally and through shallow faster pathways (*Bonell, 1993*).

Here we present a new index to capture how subsurface anisotropy controls the relative partitioning of water between lateral flow and vertical percolation, which builds upon work by *Jackson et al. (2014)* who developed the metric known as downslope travel distance. The *Jackson et al. (2014)* metric calculates the theoretical displacement of a parcel of water laterally downslope before that parcel infiltrates fully into a lower impeding horizon and was initially developed to calculate lateral travel distances in sequenced soil layers. Although the downslope travel distance calculation results in a theoretical distance, to date this distance has not been directly mapped to physical flowpath lengths – in a single catchment or across catchments. We modify the downslope travel distance to focus specifically on the soil-bedrock interface and we integrate it with DEM-based physical flowpath measurements to construct a new landscape scale anisotropy index that identifies broad landscape trends of water redistribution in the subsurface. We use this index to explore the relationship between geology, landscape structure and water transit time through the lens of subsurface anisotropy.

Specifically, we ask:

- i. How do landscape form and subsurface flow partitioning control the tendency of a catchment to store or shed water?
- ii. Can this tendency towards shedding versus storage be captured by a simple index, and does that index capture observed variations in catchment streamwater MTT?

We test this new index at 8 well-studied headwater catchments in 4 geologically diverse regions within the Pacific Rim and compare differences in mean catchment index values with previously observed streamwater MTT. We focus here initially on humid temperate catchments with thin soils and annual precipitation that greatly exceeds evapotranspiration, and specifically where previous work has shown that despite similar rainfall-runoff characteristics these catchments hide different geologically mediated subsurface runoff generation processes, thus providing an opportunity to highlight the role of subsurface architecture in differentially controlling catchment function (McGuire *et al.*, 2005; Katsuyama *et al.*, 2010; Sayama *et al.*, 2011; Gabrielli *et al.*, 2012; Hale and McDonnell, 2016).

4.3 Theory

Downslope travel distance is calculated as:

$$L_D = \frac{K_u}{K_L} * \frac{\sin \theta}{\frac{N+C_n}{C_n}} * N \quad (\text{Eq. 4.1})$$

Where K_u is the saturated hydraulic conductivity (Ksat) of overlying soil layer, and K_L is the Ksat of the underlying impeding layer, here the bedrock horizon. N is the normal thicknesses of the saturated soil lens above the bedrock horizon, C_n is the thickness of saturated bedrock, and θ is the local slope angle. For a more complete description of downslope travel distance development and calculation see Jackson *et al.* (2014).

We relate L_d to the physical landscape by dividing L_d by the flowpath length (L_f) from the point of measurement on the landscape to the stream channel, to create the new Anisotropy Index (AI). Figure 4.1 shows conceptually how the AI index functions. When AI is greater than 1, a parcel of water would require greater slope length to fully infiltrate into the underlying bedrock than is possible from the slope, and thus the parcel of water is delivered to the stream channel. Conversely, when AI is less than 1, a parcel of water would move vertically through the soil and fully infiltrate into the bedrock horizon before reaching the stream channel, and thus that parcel of water would

be lost to deeper storage. Applying this calculation to each grid cell within a DEM provides a spatially distributed assessment of how a catchment internally redistributes its water. Taken in aggregate, the mean AI for a catchment provides information on the general tendency of the landscape to shed water laterally to the stream channel or infiltrate water to depth. We hypothesize that catchments with a lower mean AI, and thus a greater proportion of water moving to depth through longer more tortuous flowpaths will tend towards longer catchment MTT, and vice versa (Jiang *et al.*, 2009; Ameli *et al.*, 2016).

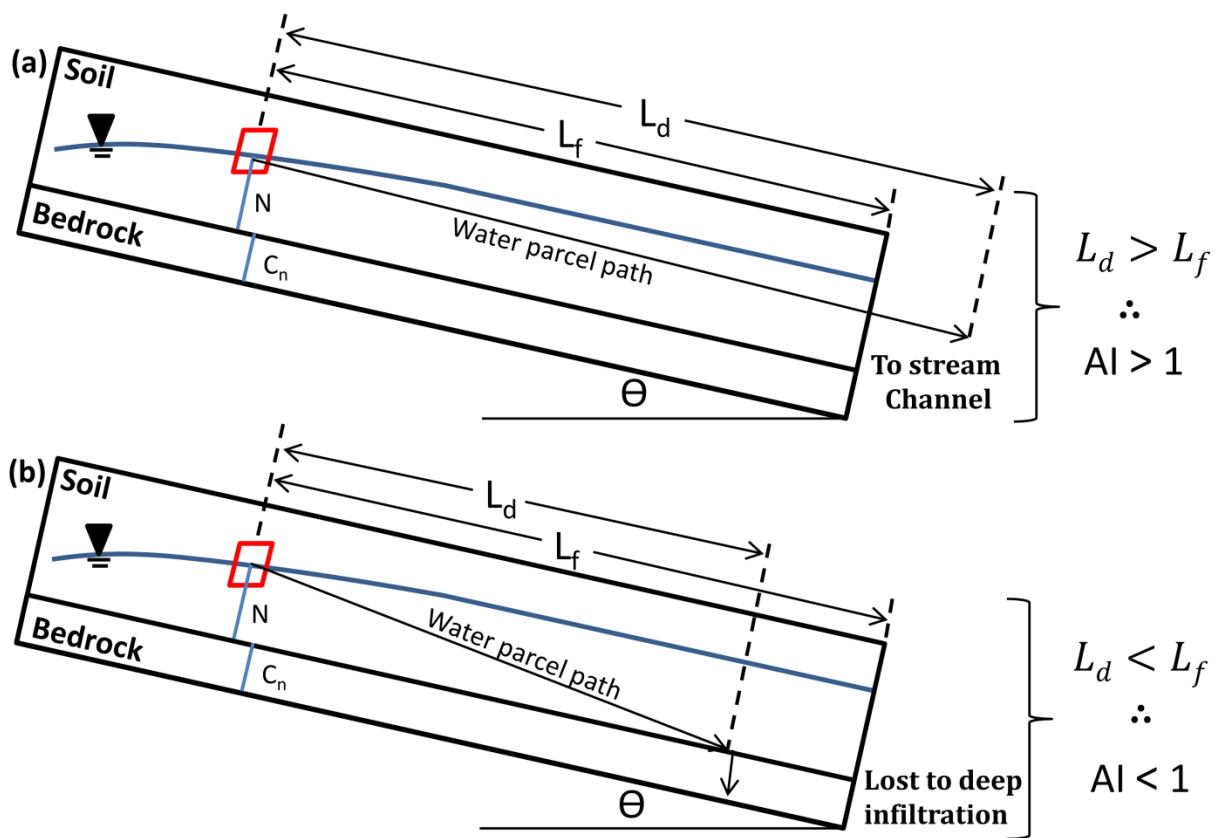


Figure 4.1 When the Anisotropy Index (AI) is greater than 1, the downslope travel distance (L_d) of a parcel of water (here represented by the red box) is greater than the flowpath length (L_f) that the parcel of water would travel down the hillslope to the stream channel. This results in the parcel of water being delivered to stream (a). When AI is less than 1, then L_d is greater than L_f and the parcel of water is lost instead to deep percolation. Figure adapted from Jackson *et al.* (2014).

4.4 Methods

We test this new index on 8 well-studied watersheds in 4 geologically distinct regions around the Pacific Rim. Specifically, the M8 sub-catchment within the Maimai Experimental Watershed, New Zealand (*McGlynn et al.*, 2002); catchments WS1, WS9 and WS10 at the H.J. Andrews Experimental Forest Long Term Ecological Research site in the Cascade range of Oregon, USA (*Swanson and Jones*, 2002); catchments NB12, NB35 and NB86 recently studied by *Hale and McDonnell* (2016) and *Hale et al.* (2016) within the Coast range of Oregon, USA; and finally catchment K at the Kiryu Experimental Watershed (KEW) in the Shiga Prefecture, Japan (*Katsuyama et al.*, 2008).

Table 4.1 Summary of catchment characteristics

Catchment	Location	Area, ha	Annual rainfall, [mm]	Annual runoff, [mm]	Runoff ratio, [-]	Mean soil depth, [m]	Elevation min, [m.a.s.l]	Elevation max, [m.a.s.l]	Geology
M8	Maimai Experimental Watershed, New Zealand	4.5	2600 ^a	1550 ^a	0.60	0.6 ^a	250	348	Weakly Cemented conglomerate ^b
WS1	HJ Andrews, LTER, OR, USA	96	2800 ^c	1354 ^d	0.48	0.9 ^d	460	990	volcanic tuff and coarse breccia ^e
WS9	HJ Andrews, LTER, OR, USA	8.5	2800 ^c	1673 ^d	0.60	0.9 ^d	451	692	volcanic tuff and coarse breccia ^e
WS10	HJ Andrews, LTER, OR, USA	10.2	2800 ^c	1475 ^c	0.53	3.0 ^f	424	710	volcanic tuff and coarse breccia ^e
KEW	Kiryu Experimental Watershed, Japan	5.99	1631 ^g	936 ^h	0.57	0.6 ⁱ	178	253	Biotite Granite ^j
NB12	Coast Range, OR, USA	12	2500 ^c	1627	0.65	1.0 ^c	686	1212	Marine Derived silt and sandstones ^k
NB35	Coast Range, OR, USA	35	2500 ^c	1588	0.64	1.0 ^c	540	1212	Marine Derived silt and sandstones ^k
NB86	Coast Range, OR, USA	86	2500 ^c	1548	0.62	1.0 ^c	426	1212	Marine Derived silt and sandstones ^k

^a*McGlynn et al.* (2002), ^b*Pearce and Rowe* (1979), ^c*Hale and McDonnell* (2016), ^d<https://andrewsforest.oregonstate.edu/>, ^e*Swanson and James* (1975), ^f*Harr and Ranken* (1972), ^g*Katsuyama et al.* (2010), ^h*Katsuyama et al.* (2001), ⁱ*Kubota et al.* (1983), ^j*Torii* (1996), ^k*Snively et al.* (1964)

General catchment characteristics are presented in Table 4.1. Catchments range in area from 4.5 ha (M8) to 86 ha (NB86), have generally shallow soils (mean: 0.9 m, SD: 0.19 m) and steep slopes (range: 1 - 65°, mean: 30°, SD: 11°). Precipitation is high for all catchments and with the exception of KEW, which receives on average 1631 mm of rainfall, all catchments receive greater than 2500 mm of rainfall annually. Previous work has established subsurface stormflow as the main runoff generating mechanism for all catchments.

Geologically, the catchments are quite diverse. M8 in New Zealand is underlain by an unfractured weakly cemented Early Pleistocene conglomerate composed primarily of sandstone clasts in a consolidated sandy matrix (*Nathan, 1974*). Bedrock at KEW is composed of a uniformly weathered Cretaceous biotite granite that is weathered in its upper layers to a saprolitic consistency (*Torii, 1996; Katsura et al., 2006*). NB12, NB35 and NB86 in the Oregon Coast Range are comprised of the Eocene-aged Tyee formation which is marine-derived layered greywacke siltstones and sandstones (*Snavely et al., 1964*). While bedrock in the Oregon Cascade Range catchments, WS1, WS9 and WS10, is composed of late Oligocene to early Miocene aged hydrothermally altered volcanic tuff and coarse breccia (*Swanson and James, 1975*).

Streamwater MTT studies were conducted previously for all catchments and we refer the reader to that primary literature as summarized in Table 4.2. The primary methodology employed to determine MTT was through lumped parameter convolution modeling using stable isotopes of water, however, tritium analysis combined with silica regression was used at M8 (Table 4.2). MTT values ranged from 0.33 y (M8) to 5.0 y (NB12). Previous work also investigated a range of catchment attributes which were observed to scale with or act as primary controls on catchment MTT (Table 4.2). This includes magnitude of annual bedrock infiltration (KEW (*Katsuyama et al., 2010*)), catchment area (NB12, NB35 & NB86 (*Hale and McDonnell, 2016*)), median sub-catchment size (M8 (*McGlynn et al., 2003*)), and flow path distance and gradient (WS9 & WS10 (*McGuire et al., 2005*)).

Table 4.2 Summary of catchment MTT characteristics

Catchment	MTT, y	MTT determination method	MTT found to scale with:
M8	0.4 ^a	Tritium and Silica Regression	^b Median subcatchment area
WS1	1.3 ^c	Stable isotopes of water and lumped-parameter convolution modeling	^c Topographic characteristics, flowpath length and gradient
WS9	1.4 ^c	Stable isotopes of water and lumped-parameter convolution modeling	^{c,d} Topographic characteristics, flowpath length and gradient
WS10	1.2 ^c	Stable isotopes of water and lumped-parameter convolution modeling	^{c,d} Topographic characteristics, flowpath length and gradient
KEW	3.8 ^e	Stable isotopes of water and lumped-parameter convolution modeling	^e Bedrock infiltration
NB12	5.0 ^c	Stable isotopes of water and lumped-parameter convolution modeling	^c Catchment area
NB35	3.7 ^c	Stable isotopes of water and lumped-parameter convolution modeling	^c Catchment area
NB86	4.0 ^c	Stable isotopes of water and lumped-parameter convolution modeling	^c Catchment area

^aGabrielli *et al.* (2017), ^bMcGlynn *et al.* (2003), ^cHale and McDonnell (2016), ^dMcGuire *et al.* (2005), ^eKatsuyama *et al.* (2010)

Values for K_u and K_L in Equation 4.1 were established from catchment-specific literature as shown in Table 4.3. The thickness of the saturated lens above the impeding bedrock boundary, N , will vary both spatially and temporally and can take values ranging from 0 to the full thickness of the soil column. For simplicity, we used a spatially constant N equal to 0.5 times the mean catchment soil depth for all catchments, which corresponds well to piezometric observations at Maimai (McDonnell, 1990) and to observations made at similar catchments near both Oregon sites (Dhakal and Sullivan, 2014) for median-sized and larger storms. Similarly, the saturated bedrock thickness, C_n , can also vary spatially throughout a catchment and temporally under different catchment wetness conditions. Jackson *et al.* (2014) noted that C_n likely takes values ranging from very thin (< 0.1 m) to very thick (> 10 m). For simplicity we used a spatially constant value of C_n equal to 1.0 m. However, we tested a range of values for both N and C_n and discuss the sensitivity of these variations to our final results in the discussion below. Local slope, Θ , was calculated for each catchment using a 5 m grid DEM, except for NB12, NB35 and NB86 in which a 10 m grid DEM was used.

L_f was calculated using the D8 flow algorithm (Jenson and Domingue, 1988) to determine flowpath length from each grid cell to the stream channel. Stream channels were delineated based

on stream initiation threshold values found in literature. AI was calculated for each DEM grid establishing a spatially distributed AI map for each catchment. We calculated basic statistics for each catchment, as well as mean AI and the percent of each catchment with an AI value greater than 1 ($AI_{>1}$) and compared these values to observed catchment MTT.

Table 4.3 Catchment variables used to calculate the Anisotropy Index.

Catchment	Soil Ksat, K_u [m/s]	Bedrock Ksat, K_L [m/s]	^a Soil saturated thickness depth: N, [m]	Bedrock saturated thickness: Cn, [m]	Slope range, Θ , [°]
M8	6.94E-05 ^b	9.90E-08 ^c	0.3	1.0	2 - 51
WS1	1.00E-04 ^d	1.42E-07 ^e	0.5	1.0	1 - 69
WS9	1.00E-04 ^d	1.42E-07 ^e	0.5	1.0	4 - 45
WS10	1.00E-04 ^d	1.42E-07 ^e	1.5	1.0	1 - 45
KEW	4.70E-04 ^f	1.00E-06 ^g	0.3	1.0	1 - 41
NB12	2.78E-04 ^h	4.70E-07 ⁱ	0.5	1.0	1 - 44
NB35	2.78E-04 ^h	4.70E-07 ⁱ	0.5	1.0	1 - 44
NB86	2.78E-04 ^h	4.70E-07 ⁱ	0.5	1.0	1 - 46

^aDepth of saturation was set equal to 0.5 times mean soil depth as reported in the listed literature in table 4.2.

^bMcKie (1978), ^cGabrielli *et al.* (2017) ^dRanken (1974), ^eGraham *et al.* (2010), ^fOhte *et al.* (1989), ^gKatsura *et al.* (2006), ^hHale and McDonnell (2016)

^mValues based on nearby bedrock groundwater studies at the CB1 ridge (Montgomery *et al.*, 2002) which were noted to have similar bedrock characteristics by Hale and McDonnell (2016)

4.5 Results

Table 4.4 presents mean values of L_f , L_D , AI, and $AI_{>1}$ for each of the 8 studied catchments. Mean catchment AI ranged from 0.3 ± 0.6 at NB86 to 8.0 ± 6.8 at M8. The 3 Oregon Coast Range catchments, NB12, NB36 and NB86, had the lowest mean AI as a result of a lower permeability contrast at the soil-bedrock interface and long hillslope lengths which correspond with shorter downslope travels distances and longer flowpath lengths. This suggests that water redistribution at these sites tends to be vertically downward into the bedrock horizon. Catchment M8 had the highest mean AI. The high soil-bedrock permeability contrast resulted in large downslope distances and when combined with the short physical slope lengths AI values were high.

Table 4.4 Mean flowpath length (L_f), mean downslope travel distance (L_d), mean AI, and percent $AI_{>1}$.

Catchment	L_f mean [m]	$L_f \pm SD$ [m]	L_d mean [m]	$\pm SD$ [m]	AI mean [-]	$\pm SD$ [-]	Percent $AI_{>1}$ [%]
M8	25	22	98	15	8.0	6.8	1
WS1	121	34	122	76	3.8	6.3	34
WS9	119	22	126	76	3.8	6.4	35
WS10	100	49	228	64	6.9	11.5	8
KEW	26	12	38	16	3.3	2.7	18
NB12	254	12	32	151	0.4	0.8	92
NB35	256	12	54	195	0.4	0.6	92
NB86	287	12	56	214	0.3	0.6	93

Figure 4.2 shows the spatial distribution of each of these variables for 4 of the 8 catchments – one each from the 4 geologic regions. Generally, catchments M8, WS1 and KEW had much higher AI in areas directly surrounding the stream channel. Values quickly dropped with distance upslope. Figure 4.2e shows the spatial distribution of $AI_{>1}$, distinguishing between grid cell values greater or less than 1. At M8, $AI_{>1}$ is present only in ridgeline locations, while at NB86 the inverse pattern was observed, and values were less than 1 across the majority of the catchment except directly along the stream channel. These two catchments provide bookend examples of landscape structures that tend to shed water (M8) versus infiltrate water (NB86).

We compared catchment MTT to catchment mean L_f , mean flow path length divided by gradient (L_f/G), catchment area, mean L_d , mean AI and $AI_{>1}$ (Figure 4.3). Both mean L_f and mean L_f/G explained about half of the variance observed in catchment MTT between the 8 catchments (R^2 : 0.45 and 0.48, $p < 0.01$ and 0.02, respectively), while catchment area showed no correlation to MTT ($R^2 = 0.01$, $p < 0.85$). Mean L_d had a slightly stronger relation with MTT than L_f or L_f/G , but still only explained slightly more than half of the variability observed in MTT. Mean AI, however, was strongly correlated to catchment MTT and explained nearly 80% of the observed variation in age ($R^2 = 0.77$, $p < 0.01$).

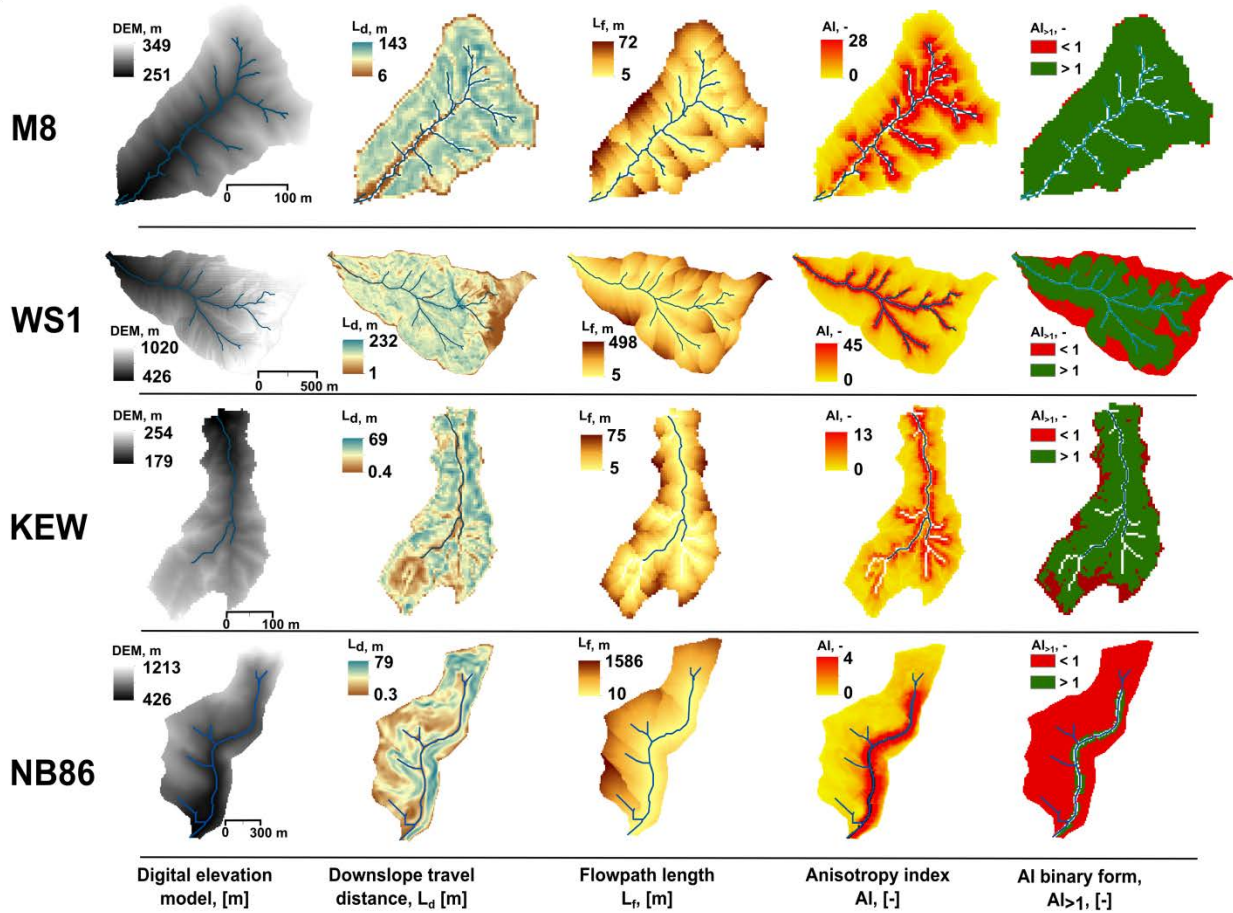


Figure 4.2 Catchment examples from the 4 different geologic settings. This figure shows, from left to right for each catchment, the sequence of analysis to calculate AI. The final graphic (far right) for each site shows the binary form of AI.

Since distributed field observations of soil and/or bedrock saturated thickness (N and C_n) are the most difficult data sets to obtain for this analysis, and thus the most likely to contain large degrees of uncertainty due to estimation, we varied both N and C_n through a range of values and observed the sensitivity of the relationship between catchment mean AI and MTT through changes in the coefficient of determination (i.e. R^2). We varied N from 0.01 to 1 times the mean catchment soil depth, and C_n from 0.1 m to 10 m. Overall, the range in R^2 varied from 0.56 to 0.84 indicating the AI index still had a strong relation with catchment MTT even if estimates of either parameter contained considerable uncertainty (Figure 4.4).

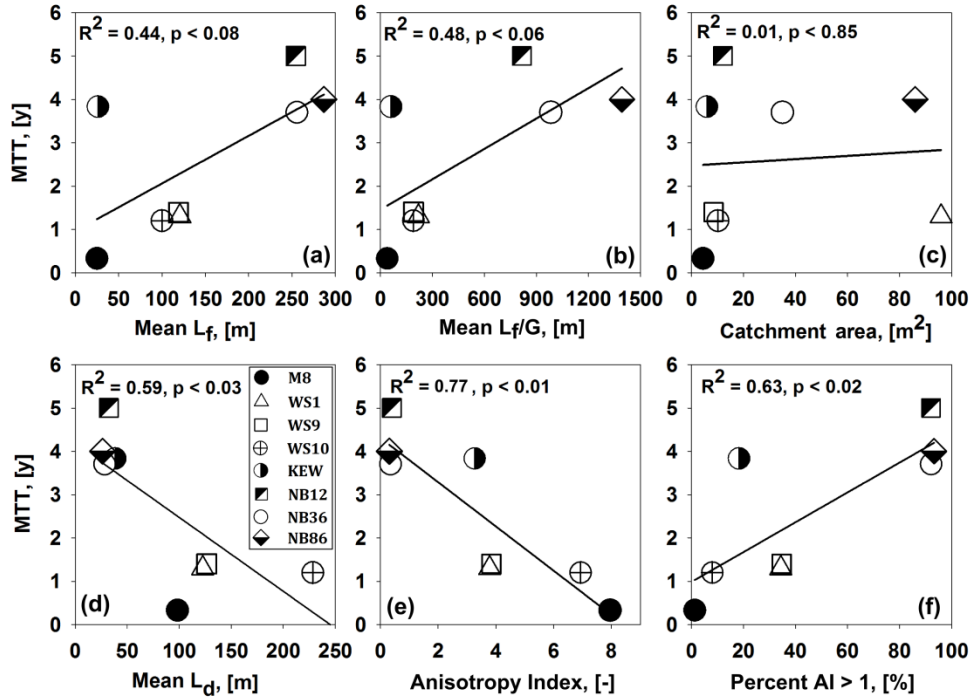


Figure 4.3 Relationship between the AI and catchment MTT for the 8 studied catchments. The solid line shows the liner regression relationship between the two variables and the associated coefficient of determination. Note, catchment legend markers shown in (d) are consistent through all plots.

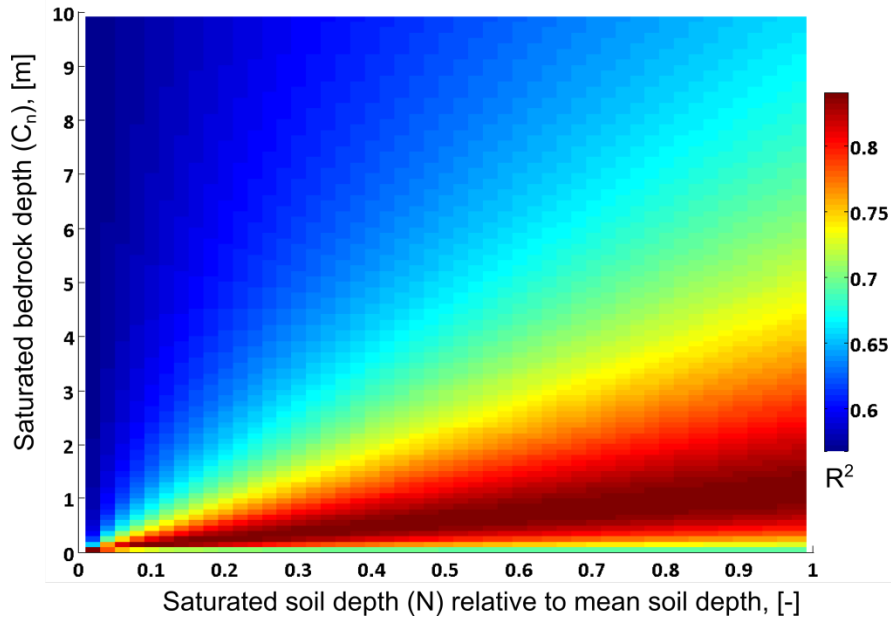


Figure 4.4 Coefficient of determination (R^2) values for the regression fit between catchment mean AI and MTT through a range of saturated soil depths (N) and saturated bedrock depths (C_n).

4.6 Discussion

4.6.1 On the value of the new index

While many studies have found landscape derived metrics at single sites that scale to MTT (*McGlynn et al.*, 2003; *McGuire et al.*, 2005; *Rodgers et al.*, 2005; *Tetzlaff et al.*, 2009a; *Katsuyama et al.*, 2010; *McNamara et al.*, 2011; *Buttle*, 2016; *Hale and McDonnell*, 2016), we are unaware of any metric which successfully combines internal catchment structure with topographically based data to capture the observed variability in catchment discharge MTT across multiple geologically diverse sites. Our simple landscape anisotropy index builds on the *Jackson et al.* (2014) downslope travel distance index and combines simple field-measurable data with topographic DEM analysis into a single new composite index that captures the general tendencies of how catchments capture, store and release their subsurface water. As the propensity to shed water laterally within a catchment increases (due to greater anisotropy at the soil-bedrock interface and/or shorter slopes lengths), greater relative volumes of water transit the subsurface domain through shallower faster flowpaths, resulting in shorter MTT, and vice versa. Although streamwater MTT is highly complex and varies considerably in time with catchment storage conditions (*Maloszewski and Zuber*, 1982; *Morgenstern et al.*, 2010; *Heidbüchel et al.*, 2012; *Tetzlaff et al.*, 2014; *Harman*, 2015), the general tendencies of subsurface storage and flow within a catchment are still reflected by their MTT values. Our results show a clear and significant relationship between mean AI and catchment MTT for 8 catchments in 4 geological settings, highlighting the first order control of subsurface anisotropy and catchment form on storage-release processes.

4.6.2 On the meaning of the anisotropy index

The AI index offers two levels of information: first through its spatially distributed pattern at the grid-scale within each catchment, and second through the aggregated catchment-scale value. At the grid-scale, an individual grid value less than 1 indicates that a parcel of water originating from that grid cell will fully infiltrate into the underlying bedrock before reaching the stream channel. A grid-scale value greater than 1 indicates lateral movement of water to the stream and provides spatial information on variable source areas that contribute more extensively to the stream channel

(Walter *et al.*, 2000; Jackson *et al.*, 2014). It is worth noting, however, that for grid values greater than 1, ‘transmission losses’ to the bedrock horizon still occur as the parcel of water transits the hillslope. A grid value nearer to 1 implies greater transmission losses than a grid value further from 1, providing a means to compare the degree to which catchments shunt water to depth. This is captured by the difference in regression fit between $AI_{>1}$ and MTT versus the regression fit between mean AI and MTT (Figure 4.3e versus 4.3f, respectively). The binary form of AI does not account for contributions to deeper infiltration from grid cells with values greater than 1, when in fact these locations would contribute some portion of water to depth, which explains the only moderate correlation with MTT. However, mean AI captures this partial infiltration and thus more completely captures the general catchment flux trends. Consequently, the correlation between mean AI and MTT is much stronger across the tested catchments.

While many of the individual catchments studied in this work have shown clear MTT scaling relationships with different topographic or landscape-based metrics (McGlynn *et al.*, 2003; McGuire *et al.*, 2005; Hale and McDonnell, 2016), these metrics are not necessarily transferable between catchments in different geologic regions. This implies that the local metrics like area, slope gradient, and flowpath distance still do not capture the full range of possible controls on MTT generally. Our new anisotropy index for the first time captures between-region variability in MTT and provides strong evidence that it also captures the underlying relationships governing subsurface storage and release. This transcends single catchments finding and shows – at least for the environments tested here – that AI is able to subsume the previously identified dominant factors that mediate MTT at each individual catchment into a single value that captures broader controls on the relationship between geology, landscape structure and catchment transit time.

So why does the AI outperform topographic metrics? In catchments with more than one major subsurface storage unit, bedrock permeability and thus subsurface anisotropy, acts as a first-order control on the depth of active flowpaths. In turn, depth of active flowpaths controls total mixing volume and the general flux rates of catchment storage such that shallow flowpaths tend to be faster and therefore younger (McGlynn *et al.*, 2003; Hrachowitz *et al.*, 2009a), while deeper flowpaths implicate larger storage and slower groundwater movement and tend to be older

(McNamara *et al.*, 2011; Asano and Uchida, 2012). The AI identifies how MTT varies *between* catchments with different subsurface structures, while topographic metrics capture how MTT varies *within* catchments of generally similar geologic characteristics. In this manner, AI does not outperform topographic metrics, so much as it may be able to predict which metrics within a similar geologic unit scale with local catchment MTT. For example, catchments with similar geologic characteristics and a high AI would generally be associated with high permeability contrasts, shallow flowpaths and thus young transit times which would likely scale to topographic metrics such as flowpath length or gradient. While the inverse would be true of catchments with low AI values in which MTT would scale with catchment area or depth of active flowpaths.

4.6.3 Beyond the initial Pacific Rim testing

While our index in no way replaces (nor do we argue against) on going work with particle tracking models (Davies *et al.*, 2011; Ameli *et al.*, 2017) and storage selection functions (Klaus *et al.*, 2015; Kim *et al.*, 2016) this parallel learning track, with its simple approach, perhaps warrants further examination elsewhere. For ungauged catchments without MTT information the AI index – with its ease of calculation and modest data requirements – offers an opportunity to explore how underlying bedrock structure and landscape form might shape the distribution of water ages discharged from catchments in various settings. This could be a useful hypothesis generating tool for field work and catchment modeling where such soft data exists (Seibert and McDonnell, 2002); especially in instances where theoretically, mathematically and computationally intensive transit time models would be difficult to run.

Clearly, more testing needs to be done. The 8 catchments tested in this study – while diverse geologically – are similar with respect to their high annual rainfall, high rainfall-runoff ratios and thin soils. Groundwater recharge at these sites would be categorized as lithologically limited (Sanford, 2002), that is, deep infiltration is constrained by the ability of the subsurface to move water to depth, as opposed to water availability. We need to test this index at drier sites. We expect that climates with less precipitation or a higher evaporative index may be less likely to show similar trends with MTT, as the redistribution of moisture to depth would be controlled to a greater extent by factors other than geology. Additionally, for example, the well-known Scottish catchments of

Rodgers et al. (2005) or *Tetzlaff et al. (2009a)* and Ecuador sites of *Mosquera et al. (2016)* may reveal a different relation with the AI index due to peculiarities of soil drainage class, despite similar total rainfall patterns to the catchments tested here. Although we suspect this index may be limited to lithologically controlled groundwater systems, a larger analysis covering a wider array of catchment geologies, soil covers and climates would be required to determine the full extent of these limitations, and in so doing may shed light on alternative controls of MTT in different environments.

Lastly, while promising, our sensitivity analyses suggest that the index, while simple, may be partially limited by the availability of spatially robust soil and bedrock data sets or the ability to appropriately constrain effective catchment-scale hydraulic conductivity parameters. However, we showed strong correlations between catchment MTT and mean AI through a range of different C_n and N values indicating a general lack of sensitivity to uncertainty in these values. This also suggests that the soil-to-bedrock permeability contrast is indeed the most critical component of the anisotropy index and its relation to catchment MTT – something that hillslope hydrological models have shown repeatedly for subsurface stormflow generation (*Hopp and McDonnell, 2009; Jackson et al., 2016*).

Further analyses may consider using spatially distributed soil thickness data where available. Additionally, where we used a spatially constant saturated soil thickness for this current analysis, it may be possible to incorporate a spatially distributed data set using proxy relationships between topographic indices, such as the topographic wetness index, and soil moisture (*Woods and Sivapalan, 1997; Sayama and McDonnell, 2009*) to construct a more precise spatially distributed catchment map of AI. Further, this analysis may also be scaled to leverage recently established continental-scale permeability mapping (*Gleeson et al., 2011*) in an effort to predict large scale MTT trends which could provide a baseline for hypothesis testing to identify if landscapes follow or do not follow trends outlined by this index.

4.7 Summary

We show proof of concept for a new index that builds on recent work by *Jackson et al. (2014)* to quantify the relationship between geology, landscape structure and water transit time. The anisotropy index successfully captures landscape scale water redistribution characteristics. We tested this relationship for 8 catchments in 4 geologic settings and found a strong positive correlation between mean catchment AI and catchment streamwater MTT that explained 77% of the variance in MTT. This suggests that permeability contrasts at the soil-bedrock interface in combination with hillslope flowpath length, act to control catchment scale storage characteristics which may account for the observed gross variability in catchment MTT.

4.8 Transition statement

Chapter 3 built upon the general control of bedrock characteristics in hydrologic functioning identified in Chapter 2, and found that bedrock properties, in concert with seasonality of evapotranspiration, controlled the timing of bedrock groundwater recharge. Both studies identified bedrock permeability as critical in controlling water redistribution in the subsurface at Maimai, which in turn controlled the nature of the recharge-discharge relationship of the bedrock groundwater aquifer. These findings provided the context of Chapter 4, in which I expanded beyond the Maimai catchment to construct a new catchment-scale index that captured the link between permeability contrasts at the soil-bedrock interface, landscape form and streamwater mean transit time at various geologically distinct catchments within the Pacific Rim.

4.9 Acknowledgments

The authors thank Ken Kosugi for the Kiryu Experimental Watershed DEM and Kevin McGuire and Cody Hale for their generous provision of data. Additionally, DEM data were provided by the HJ Andrews Experimental Forest and Long Term Ecological Research program, administered cooperatively by the US Department of Agriculture, Forest Service Pacific Northwest Research Station, Oregon State University, and the Willamette National Forest. This material is based upon work supported by the National Science Foundation under Grant No. DEB-1440409. The Oregon Geospatial Enterprise Office supplied the DEM data associated with the Needle Branch (NB)

catchments. This work was supported through funding by NSERC Discovery grant to J.J. McDonnell and a Horton Research Grant to C.P. Gabrielli. Finally, Ali Ameli, Julian Klaus, Uwe Morgenstern and Mike Stewart are thanked for early discussions on MTT.

4.10 Author contributions

CPG and JJM brainstormed the manuscript outline. CPG carried out all fieldwork, data collection, analyses and general writing of the manuscript, while JJM contributed to editing, feedback and final text.

4.11 References

Ameli, A., J. McDonnell and K. Bishop (2016), The exponential decline in saturated hydraulic conductivity with depth: A novel method for exploring its effect on water flow paths and transit time distribution, *Hydrol. Processes*, 30(14), 2438-2450. 10.1002/hyp.10777.

Ameli, A.A., K. Beven, M. Erlandsson, I.F. Creed, J.J. McDonnell and K. Bishop (2017), Primary weathering rates, water transit times, and concentration-discharge relations: A theoretical analysis for the critical zone, *Water Resour. Res.*, 53(1), 942-960. 10.1002/2016WR019448.

Asano, Y. and T. Uchida (2012), Flow path depth is the main controller of mean base flow transit times in a mountainous catchment, *Water Resour. Res.*, 48(3), W03512. 10.1029/2011WR010906.

Birkel, C., C. Soulsby, D. Tetzlaff, S. Dunn and L. Spezia (2012), High-frequency storm event isotope sampling reveals time-variant transit time distributions and influence of diurnal cycles, *Hydrol. Processes*, 26(2), 308-316. 10.1002/hyp.8210.

Bonell, M. (1993), Progress in the understanding of runoff generation dynamics in forests, *J. Hydrol.*, 150, 217-275. 10.1016/0022-1694(93)90112-M.

Botter, G., E. Bertuzzo and A. Rinaldo (2011), Catchment residence and travel time distributions: The master equation, *Geophys. Res. Lett.*, 38(11). 10.1029/2011GL047666.

Buttle, J.M. (2016), Dynamic storage: A potential metric of inter-basin differences in storage properties, *Hydrol. Processes*, 30(24), 4644-4653. 10.1002/hyp.10931.

Davies, J., K. Beven, L. Nyberg and A. Rodhe (2011), A discrete particle representation of hillslope hydrology: Hypothesis testing in reproducing a tracer experiment at gårdsjön, sweden, *Hydrol. Processes*, 25(23), 3602-3612. 10.1002/hyp.8085.

Davies, J., K. Beven, A. Rodhe, L. Nyberg and K. Bishop (2013), Integrated modeling of flow and residence times at the catchment scale with multiple interacting pathways, *Water Resour. Res.*, 49(8), 4738-4750. 10.1002/wrcr.20377.

Dhakal, A.S. and K. Sullivan (2014), Shallow groundwater response to rainfall on a forested headwater catchment in northern coastal California: Implications of topography, rainfall, and throughfall intensities on peak pressure head generation, *Hydrol. Processes*, 28(3), 446-463. 10.1002/hyp.9542.

Duffy, C.J. (2010), Dynamical modelling of concentration–age–discharge in watersheds, *Hydrol. Processes*, 24(12), 1711-1718. 10.1002/hyp.7691.

Gabrielli, C.P., J.J. McDonnell and W.T. Jarvis (2012), The role of bedrock groundwater in rainfall–runoff response at hillslope and catchment scales, *J. Hydrol.*, 450, 117-133. 10.1016/j.jhydrol.2012.05.023.

Gabrielli, C.P., J.J. McDonnell, U. Morgenstern and M. Stewart (2017), Bedrock groundwater age, water table dynamics and time-varying transit time at the maimai watershed *Water Resour. Res.*, In Review.

Gleeson, T., L. Smith, N. Moosdorf, J. Hartmann, H.H. Dürr, A.H. Manning, L.P. Van Beek and A.M. Jellinek (2011), Mapping permeability over the surface of the earth, *Geophys. Res. Lett.*, 38(2). 10.1029/2010GL045565.

Graham, C.B., W. Van Verseveld, H.R. Barnard and J.J. McDonnell (2010), Estimating the deep seepage component of the hillslope and catchment water balance within a measurement uncertainty framework, *Hydrol. Processes*, 24(25), 3631-3647. 10.1002/hyp.7788.

Hale, V.C. and J.J. McDonnell (2016), Effect of bedrock permeability on stream base flow mean transit time scaling relations: 1. A multiscale catchment intercomparison, *Water Resour. Res.*, 52(2), 1358-1374. 10.1002/2014WR016124.

Hale, V.C., J.J. McDonnell, M.K. Stewart, D.K. Solomon, J. Doolittle, G.G. Ice and R.T. Pack (2016), Effect of bedrock permeability on stream base flow mean transit time scaling relationships: 2. Process study of storage and release, *Water Resour. Res.*, 52(2), 1375-1397. 10.1002/2015WR017660.

Harman, C.J. (2015), Time-variable transit time distributions and transport: Theory and application to storage-dependent transport of chloride in a watershed, *Water Resour. Res.*, 51(1), 1-30. 10.1002/2014WR015707.

Harr, R.D. and D.W. Ranken (1972), Movement of water through forested soils in steep topography, p. 19, University of Washington, Coniferous Forest Biome Internal Rep. 117., Seattle, WA.

Heidbüchel, I., P.A. Troch, S.W. Lyon and M. Weiler (2012), The master transit time distribution of variable flow systems, *Water Resour. Res.*, 48(6). 10.1029/2011WR011293.

Heidbüchel, I., P.A. Troch and S.W. Lyon (2013), Separating physical and meteorological controls of variable transit times in zero-order catchments, *Water Resour. Res.*, 49(11), 7644-7657. 10.1002/2012WR013149.

Hopp, L. and J.J. McDonnell (2009), Connectivity at the hillslope scale: Identifying interactions between storm size, bedrock permeability, slope angle and soil depth, *J. Hydrol.*, 376(3-4), 378-391. 10.1016/j.jhydrol.2009.07.047.

Hrachowitz, M., C. Soulsby, D. Tetzlaff, J. Dawson, S. Dunn and I. Malcolm (2009a), Using long-term data sets to understand transit times in contrasting headwater catchments, *J. Hydrol.*, 367(3), 237-248. 10.1016/j.jhydrol.2009.01.001.

Hrachowitz, M., C. Soulsby, D. Tetzlaff, J.J.C. Dawson, S.M. Dunn and I.A. Malcolm (2009b), Using long-term data sets to understand transit times in contrasting headwater catchments, *J. Hydrol.*, 367(3), 237-248. 10.1016/j.jhydrol.2009.01.001.

Hrachowitz, M., C. Soulsby, D. Tetzlaff, I. Malcolm and G. Schoups (2010), Gamma distribution models for transit time estimation in catchments: Physical interpretation of parameters and implications for time-variant transit time assessment, *Water Resour. Res.*, 46(10). 10.1029/2010WR009148.

Jackson, C.R., M. Bitew and E. Du (2014), When interflow also percolates: Downslope travel distances and hillslope process zones, *Hydrol. Processes*, 28(7), 3195-3200. 10.1002/hyp.10158.

Jackson, C.R., E. Du, J. Klaus, N.A. Griffiths, M. Bitew and J.J. McDonnell (2016), Interactions among hydraulic conductivity distributions, subsurface topography, and transport thresholds revealed by a multitracer hillslope irrigation experiment, *Water Resour. Res.*, 52(8), 6186-6206. 10.1002/2015WR018364.

Jenson, S.K. and J.O. Domingue (1988), Extracting topographic structure from digital elevation data for geographic information system analysis, *Photogrammetric engineering and remote sensing*, 54(11), 1593-1600.

Jiang, X.W., L. Wan, X.S. Wang, S. Ge and J. Liu (2009), Effect of exponential decay in hydraulic conductivity with depth on regional groundwater flow, *Geophys. Res. Lett.*, 36(24). 10.1029/2009GL041251.

Katsura, S.Y., K.I. Kosugi, N. Yamamoto and T. Mizuyama (2006), Saturated and unsaturated hydraulic conductivities and water retention characteristics of weathered granitic bedrock, *Vadose Zone Journal*, 5(1), 35-47. 10.2136/vzj2005.0040.

Katsuyama, M., N. Ohte and S. Kobashi (2001), A three-component end-member analysis of streamwater hydrochemistry in a small Japanese forested headwater catchment, *Hydrol. Processes*, 15(2), 249-260. 10.1002/hyp.155.

Katsuyama, M., K. Fukushima and N. Tokuchi (2008), Comparison of rainfall-runoff characteristics in forested catchments underlain by granitic and sedimentary rock with various forest age, *Hydrological Research Letters*, 2, 14-17. 10.3178/hrl.2.14.

Katsuyama, M., M. Tani and S. Nishimoto (2010), Connection between streamwater mean residence time and bedrock groundwater recharge/discharge dynamics in weathered granite catchments, *Hydrol. Processes*, 24(16), 2287-2299. 10.1002/hyp.7741.

Kim, M., L.A. Pangle, C. Cardoso, M. Lora, T.H. Volkmann, Y. Wang, C.J. Harman and P.A. Troch (2016), Transit time distributions and storage selection functions in a sloping soil lysimeter with time-varying flow paths: Direct observation of internal and external transport variability, *Water Resour. Res.*, 52(9), 7105-7129. 10.1002/2016WR018620.

Klaus, J., K.P. Chun, K.J. Mcguire and J.J. McDonnell (2015), Temporal dynamics of catchment transit times from stable isotope data, *Water Resour. Res.*, 51(6), 4208-4223. 10.1002/2014WR016247.

Kubota, J., Y. Fukushima and M. Suzuki (1983), Runoff characteristics and soil moisture variation of topsoil in head-waters of a mountain small catchment: The observation in weathered granitic mountains at the south-east of Shiga prefecture [Japan], *Bulletin of the Kyoto University Forests (Japan)*.

Maloszewski, P. and A. Zuber (1982), Determining the turnover time of groundwater systems with the aid of environmental tracers. 1. Models and their applicability, *J. Hydrol.*, 57, 207-231. 10.1016/0022-1694(82)90147-0.

Małoszewski, P. and A. Zuber (1982), Determining the turnover time of groundwater systems with the aid of environmental tracers: 1. Models and their applicability, *J. Hydrol.*, 57(3), 207-231. 10.1016/0022-1694(82)90147-0.

Mcdonnell, J.J. (1990), A rationale for old water discharge through macropores in a steep, humid catchment, *Water Resour. Res.*, 26(11), 2821-2832. 10.1029/WR026i011p02821.

Mcglynn, B., J. Mcdonnell, M. Stewart and J. Seibert (2003), On the relationships between catchment scale and streamwater mean residence time, *Hydrol. Processes*, 17(1), 175-181. 10.1002/hyp.5085.

Mcglynn, B.L., J.J. Mcdonnell and D.D. Brammer (2002), A review of the evolving perceptual model of hillslope flowpaths at the maimai catchments, new zealand, *J. Hydrol.*, 257, 1-26. 10.1016/S0022-1694(01)00559-5.

Mcguire, K.J., J.J. Mcdonnell, M. Weiler, C. Kendall, B.L. McGlynn, J.M. Welker and J. Seibert (2005), The role of topography on catchment-scale water residence time, *Water Resour. Res.*, 41(5). 10.1029/2004WR003657.

Mcguire, K.J. and J.J. Mcdonnell (2006), A review and evaluation of catchment transit time modeling, *J. Hydrol.*, 330(3), 543-563. 10.1016/j.jhydrol.2006.04.020.

Mckie, D. (1978), A study of soil variability within the blackball hill soils, reefton, new zealand, Lincoln College, University of Canterbury.

Mcnamara, J.P., D. Tetzlaff, K. Bishop, C. Soulsby, M. Seyfried, N.E. Peters, B.T. Aulenbach and R. Hooper (2011), Storage as a metric of catchment comparison, *Hydrol. Processes*, 25(21), 3364-3371. 10.1002/hyp.8113.

Montgomery, D.R., W.E. Dietrich and J.T. Heffner (2002), Piezometric response in shallow bedrock at cb1: Implications for runoff generation and landsliding, *Water Resour. Res.*, 38(12). 10.1029/2002WR001429.

Morgenstern, U., M.K. Stewart and R. Stenger (2010), Dating of streamwater using tritium in a post nuclear bomb pulse world: Continuous variation of mean transit time with streamflow, *Hydrol. Earth Syst. Sci.*, 14(11), 2289-2301. 10.5194/hess-14-2289-2010.

Mosquera, G., C. Segura, K. Vaché, D. Windhorst, L. Breuer and P. Crespo (2016), Insights on the water mean transit time in a high-elevation tropical ecosystem 2, *Hydrol. Earth Syst. Sci.*, 20(1), 1-1. 10.5194/hess-20-2987-2016.

Nathan, S. (1974), Stratigraphic nomenclature for the cretaceous-lower quaternary rocks of buller and north westland, west coast, south island, new zealand, *New Zealand journal of geology and geophysics*, 17(2), 423-445.

Ohte, N., M. Suzuki and J. Kubota (1989), Hydraulic properties of forest soils (i), *Journal of Japanese Forestry Society* 71(4), 137-147.

Pearce, A.J. and L.K. Rowe (1979), Forest management effects on interception, evaporation, and water yield, *J. Hydrol.*, 18(2), 73-87.

Pfister, L., N. Martínez-Carreras, C. Hissler, J. Klaus, G.E. Carrer, M.K. Stewart and J.J. McDonnell (2017), Bedrock geology controls on catchment storage, mixing and release: A comparative analysis of 16 nested catchments, *Hydrol. Processes*, 31(10), 1828-1845. 10.1002/hyp.11134.

Ranken, D.W. (1974), Hydrologic properties of soil and subsoil on a steep, forested slope. M.S., Oregon State University, Corvallis.

Rinaldo, A., P. Benettin, C.J. Harman, M. Hrachowitz, K.J. McGuire, Y. Van Der Velde, E. Bertuzzo and G. Botter (2015), Storage selection functions: A coherent framework for quantifying how catchments store and release water and solutes, *Water Resour. Res.*, 51(6), 4840-4847. 10.1002/2015WR017273.

Rodgers, P., C. Soulsby, S. Waldron and D. Tetzlaff (2005), Using stable isotope tracers to assess hydrological flow paths, residence times and landscape influences in a nested mesoscale catchment, *Hydrology and Earth System Sciences Discussions*, 9(3), 139-155. hal-00304813.

Sanford, W. (2002), Recharge and groundwater models: An overview, *Hydrogeol. J.*, 10(1), 110-120. 10.1007/s10040-001-0173-5.

Sayama, T. and J.J. McDonnell (2009), A new time-space accounting scheme to predict stream water residence time and hydrograph source components at the watershed scale, *Water Resour. Res.*, 45(7). 10.1029/2008WR007549.

Sayama, T., J.J. McDonnell, A. Dhakal and K. Sullivan (2011), How much water can a watershed store?, *Hydrol. Processes*, 25, 3899-3908. 10.1002/hyp.8288.

Seibert, J. and J.J. McDonnell (2002), On the dialog between experimentalist and modeler in catchment hydrology: Use of soft data for multicriteria model calibration, *Water Resour. Res.*, 38(11), 231-2314. 10.1029/2001WR000978.

Snively, P.D., H.C. Wagner and N.S. Macleod (1964), Rhythmic-bedded eugeosynclinal deposits of the tyee formation, oregon coast range, *Kansas Geological Survey Bulletin*, 169, 461-480.

Soulsby, C., K. Piegat, J. Seibert and D. Tetzlaff (2011), Catchment-scale estimates of flow path partitioning and water storage based on transit time and runoff modelling, *Hydrol. Processes*, 25(25), 3960-3976. 10.1002/hyp.8324.

Staudinger, M., M. Stoelzle, S. Seeger, J. Seibert, M. Weiler and K. Stahl (2017), Catchment water storage variation with elevation, *Hydrol. Processes*, 31(11), 2000-2015. 10.1002/hyp.11158.

Stewart, M.K., J. Mehlhorn and S. Elliott (2007), Hydrometric and natural tracer (oxygen-18, silica, tritium and sulphur hexafluoride) evidence for a dominant groundwater contribution to pukemanga stream, new zealand, *Hydrol. Processes*, 21(24), 3340-3356. 10.1002/hyp.6557.

Stewart, M.K., U. Morgenstern, M.A. Gusyev and P. Małozzewski (2016), Aggregation effects on tritium-based mean transit times and young water fractions in spatially heterogeneous catchments and groundwater systems, and implications for past and future applications of tritium, *Hydrol. Earth Syst. Sci. Discuss.*, 10. 10.5194/hess-2016-532.

Swanson, F.J. and M.E. James (1975), Geology and geomorphology of the h.J. Andrews experimental forest, western cascades, oregon., p. 14, U.S. Department of Agriculture, Forest Service, Pacific Northwest Forest and Range Experiment Station, Portland, OR.

Swanson, F.J. and J.A. Jones (2002), Geomorphology and hydrology of the hj andrews experimental forest, blue river, oregon, *Field Guide to Geologic Processes in Cascadia*, 289-313.

Tetzlaff, D., J. Seibert, K.J. Mcguire, H. Laudon, D.A. Burns, S.M. Dunn and C. Soulsby (2009a), How does landscape structure influence catchment transit time across different geomorphic provinces?, *Hydrol. Processes*, 23(6), 945-953. 10.1002/hyp.7240.

Tetzlaff, D., J. Seibert and C. Soulsby (2009b), Inter-catchment comparison to assess the influence of topography and soils on catchment transit times in a geomorphic province; the cairngorm mountains, scotland, *Hydrol. Processes*, 23(13), 1874-1886. 10.1002/hyp.7318.

Tetzlaff, D., C. Birkel, J. Dick, J. Geris and C. Soulsby (2014), Storage dynamics in hydrogeological units control hillslope connectivity, runoff generation, and the evolution of

catchment transit time distributions, *Water Resour. Res.*, 50(2), 969-985.
10.1002/2013WR014147.

Torii, A. (1996), Development of immature soils after afforestation on bare hills, with special reference to their mineralogical changes, *Journal of Forest Environment (Japan)*.

Walter, M.T., M.F. Walter, E.S. Brooks, T.S. Steenhuis, J. Boll and K. Weiler (2000), Hydrologically sensitive areas: Variable source area hydrology implications for water quality risk assessment, *Journal of Soil and Water Conservation*, 55(3), 277-284.

Woods, R.A. and M. Sivapalan (1997), A connection between topographically driven runoff generation and channel network structure., *Water Resour. Res.*, 33(12), 2939-2950.
10.1029/97WR01880.

CHAPTER 5

CONCLUSIONS AND FUTURE WORK

5.1 Conclusions

The central questions addressed by my PhD research was, what is the role of bedrock groundwater in controlling the processes, patterns, storage and transit time through a headwater catchment? My coupled water table monitoring, water chemistry analysis, tritium age dating and streamflow measurements assessed, mechanistically, the role of the low permeability bedrock on the rainfall-runoff regime and identified the processes, patterns, storages and transit times associated with bedrock groundwater contributions to the Maimai headwater catchment. Although by volume bedrock storage was considerable, the low permeability formation prevented rapid bedrock groundwater flow, limiting overall flux rates and contributions to the stream channel. Lack of bedrock fracturing was also critical to the nature of the flow regime and drove diffuse porous groundwater flow, a much slower flow system than fracture-flow. This created a highly anisotropic catchment scale flow regime defined by fast shallow soil-based flowpaths overlying a slow and deeper groundwater system with a considerable unsaturated bedrock zone that damped hillslope groundwater storm response and acted as a considerable storage unit. The ages of these stored waters likewise followed the vertically layered pattern associated with the flow regime: young water in the soil and shallow bedrock layers; older water with depth. Limited total and available storage in the thin soils combined with large annual rainfall totals maintained short soil water residence times of weeks to months, while large bedrock storage volumes and minimal annual groundwater recharge considerably lengthened deeper turn-over times, resulting in groundwater ages on the order of 1-2 decades.

The slow movement of the bedrock aquifer limited its volumetric contributions to the stream channel. Although it was an order of magnitude older than the younger soil-based storage, the large relative volume of younger soil water discharging from the catchment swamped the bedrock groundwater age signal throughout most of the year, except in the driest of times. This drove a time-varying streamwater transit time that was extremely young during storm runoff, young for

much of the hydrograph recession period and only old, in a relative sense, during infrequent extended summer periods without rainfall.

Noble gas and excess air measurements accompanying the groundwater tritium analysis revealed mean annual recharge temperatures that aligned with mean winter air temperature, *not* mean annual air temperature, suggesting a seasonally focused recharge regime. Further analysis revealed the critical role of bedrock structure – in combination with evapotranspiration – in this seasonal pattern. The Maimai catchment did experience a dry season during summer months, however, this was relative and mean monthly precipitation remained considerable. Additionally, storm runoff ratios also remained high during this period, implying an excess of available moisture in the catchment – enough to drive a high, 40% summer rainfall-runoff ratio. But despite the summer runoff, Maimai experienced essentially no summer recharge. This apparent contradiction was resolved through assessment of a long term data set and an energy balance recharge model. The lack of fractures within the bedrock and associated matrix flow dominance limited the volume of event-based groundwater recharge. Instead, recharge was controlled primarily by long term wetness conditions. During winter months, when the low evapotranspiration rates limited soil water extraction between storm events, the catchment remained wet and the slow trickle charge of bedrock groundwater recharge occurred. During summer, although storm events regularly introduced additional moisture into the system, the shallow soils and highly networked preferential flowpaths quickly shed this water as stormflow. Between storm events, the much higher evapotranspiration rates wicked additional moisture from the soil. Ultimately, the soil water that would have otherwise moved vertically downward into the bedrock as recharge instead moved vertically up through the canopy, and summer bedrock groundwater recharge was volumetrically inconsequential. Although seasonal recharge is common in many climate regimes across the world, the lack of seasonality in both the input signal (P) and output signal (Q) at Maimai masked the recharge seasonality. This highlights the importance of continued field-based research to inform and identify hydrologic processes that may otherwise be overlooked or assumed based on poor characterization of internal processes.

Where Chapter 2 and Chapter 3 focused specifically on bedrock groundwater processes at Maimai, Chapter 4 aimed to distill the basic understanding of the control of bedrock characteristics on catchment scale hydrologic processes. Specifically it highlighted the controls on the storage-release relationship across the headwater landscape and how these translate into varied streamwater mean transit time at geologically diverse sites. Previous studies have shown the importance of bedrock permeability in controlling catchment residence time dynamics (*Hale and McDonnell, 2016; Pfister et al., 2017*), however, a simple index to capture these controls across different catchment geologies had not yet been developed. A simple hypothesis was tested: catchments with longer hillslope lengths and a lower permeability contrast between at soil bedrock interface would tend towards greater mean transit times, and vice versa. A small meta-analysis was conducted of 8 catchments in 4 geologically diverse regions which had streamwater MTT established by previous studies. Indeed, the new anisotropy index developed in Chapter 4 was able to explain the variability in observed MTT at the 8 catchments based on geologic characteristics and landscape structure. As such, it offers a simple, data-driven approach to understand how bedrock properties, in part, control the redistribution tendencies and storage-release relationships that set the time scales of water transiting through the landscape. This new index and its presented application provide a promising new approach to evaluate headwaters. There is considerable potential to expand upon this index and apply it to larger landscapes across more varied hydroclimatic settings to further improve our understanding of the role of bedrock properties in controlling headwater hydrologic processes.

The results of this PhD research have advanced our understanding of runoff generation and catchment storage-release processes through the lens of bedrock characteristics and the contribution of bedrock groundwater to hydrologic functioning in headwaters. Through an extensive field campaign coupled with analysis of the processes, patterns, storage and transit times, I have demonstrated the critical role of bedrock characteristics, specifically permeability, in controlling the redistribution of water in the subsurface and its link to catchment scale hydrologic behavior.

Notwithstanding these advancements, much work remains to be done to shed light on the patterns and processes linked with the deeper geologic properties underlying most of our headwater basins. Specifically, connecting catchment hydrologists with the methods and expertise of groundwater hydrologists and hydrogeologists seems an obvious path forward. From basic drilling technology to mapping the subsurface, studies must probe to greater depths to understand and redefine the headwater catchment boundary. In keeping with the Critical Zone Observatory philosophy (Lin, 2010), new approaches must be adopted and developed to keep pace with ever more challenging questions.

Catchment hydrologists are often burdened by the uniqueness of individual catchments and their inability to transfer observations and knowledge from one scale to another and one region to another. This problem, in many ways, is magnified when considering bedrock groundwater movement within individual catchments. Single bedrock fractures may transport the majority of a hillslope's bedrock flow, which in turn may considerably alter streamwater chemistry, age and baseflow volume within an entire catchment. Yet defining effective characteristics for that bedrock zone, or that hillslope or the entire catchment based on measurements from single fractures can be impossibly difficult. Secondly, and conversely, topographically based watershed divides at the land surface are often at odds with the area contributing to the underlying aquifer system. This can add significant complexity to calculating specific water balance components or to modeling specific catchments processes when stream discharge at the catchment outlet is used as the reference. Managing both the randomness and heterogeneity of the small scale while also appreciating the integrated response of the larger scale is not new (Blöschl and Sivapalan, 1995), but it remains highly pertinent for bedrock groundwater studies, especially in dual porosity fracture flow systems. Particle tracking models (e.g. Davies *et al.* (2011) and Ameli *et al.* (2017)) are presenting researchers with new methods to view and study the subsurface domain and as bedrock horizons are included, more complex field campaigns will be required to both ground truth these models, as well as provide the basic data sets to run them.

Finally, the explicit recognition of the deeper storage zones represented by weathered and unweathered rock in headwater catchments has significance to the biogeochemical-ecological-

geomorphological connection that shapes landscape evolution (*Welch and Allen, 2014; Brantley et al., 2016; Riebe et al., 2017*) . The continued meshing of disciplines will likely usher in more directed studies of bedrock and bedrock groundwater less for simple mass-balance and storage inquires, but more towards understanding how weathering fronts, bedrock structure and biologic development are connected by subsurface water redistribution.

5.2 References

- Ameli, A.A., K. Beven, M. Erlandsson, I.F. Creed, J.J. McDonnell and K. Bishop (2017), Primary weathering rates, water transit times, and concentration-discharge relations: A theoretical analysis for the critical zone, *Water Resour. Res.*, 53(1), 942-960. 10.1002/2016WR019448.
- Blöschl, G. and M. Sivapalan (1995), Scale issues in hydrological modelling: A review, *Hydrol. Processes*, 9, 251-290.
- Brantley, S.L., M.I. Lebedeva, V.N. Balashov, K. Singha, P.L. Sullivan and G. Stinchcomb (2016), Toward a conceptual model relating chemical reaction fronts to water flow paths in hills, *Geomorphology*.
- Davies, J., K. Beven, L. Nyberg and A. Rodhe (2011), A discrete particle representation of hillslope hydrology: Hypothesis testing in reproducing a tracer experiment at gårdsjön, sweden, *Hydrol. Processes*, 25(23), 3602-3612. 10.1002/hyp.8085.
- Hale, V.C. and J.J. McDonnell (2016), Effect of bedrock permeability on stream base flow mean transit time scaling relations: 1. A multiscale catchment intercomparison, *Water Resour. Res.*, 52(2), 1358-1374. 10.1002/2014WR016124.
- Lin, H. (2010), Earth's critical zone and hydrogeology: Concepts, characteristics, and advances, *Hydrol. Earth Syst. Sci.*, 14(1), 25.
- Pfister, L., N. Martínez-Carreras, C. Hissler, J. Klaus, G.E. Carrer, M.K. Stewart and J.J. McDonnell (2017), Bedrock geology controls on catchment storage, mixing and release: A comparative analysis of 16 nested catchments, *Hydrol. Processes*, 31(10), 1828-1845. 10.1002/hyp.11134.
- Riebe, C.S., W.J. Hahm and S.L. Brantley (2017), Controls on deep critical zone architecture: A historical review and four testable hypotheses, *Earth Surf. Processes Landforms*, 42(1), 128-156. 10.1002/esp.4052.
- Welch, L.A. and D.M. Allen (2014), Hydraulic conductivity characteristics in mountains and implications for conceptualizing bedrock groundwater flow, *Hydrogeol. J.*, 1-24. 10.1007/s10040-014-1121-5.